1-1-2002

Nanostructures of crystalline block copolymers.

Sheng Hong
University of Massachusetts Amherst

NANOSTRUCTURES OF

CRYSTALLINE BLOCK COPOLYMERS

A Dissertation Presented

by

SHENG HONG

Submitted to the Graduate School of the

University of Massachusetts Amherst in partial fulfillment

of the requirements for the degree of

DOCTOR OF PHILOSOPHY

May 2002

Polymer Science and Engineering

NANOSTRUCTURES OF CRYSTALLINE BLOCK COPOLYMERS

A Dissertation Presented

by

SHENG HONG

Approved as to style and content by:

Samuel P. Gido, Chair

William J. MacKnight, Co-Chair

Thomas P. Russell, Member

H. Henning Winter, Member

Thomas J. McCarthy, Head
Department of Polymer Science & Engineering

DEDICATION

To my family

for their love and supports

ACKNOWLEDGEMENTS

First of all, I need to acknowledge my dissertation advisors, Prof. Sam Gido and Prof. MacKnight. It is a great pleasure of me to work with Sam during the past years and there are many enjoyable moments I have spent in Sam's research group. Without doubt, I have learnt a lot from Sam, both in the field of scientific research and in many practical matters, which will surely serve me well in the future. Prof. MacKnight is a great mentor and it was him that first introduced me to the field of crystalline block copolymers. His advices were invaluable to the progress of this research projects. It is also my distinct pleasure to work with both Prof. Tom Russell and Prof. Henning Winter during the course of my dissertation research, and I owe them thanks for their valuable time and input. Especially, I need to thank Prof. Tom Russell, whom I collaborated closely on the thin film project of this research. Although formally I am not his student, he took great time and effort to help and advise me. I must also pay due credit to Dr. David Lohse at ExxonMobile Company who contributed invaluable effort in providing the polyethylene diblock copolymer samples used in part of this study.

It is a great pleasure and privilege to work in this department. Lizhang and Tew helped me on the initial stages of my research and gave me many excellent suggestions. Yuqing, Robin, Sungkyun, Engin and Ken keep Gido group a fun and enjoyable place to work. Lou helped me a lot on microscopy. Eileen, Nancy, Susan, and many other secretaries made the life around us easy.

I have been lucky to have many friends during the last four years. Lizhang gave me tremendous help during my graduate study. With Lei, I shared many trips from Amherst to State College, Pennsylvania. The eight-hour driving is tiresome. However, they will always be enjoyable memories. Xiaodong, Shulan, Tao Xu, Chuntao and Tao Xie have been great friends for showing me how colorful life is in Amherst.

My family has been the foundation of my graduate study. I want to thank all of them from the deepest of my heart. Without them, my accomplishment would not have been possible. Especially, to my wife Yanmei, without her love and support, I will not endure the past years with joyful memories, and for her, all the efforts are worthwhile.

ABSTRACT

NANOSTRUCTURES OF CRYSTALLINE BLOCK COPOLYMER

MAY 2002

SHENG HONG

B.S., BEIJING UNIVERSITY

M.S., PENNSYLVANIA STATE UNIVERSITY STATE COLLEGE

Ph.D., UNIVERSITY OF MASSACHUSETTS AMHERST

Directed by: Professor Samuel P. Gido and Professor William J. MacKnight

The phase behavior and properties of strongly segregated crystalline–amorphous diblock copolymers with rubbery amorphous block were investigated. For low crystallinity PE-containing diblock copolymers, well-ordered microphase separated morphology was observed in the melt-state. Upon crystallization, in most cases, two-dimensional crystallization confined within the microphase-separated microdomains was observed with retention of the microphase-separated morphology formed in the melt-state. However, the crystallization temperature was found to have significant effect on morphology. Both the extent of microdomain confinement on crystallization and the crystalline chain orientation inside the microdomain were observed to be crystallization temperature dependent. Utilizing the unique properties of crystalline polymers, a novel method for preparing photonic band gap crystals was developed based on self-assembly

behavior of crystalline block copolymers. It opened up avenues to fabricate novel polymeric optical devices.

For high crystallinity PEO containing diblock copolymers, TEM coupled with electron diffraction revealed a microphase separated, alternating lamellar morphology with PEO crystalline chains oriented perpendicular to the microdomain interface regardless of the crystallization temperature. As suggested from optical microscopy and TEM experiments, the melt microphase separated morphology acted as template for crystallization. In contrast to the extended chain crystals always preferred by homopolymers, folded chain crystals were formed for crystalline/amorphous block copolymers at equilibrium state. The results were interpreted based on thermodynamic consideration of the system. The morphology of block copolymers where both block were crystalline was also investigated in this study. The effect of soft and rigid confinement on crystallization in P(E-*b*-EO), a crystalline/crystalline block copolymer, was evaluated.

The morphological evolution of crystalline block copolymers in thin films was studied. Multiple parallel layers of crystalline PEO were found to be in *perfect orientational registry* even though they were separated by approximately 10 nm thick layers of amorphous polymer.

TABLE OF CONTENTS

LIST OF TABLES

LIST OF FIGURES

CHAPTER 1

BACKGROUND AND LITERATURE REVIEW

1.1 Introduction

It is well known that diblock copolymers in the melt state can form microphase-separated morphology on the length scale of nanometers.[1] Most morphological studies on microphase separation are focused on block copolymers containing only non-crystallizable amorphous chains. Cooling such samples from the melt to the solid state is accompanied by glass transition of one of the blocks, which generally leads to trapping of the melt morphology. Consequently, there is usually little distinct thermodynamics in the phase behavior of block copolymers in the glassy state compared to the melt. Until recently, there is much less investigation on the morphology and phase behaviors of block copolymers containing crystallizable blocks. The transition from melt-state to the solid-state of crystallizable block copolymers will involve crystallization, which prefers to form crystalline lamellae on the length scale of nanometer, similar to microphase separation. The morphological evolution of crystallizable block copolymers upon transition to the solid state is thus accompanied by a competition between crystallization and microphase separation.

For pure amorphous block copolymers, the most important parameter in controlling the phase behavior is χN and ϕ. However, for crystallizable block copolymers, the situation is more complex. Besides χN and ϕ, the melting temperature of the crystalline block (T_m), the glass transition temperature of the amorphous block (T_g) and the

crystallization temperature (T_c) employed all play important role in determine the final morphology of the system.

1.2 Equilibrium Morphology of Crystalline-Amorphous Diblock Copolymers

Theoretical predictions concerning the morphology of symmetric crystalline / amorphous diblock copolymers have been developed by DiMarzio and coworkers[2], Whitmore and Noolandi[3], and Vilgis and Halperin[4] assuming that a thermodynamic equilibrium state can be achieved. As shown in Figure 1.1, this model assumes a structure of alternating crystalline and amorphous layers. In the crystalline layers there is regular chain folding with the chain stems oriented perpendicular to the interface with the amorphous domains.

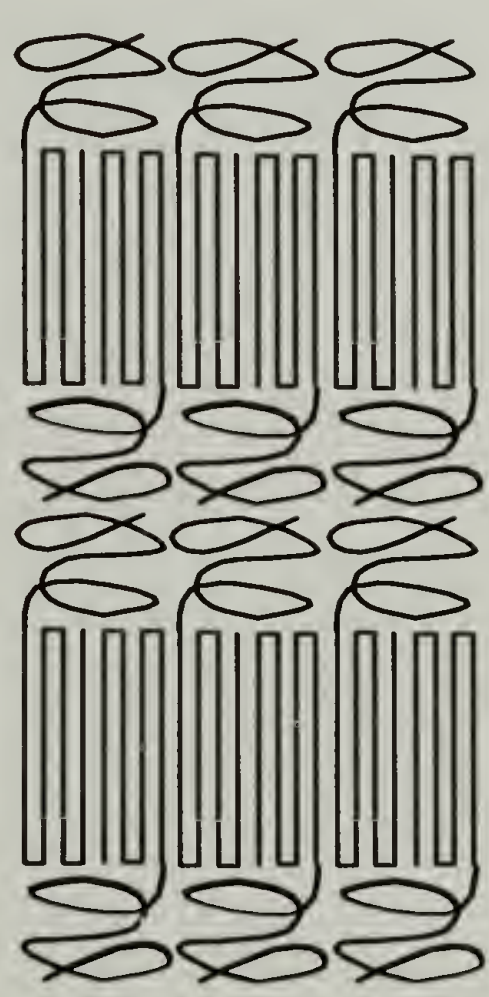

Figure 1.1: Equilibrium Morphology of Symmetric Crystalline / Amorphous Diblock Copolymers

The interaction between enthalpic driving force to minimize fold surface and the entropic term from stretching of the amorphous chain will result in an equilibrium chain folded crystalline thickness. This clearly differs from the structures formed by homopolymers where the extended chain crystals are the most stable species. Based on this consideration and minimizing the free energy with respect to the interfacial area, the equilibrium thickness of the crystalline and amorphous layer can be derived:[2]

$$L_a = \frac{N_a^{2/3}(\gamma_a + \gamma_c \rho_c)^{1/3}}{(3kT\rho_a)^{1/3}} \qquad L_c = \frac{N_c \rho_a^{2/3}(\gamma_a + \gamma_c \rho_c)^{1/3}}{\rho_c N_a^{1/3}(3kT\rho_a)^{1/3}}$$

L_i, N_i, and ρ_i are the domain spacing, molecular weight and density of the amorphous (a) and crystalline (c) block respectively. The interfacial area energy is γ_a and fold energy due to crystalline chain folding is γ_c. Accordingly, the scaling relationship between the equilibrium lamellar spacing (L_i) and block copolymer molecular weight , as obtained by DiMarzio and coworkers, are $L_a \sim N_a^{2/3}$ and $L_c \sim N_c N_a^{-1/3}$ respectively. Whitmore and Noolandi used a different method and obtained similar scaling relationship with slightly different exponentials: $L_a \sim N_a^{7/12}$ and $L_c \sim N_c N_a^{-5/12}$. This clearly differs from pure amorphous diblock copolymer where $L \sim N^{2/3}$.

Vilgis and Halperin conducted scaling analysis of aggregates formed by coil-crystalline diblock copolymers in a selective solvent.[4] Micelles, Cylinder and Lamella structures were considered. The crystalline core was considered to be intermediate between the melt like core formed by flexible immiscible blocks and the core of rod-coil

aggregates where chain folding was prohibited. For *lamellar* forming diblocks, a slightly different scaling law was obtained:

$$\frac{L_a}{a} \approx N_a^{9/11}\left(\frac{\sigma_f a^2}{kT}\right)^{2/11} \qquad \frac{L_c}{a} \approx N_c N_a^{-6/11}\left(\frac{\sigma_f a^2}{kT}\right)^{6/11}$$

where L_i and N_i are the domain spacing and molecular weight of the amorphous (a) and crystalline (c) block respectively. The σ_f is the lateral surface energy and a corresponds to molar volume of the monomer unit. For micelle structures, the cores were considered as cylindrical "pan cakes" as shown in Figure 2. In this case, the thickness of the crystalline "pan cake" (L_c) and the size of the amorphous corona (R_a) were found to scale as:

$$\frac{L_c}{a} \sim N_c^{3/5} \qquad \frac{R_a}{a} \sim N_c^{4/25} N_a^{3/5}$$

In the case of cylindrical morphology, the system was treated as cylindrical rod with rectangular shaped crystalline rod in the center with amorphous corona wrapped around it (Figure 1.2). It was derived that:

$$\frac{L_c}{a} \sim N_a^{-1/6} N_c^{13/18} \qquad \frac{W_c}{a} \sim N_a^{1/6} N_c^{13/18} \qquad \frac{R_a}{a} \sim N_a^{2/3} N_c^{1/9}$$

where L_c, W_c and R_a corresponded to the thickness and width of the crystalline rod and the size of the amorphous corona respectively.

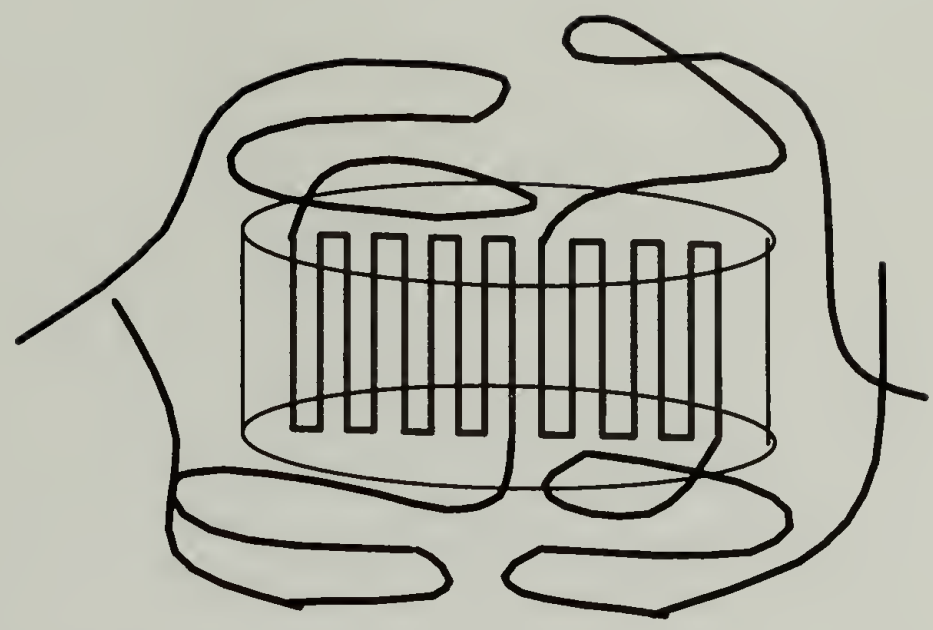

Figure 1.2: Pancake Structure of Crystalline-Amorphous Diblock Copolymer Micelles

1.3 Previous Studies on Crystalline-Amorphous Block Copolymers

Many diblock copolymer systems with a crystallizable block have been investigated. Crystallizable blocks including poly(ethylene),[5-26] poly(ethylene oxide),[22,27-37] poly(ε-caprolactone)[36,38] and poly(tetrahydrofuran)[39,40] have been studied. The amorphous blocks investigated vary considerably, in term of their glass transition temperatures and segregation interactions with the crystallizable block. Table 1 shows a summary of previously studied systems.

1.3.1 Poly(ethylene)-Containing Block Copolymers

The polyethylene containing crystalline / amorphous diblock copolymers are among the most studied systems.[6-26,41-44] The PE block is a hydrogenated derivative of polybutadiene containing diblock copolymers. The diblock copolymers are synthesized via sequential anionic polymerization followed by hydrogenation.[23] Anionic polymerization of butadiene can proceed with predominantly 1,4 microstructure, which

becomes PE after hydrogenation. However, during polymerization, there is inevitable 1,2 insertion of butadiene unit, which becomes ethyl branch on PE backbone after hydrogenation. Consequently, all PE containing diblock copolymers synthesized via this method has low crystallinity ~30% and is LDPE like. Recently advancement in living ring opening metathesis polymerization (ROMP) provides opportunities to prepare HDPE containing diblock copolymers.[45,46] However, the choice of the amorphous block is very limited. All the morphological studies on PE containing block copolymers available in the literatures are based on anionic synthesis.

1.3.1.1 Morphology formation of PE containing block copolymers

Crystallization has dramatic effect on the morphology of the system. Seguela and Prud'homme[5] investigated a poly(ethylene-b-(ethylene-alt-propylene)-b-ethylene) triblock copolymer containing 27wt% PE cast from a neutral solvent close to T_m of PE and well below it. The samples cast above T_m crystallized within the assumed hexagonal-packed cylinder microphase-separated structure. However, SAXS experiments performed on the samples cast at room temperature suggested that crystallization occurred without prior microphase separation in the melt.

Cohen and coworkers[6] studied the morphology of poly(ethylene-b-styrene) block copolymers and found the final morphology was path dependent. As shown in Figure 1.3, if the sample film was cast from solution below T_m of the PE block, crystallization preceded microphase separation (region I). Once crystallized, however, the diblock copolymer is kinetically locked into the morphology formed in region I. On the other hand, if the sample film was cast above T_m, microphase separation occurred first (region III) and crystallization proceeds within the framework of microphase-separated domains

(region II). This path dependence on casting conditions is a general feature of crystallization in block copolymers.

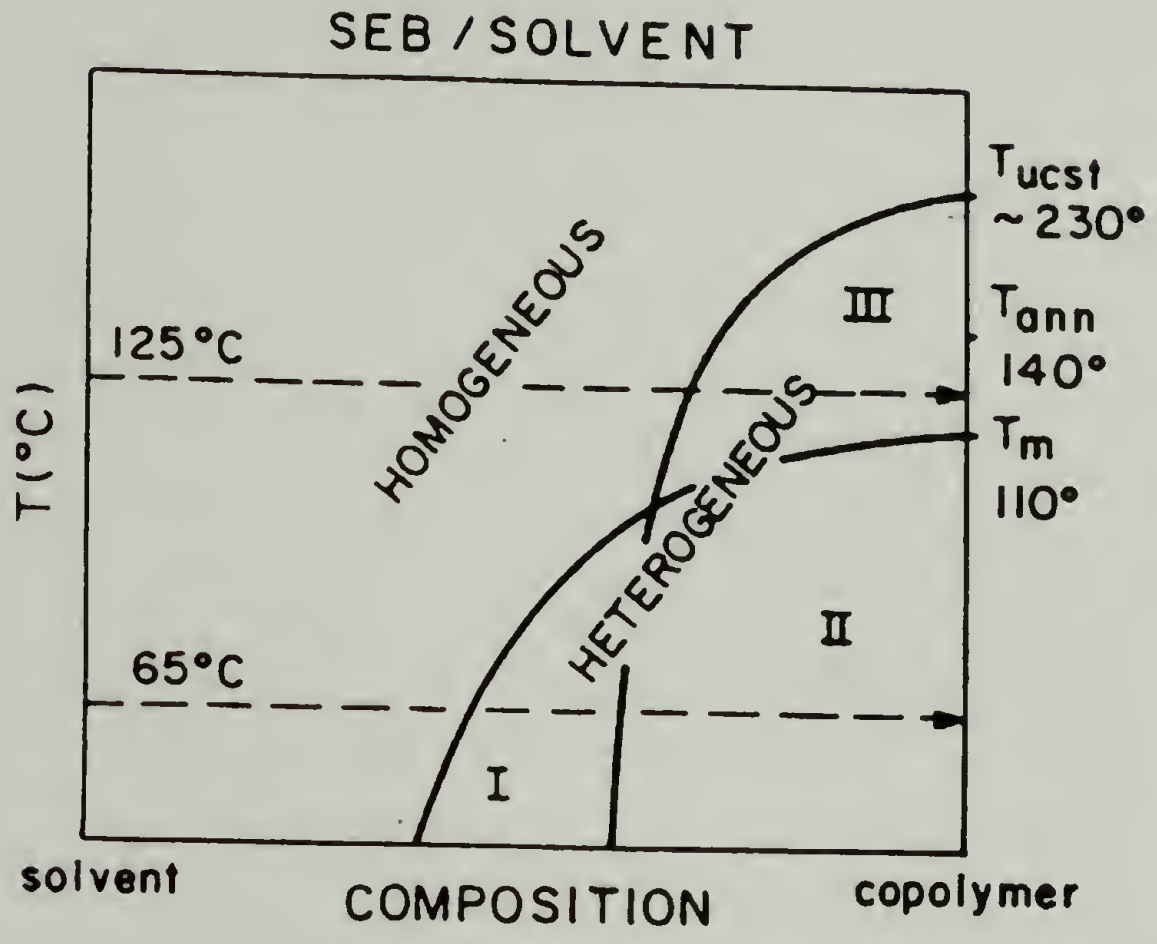

Figure 1.3: Casting Condition Dependent Morphology Formation of PE-b-PS Diblock Copolymers

Ryan, Hamley and coworkers studied a series of PE-containing diblock copolymers: poly(ethylene-*b*-ethylethylene) (PE-*b*-PEE), poly(ethylene-*b*-ethylene-*alt*-propylene) (PE-*b*-PEP) and poly(ethylene-b-vinylcylohexane) (PE-*b*-PVCH) using simultaneous small angle (SAXS) and wide angle X-ray scattering (WAXS).[10,22] The PEE, PEP are rubbery block, whereas PVCH is glassy with T_g=140°C. For diblocks with a rubbery amorphous block, the domain spacing, as obtained by SAXS, was found to increase discontinuously upon crystallization, as indicated by the shift of the principal peak position. It is suggested that the melt morphologies were destroyed due to PE chain folding upon crystallization. The PE crystalline lamellar thickness, obtained from a correlation function analysis of the SAXS data, was found for all samples to be

independent of quench temperature. It was argued to be due to the constant 5% branch density of PE, which was inevitably introduced during anionic polymerization of PBD. In contrast, the total lamellar domain spacing was found to decrease for deeper quenches, which was explained as a consequence of increased degree of crystallinity at lower T_c.

Register and coworkers studied a series of miscible PE containing block copolymers: poly(ethylene-*b*-(ethylene-*alt*-propylene)) (PE-*b*-PEP).[18,20] The amorphous block had a low T_g (~ -60°C). The diblock copolymer was melt miscible and formed a single phase in the melt. Crystallization occurred directly from the homogenous melt. The development of SAXS invariant Q was compared to development of WAXS profile. It was found that the SAXS and WAXS profiles grew concurrently upon crystallization. The primary q* peak showed no discernable change in the primary state ($t < t_{½}$) but decreased slight for $t > t_{½}$. The block copolymer adopted a crystalline lamellar morphology over the full range of compositions studied and also exhibited spherulitic superstructure. The formed morphology did not have a well ordered alternating lamellar structure as shown in Figure 1.1 but rather very similar to low density polyethylene with loosely developed spherulitic morphology.

Crystallization of weakly segregated poly(ethylene-*b*-(head to head propylene)) (PE-*b*-hhPP) containing diblock copolymers with low T_g amorphous block were also investigated by Register and coworkers by time resolved simultaneous SAXS and WAXS experiments.[19] Although microphase separation was found to occur prior to crystallization, spherulite texture was observed after PE crystallization. During crystallization, the 1st order SAXS peak shifts to lower q with a concurrent increase in

peak width. The peak shape and position during crystallization could be adequately approximated by a linear addition of the peaks observed before and after crystallization, indicating that the melt morphology was simply converted to a crystalline morphology. The SAXS results of the block copolymers were found to be very sensitive to sample's thermal history. The overall domain periodicity increased during crystallization and its value varied with cooling rate.

Crystallization in strongly segregated block copolymers with rubbery amorphous block, such as poly(ethylene-*b*-(3-methyl-1-butylene)) (PE-*b*-PMB), was studied by Register's group also.[16] SAXS results indicated that there was almost no spacing change upon crystallization. This observation is in contrast to the PE-*b*-PEP and PE-b-hhPP system, where discontinuity in lamellar spacing is observed upon crystallization. It was suggested that crystallization proceeded within the confinement of microdomains based on the invariance of lamellar spacing upon crystallization.

In the study of Sakurai and MacKnight[25] on morphology of a strongly segregated poly(ethylene-*b-atactic* propylene) diblock copolymer and its blends, a combination of TEM and scattering techniques were employed. It was found that fast quenching the diblock copolymer melts by liquid nitrogen could preserve the microphase-separated morphology formed in the melt-state and PE crystallized within microdomains. On the other hand, slow cooling resulted in formation of spherulitic crystalline super structure that destroyed the melt microphase-separated morphology completely.

1.3.1.2 Orientation of PE crystalline chains inside the microphase separated domains

Confining crystallization within nano scaled microdomains will certainly affect the physical characteristics of PE crystallites. One of most important aspect is the orientation of crystalline material inside the microdomains. Cohen and coworkers studied the PE crystalline chain orientation inside the microphase-separated domains of near symmetric, lamellar forming diblock copolymers: poly(ethylene-*b*-(ethylene-alt-propylene)).[11,13,41] The samples were first shear aligned in the melt and then investigated by simultaneous SAXS and WAXS experiments. The (200) WAXS reflections were observed to be oriented in the same direction as the SAXS Bragg peaks from the lamellar structure with four oriented (110) reflections at ϕ=53° with respect to the normal to the shear direction. The results suggested that the chain axis of the PE crystalline lamellae oriented parallel to microphase separated domain interface but oriented randomly along the *a*- axis within in the lamellar plane, as shown in Figure 4. Parallel orientation of PE was also observed by Hamley and coworkers.[9] This observation is in contrary to the equilibrium theory where perpendicular orientation is believed to have a much lower free energy. It is suggested that for PE containing block copolymers adopting parallel orientation can allow crystallization to proceed without major disruption of the morphology.[9]

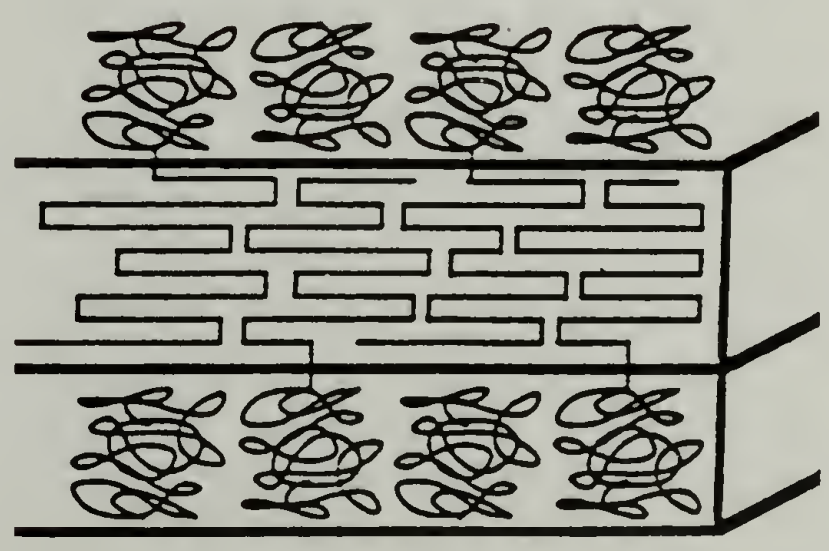

Figure 1.4: Parallel Orientation of PE crystalline chain inside Microdomains

In contrary, the study of Sakuri *et al.* indicated that the PE crystalline chain oriented randomly inside the microdomains of quenched PE-*b*-aPP diblock copolymers.[25]

The crystalline chain orientation in PE-containing block copolymers exhibiting cylindrical morphology was studied by SAXS and WAXS.[17] As shown in Figure 1.5, the SAXS and WAXS results suggested that for samples with low T_g amorphous block, slow cooling resulted in perpendicular alignment of PE crystallites with respect to the cylinder axis, while fast cooled samples displayed a slightly tilted orientation.

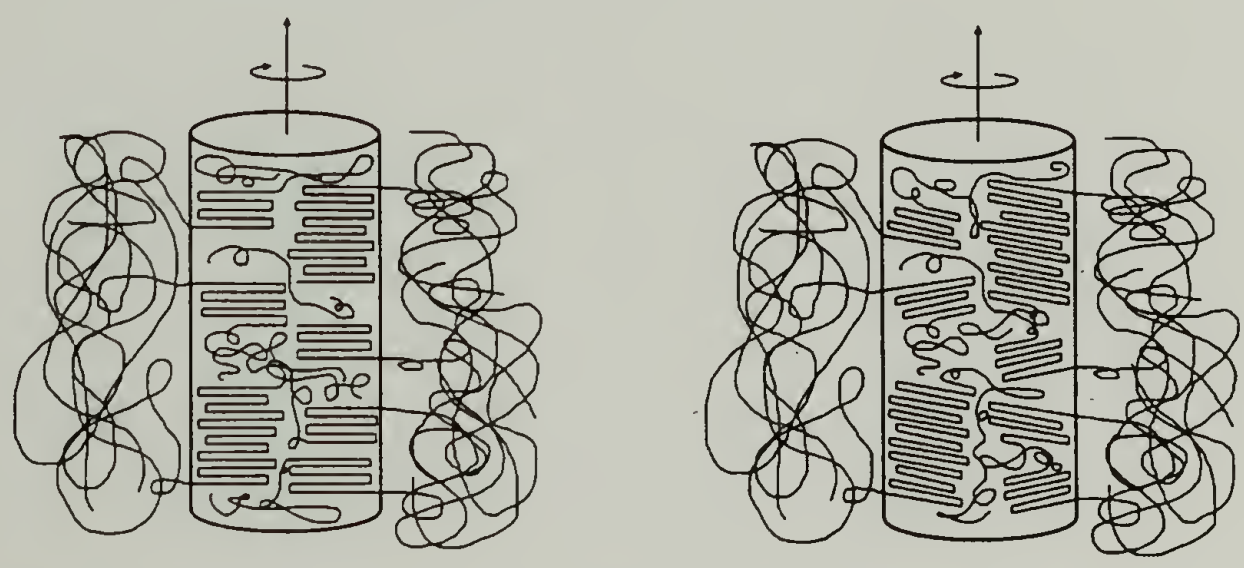

Figure 1.5: Crystalline Chain Orientation insider Cylindrical Microdomains

1.3.1.3 Morphology of PE containing block copolymer blends

Although there are many reports on PE-containing block copolymers, only a few focused on the morphology of their blends with homopolymers. Sakurai and MacKnight and coworkers investigated the morphology of PE-b-aPP diblock copolymers and their blends with atactic polypropylene with various molecular weights by TEM, SAXS and light scattering.[23-25] When the aPP chain was shorter than the aPP block, addition of aPP changed the morphology from a lamellar to a bicontinuos cylindrical and then a discrete

cylindrical and finally to a spherical structure. On the other hand, when the aPP chain was longer than the aPP block, macrophase separation was observed.

Register and coworkers studied the influence of semicrystalline homopolymer addition on the morphology of PE-b-PEP diblock copolymers. The pure diblock copolymers formed a homogeneous phase in the melt. The PE in the diblocks and the added PE homopolymers were found to readily co-crystallize. It was observed that the SAXS Bragg spacing decreased continuously and substantially as homopolymers was added. It was suggested that addition of PE homopolymer, which co-crystallized with diblocks, relaxed the strong chain stretch in the amorphous PEP block as shown in Figure 1.6, resulting observed reduction in lamellar long periods.

Figure 1.6: Effect of Homopolymer Addition

1.3.1.4 Crystallization kinetics of poly(ethylene)-containing block copolymers

The kinetics of PE crystallization in block copolymers have been studied by several research groups using either DSC or simultaneous synchrotron SAXS and

WAXS.[10,15,20,22,24] Using synchrotron radiation it is possible to obtain diffraction patterns in 6 seconds, sufficient to ensure that the development of crystallinity can be followed.

Ryan and Hamley and coworkers studied the dynamics of structure formation of a series of polyethylene containing diblock copolymers. The development of PE crystallites was followed via variation of SAXS invariant upon crystallization using Avrami analysis:[47]

$$1-\phi = \exp(-kt^n)$$

where ϕ is the relative degree of crystallinity and can be characterized by SAXS invariant, k and n are constants which depend on the nucleation and growth mechanism. The value of n ($n=a+b$) characterizes both the nucleation mechanism ($a=0$ for spontaneous nucleation or 1 for sporadic nucleation) and the growth dimension of crystallization ($b=1$ *or* 2 *or* 3). For both rubbery PE-b-PEE diblocks and glassy PE-b-PVCH, an exponent of $n=3$ was observed by Ryan, Hamley and coworkers.[10,22]

Dynamics of crystallization of homogeneous PE-b-PEP and PE-b-PEE diblocks have been studied also using time-resolved simultaneous SAXS, WAXS with a combination of DSC. It was observed that up to four orders of reflections in the SAXS profiles developed rapid and simultaneously during isothermal crystallization from the homogenous melt, suggesting a nucleation and growth structure formation mechanism driven by crystallization.

Sakurai and MacKnight and coworkers studied the crystallization kinetics of PE-b-aPP diblocks and their blends with aPP homopolymers. An Avrami exponent of 2.7-2.9

was observed for PE-b-aPP diblock copolymers in all the temperature range studied. On the other hand, a continuous decrease in Avrami exponent was observed with addition of aPP homopolymers indicating that the dimensionality of the crystallization growth geometry was reduced by blending homopolymer. In addition, blending did not affect the melting behavior of PE block but drastically altered the crystallization behavior depending on the molecular weight and composition of the blend.

1.3.2 Poly(ethylene oxide)-Containing Block Copolymers.

The PEO homopolymer is typically synthesized from ethylene oxide by either anionic or cationic polymerization. PEO containing block copolymers can be synthesized by sequential anionic polymerization. Unlike PE blocks in PE containing block copolymers, the PEO chains are perfectly linear. Consequently, the chain folds in PEO crystallites will not be affected by chain branching. The PEO homopolymer typically has very much crystallinities, which can be 90% or higher for low molecular weight polymers.

The crystallization of poly(ethylene oxide) (PEO) homopolymers has been an widely studied.[48-67] Low molecular weight PEO homopolymers were found to have the characteristic preference for integral folding. This preference is gradually lost for molecular weight higher than 10,000 g/mol.

Comparing to PE-containing block copolymers, there was less study on the morphology of PEO-containing block copolymers.[22,27,28,30,32,33,37,68-72] Crystallization of melt miscible poly(ethylene oxide-b-propylene oxide) (PEO-b-PPO) has been investigated by Ashman and Booth.[27] Predominantly, extended chain crystals were

found. However, the melting temperatures of the block copolymers were depressed as compared to perfect linear PEO homopolymers. The crystallization behaviors of melt miscible PPO-b-PEO-b-PPO triblock copolymers were also reported by Ashman and Booth in a companion paper.[28] Both extended and once or twice folded chain crystals were observed. Modified Flory-Vrij theory[73] was applied to melt miscible PEO / PPO block copolymer systems by Ashman and Booth. The free energy of formation of the amorphous layer from the melt was extrapolated from experimental data to be about 3.5 KJ/mol, while the free energy of formation of crystalline PEO and amorphous PPO interface was extrapolated to be about 3 KJ/mol.

Morphology and crystallization of poly(ethylene oxide-b-butylene oxide) (PEO-b-PBO) was studied by Ryan and coworkers.[32,33,74] Low molecular weight block copolymers formed lamellae morphology upon crystallization from homogeneous melt and the PEO chain assumed an extend chain conformation. For higher molecular weight PEO-b-PBD block copolymer crystallizing from homogeneous melt, however, extended chain crystallites became unstable and integral folded PEO crystallites were observed. Crystallization from weakly segregated melt of PEO-b-PBD block was accompanied by a change of length scale and led to integral folded crystallites. Crystallization using self-seeded process on the same block copolymer led to crystallites with less integral folding numbers. It was found that the lamellae in all crystallites formed by quenching could be thickened by annealing.

A comprehensive study on the single crystal morphology of poly(ethylene oxide-b-styrene) (PEO-b-PS) was studied by Lotz, Kovac and coworkers.[68,69] Transitions

between different crystal habits and their dependence on crystallization conditions were studied in detail. Typically, square or truncated square single crystals were observed. Layer thickness measurements based on SAXS and electron microscopy suggested that a layered structure with PEO crystalline chain sandwiched between amorphous PS.

Gervais and Gallot investigated the degree of crystallinity and chain folding in neat PEO-b-PS and as a function of selective solvent for either block. The PEO was found to form spherulitic structures. In analysis of the results, perpendicular orientation of the PEO chains to the lamellar interface was assumed and formation of highly folded PEO crystallites was suggested. The number of folds and the interfacial area per PS block were found to increase with increasing molecular weight f the PS block. Increasing the concentration of the preferential solvent for PS (diethyl phthalate), resulted in reduced melting temperature.

Recently, Cheng and coworkers studied the morphology and crystallization of a disordered PEO-b-PS (PEO: 5,000g/mol; PS: 11,00/mol) block copolymer system.[37] The order-disorder transition temperature was above the glass transition temperature of the PS block that was determined to be 44°C using dilatometer mode in thermo mechanical measurements. Depending on the crystallization temperature, several different situations were studied: $T_c > T_g$ (PS), $T_c \sim T_g$ (PS) and $T_c < T_g$ (PS). The lamellar crystals of the PEO blocks in the first case were found to grew with little morphological constraint due to initial disordered phase morphology. If T_c was only still slightly higher than the T_g (PS), the PEO crystals with a greater long period (L) than that of the disordered state was observed. The initial disordered phase morphology was gradually destroyed. When the

T_c was near but slightly lower than the T_g (PS), the crystallization took place largely within the existing phase morphology. A gradual shift of the L towards smaller q values was observed with increasing time, suggesting that the initial phase morphology was disturbed by the crystallization of the PEO blocks. In the last case, the PEO blocks was found to crystallize under a total constraint provided by the disordered phase morphology due to rapid vitrification of the PS-rich phase. Substantial decrease of crystallinity was also observed in this case.

1.3.3 Poly(ε-caprolactone)-Containing Block Copolymers

Poly(ε-caprolactone) (PCL) has a T_m around 63°C and block copolymers containing PCL can be synthesized via sequential anionic polymerization.

Nojima studied a series of PCL containing block copolymers.[38,75-81] For weakly segregated poly(ε-caprolactone-b-butadiene) (PCL-b-PBD), microphase separation was observed to occur prior to crystallization of PCL. A significant shift of SAXS q spacing to lower angle was observed upon crystallization of the PCL block. It was suggested that the microphase separated morphology was completely destroyed by the crystallization of PCL block.[38] The crystallization kinetics of the PCL-b-PBD block copolymer was compared with PCL homopolymers by time resolved SAXS experiments.[75] The Avrami analysis at the early stage of crystallization did not show any significant difference between PCL-b-PBD and PCL homopolymers, both showed an Avrami exponent about 2~3, suggesting that the initially existing microphase separated morphology does not affect the early stage of crystallization. In the late stage, however, the crystallization of PCL-b-PBD was found to be significantly retarded.

1.3.4 Poly(tetrahydrofuran)-Containing Block Copolymers

Poly(tetrahydrofuran) (PTHF) is typically synthesized via cationic polymerization. Although the PTHF chains are also linear as PEO chains, the PTHF has a much lower crystallinity, typically about 50%.

Ishikawa and coworkers studied the morphology of poly(tetrahydrofuran-b-isoprene) (PTHF-b-PIP) block copolymers by TEM and DSC.[82-84] Using N-vinyl carbazole together with osmium tetraoxide as staining reagent, TEM micrographs of the block copolymer were obtained. However, the PTHF chain orientation inside the microdomain was not determined.

Liu and coworkers studied the morphology and crystallization of poly(tetrahydrofuran-b-methylmethacrylate) (PTHF-*b*-PMMA) block copolymers and their blends with PMMA homopolymers by SAXS and DSC.[40,85-87] The PTHF block was synthesized cationically at first and an active site was then grafted at chain end so that subsequent anionic polymerization of PMMA could take place.[88] Microphase separation between the PTHF blocks and PMMA blocks were found to occur above the melting temperature of PTHF. Upon cooling from the melt, vitrification of the PMMA microphase occurred prior to crystallization. The microdomain size and shape remained unchanged after crystallization of PTHF block suggesting that the structure was locked by vitrification of the PMMA block. Strong dependence of the melting temperature and crystallization temperature of PTHF on diblock and blend composition were observed, both of which were observed to decrease continuously with increasing amount of PMMA concentration.

1.3.5 Thin Film Morphology of Crystalline / Amorphous Diblock Copolymers

Most of the recent research on the morphology of crystallizable block copolymers focused on the bulk properties. Until very recently, there is very little report on their thin film morphology.

Hamley and coworkers studied the thin crystallized film of PEO-b-PBD diblock and triblock copolymers on silicon by atomic force microscopy (AFM). The lamellar spacing of the diblock copolymer on thin film was found to be smaller than in the bulk. A tilted PEO chain model was proposed to explain the observation.

Recently, Reiter and coworkers reported experimental observations on the ordered surface patterns resulting from the crystallization of annealed thin films of microphase-separated low-molecular-weight hydrogenated poly(ethylene oxide-b-hydrogenated 1, butadiene) diblock copolymers.[34] For crystal growth rates higher than about 1 nm/sec, perpendicular orientation of the crystalline lamellae to the substrate was observed. Alignment of these lamellae on large length scales was found when crystallization occurred at boundaries created by a dewetting process.

1.3.6 Summary

In many of these previous studies, the morphology of diblock copolymers containing crystallizable blocks was found to be significantly influenced by the crystallization conditions. When crystallizing the sample from a microphase separated melt state, one of two results is obtained: (1) the microphase-separated morphology is maintained and the crystallizable block crystallizes within volume defined by the block copolymer microphase separated morphology. (2) Crystallization destroys the

microphase-separated morphology and a spherulitic texture formed. The morphology of crystalline/amorphous block copolymers was found to be heavily influenced by kinetics, similar to the case of crystallizable homopolymers. The previous works suggested that the final morphology of semicrystalline diblock copolymers is a strong function of: (1) the segregation strength of the copolymers (χN); (2) the mobility of the amorphous block (T_g); (3) the crystallization temperature (T_c) employed.

1.4 Statement of Problem and Proposed Research

Although a relatively large body of research on crystallizable block copolymers existed in the literatures, there are still many unanswered questions and further research is required to achieve a better understanding.

It is recognized that T_g of the amorphous block had significant influence on the morphological development of crystalline / amorphous block copolymers upon crystallization. Most research in the literatures has been focused mainly on crystalline / amorphous block copolymer with a high T_g amorphous block, where confinement of crystallization is from domain rigidity. In most cases, it is suggested that if T_c is higher than T_g of the amorphous block, crystallization will overwhelm the original microphase separated morphology existed in the melt state and impose a different, semi-crystalline morphology.[10,22,38] There is few report on the phase behaviors of strongly segregated crystalline / amorphous diblock copolymers with a rubbery amorphous block. It was suggested from the work of Register and coworkers[17] that strong incompatibility between the two blocks was sufficient to confine crystallization even though that the amorphous

block is rubbery at the crystallization temperature. However, few studies have focused on such systems.

The scaling behaviors between lamellar domain spacing and the molecular weight of the block copolymers and the equilibrium morphology of crystalline / amorphous block copolymers are of great interest. The lamellar domain spacing of PE-containing block copolymers with different molecular weights have been reported and results were compared to the equilibrium theory.[7,18] However, those previous work did not recognize the fact that the lamellar domain spacing in crystalline / amorphous block copolymer was heavily influenced by kinetics and the equilibrium state usually could not be obtained. In addition, the system studied did not have the same morphology as shown in Figure 1.1. First of all, the PE crystalline chain orientation was later found to be oriented parallel to the domain interface, contradicting to the equilibrium theory assumption. Second, as for the PE-b-PEP system studied by Register and coworkers,[18] the two constituent blocks were miscible with each other in the melt and the formed morphology was much like LDPE and did not have a strictly alternating lamellar morphology as assumed in the equilibrium theory calculation. Finally, the PE block has low crystallinity (~30%).

Most previous work on crystalline / amorphous block copolymers was based scattering technique and thermal analysis. Although SAXS and WAXS provide very valuable information on the morphology of the system, they do not provide direct visual evidence of the morphology formed. The structure of system, in many cases, was obtained based on indirect evidence and may lead to erroneous conclusion. The morphological study in this current research will be based on a combination of scattering,

thermal analysis and electron microscopy techniques. It is hoped that by employing different methods, a clear picture of the morphology can be unequivocally obtained.

Although the path dependent morphology of crystalline / amorphous diblock copolymers on solvent casting conditions has been studied, the effect of crystallization temperature on morphology formation has yet been investigated in detail. Sakurai et al.[25] observed that fast quenching of PE-b-aPP block copolymers from the melt could maintain the melt microphase separated morphology. On the other hand, if the sample was slowly cooled from the melt to the room temperature over of period of days, the original microphase separated morphology was substituted by a sheaf-like PE crystalline structure. However, detailed crystallization temperature studied was not carried out to define such a morphological transition. In addition, the orientation of the PE crystallites inside the quenched sample was found to be randomly oriented, different from those observed by other researchers.[8,9] In this current research, the effect of crystallization temperature on the morphology of crystalline / amorphous diblock copolymers will be investigated in detail.

It is also proposed in this research that for a system to behave similar to what is described by the equilibrium theory, it shall consist of a high crystallinity crystalline block and a low glass transition temperature amorphous block. The T_g of the amorphous block governs its mobility at crystallization temperature and is crucial for the diblock copolymer to approach its equilibrium state. Accordingly, this current research will focus on the phase behaviors of crystalline / amorphous diblock copolymers in the strong segregation limit with a rubbery amorphous block. The objective of the research is to

evaluate both the effect of crystallization on pre-existing microphase separated morphology and the effect of pre-existing microstructure on the crystallization characteristics of the crystalline block.

CHAPTER 2

PATH DEPENDENT MORPHOLOGY OF POLY(ETHYLENE-b-ATACTIC PROPYLENE)

2.1 Abstract

Transmission electron microscopy (TEM) and electron diffraction (ED) are used to study the morphology of a semicrystalline polyolefin diblock copolymer Polyethylene-*b-atactic-* polypropylene (PE-*b*-*a*PP) and its blend with polyethylene homopolymer. By using $RuCl_3$/NaClO as staining agent, both the contrast between amorphous PP and amorphous PE regions and the contrast between amorphous PE regions and crystalline PE regions can be obtained. As a result, both the larger lamellar structures due to microphase separation and the smaller crystalline PE lamellae can be resolved on TEM micrographs. Electron diffraction coupled with TEM imaging is used to elucidate the orientation of PE crystallites with respect to the interfaces of the microphase separated block copolymer lamellar domains. In most cases, two-dimensional crystallization confined within the microphase-separated microdomains was observed with retention of the microphase-separated morphology formed in the melt-state. The crystallization temperature was found to have significant effect on morphology. Both the extent of microdomain confinement on crystallization and the crystalline chain orientation inside the microdomain were observed to be crystallization temperature dependent. It was also shown in this study that utilizing the improved solvent resistance of crystalline block copolymers, a novel method to prepare photonic band gap crystals was developed.

2.2 Introduction

Theoretical predictions on the behavior of semicrystalline diblock copolymers have been developed by DiMarzio *et al.*,[2] Whitmore and Noolandi,[3] Vilgis and Halperin[4] assuming that a thermodynamically most stable state can be achieved. The most stable state of symmetrical crystalline/coil diblock copolymers is predicted to be strictly alternating lamella morphology with crystalline chain stems oriented perpendicular to the interface with the amorphous block domains. Experimental investigation of the morphology of semi-crystalline diblock copolymers has been carried out by several research groups[6,8,9,11,18,38,71]. For many systems studied, the final morphology was found to be path-dependent. When crystallizing the sample from a microphase separated melt state, one of two results is obtained: - (1) The microphase separated morphology is maintained and the crystallizable block crystallizes within the nano scale regions defined by the block copolymer microphase separation. (2) Crystallization destroys the morphology preformed in the melt state and forms spherulites. The experimental work of Cohen,[6] Nojima,[38] Register[19] and their co-works suggest that the final morphology of semicrystalline diblock copolymers is a strong function of: (1) the segregation strength of the copolymers; (2) the mobility of the amorphous block; (3) the crystallization temperature employed.

Most previous results on semicrystalline block copolymers made use of scattering techniques. Transmission Electron Microscopy (TEM) offers the opportunity to directly visualize the morphologies of these materials provided that the problem of achieving adequate contrast between different domains can be solved. TEM contrast between saturated polyolefin blocks is difficult to achieve and this has limited the use of TEM in

the study of these materials. Using RuO_4 to stain polyolefins, such as PE and PP, has been reported previously.[42,89,90] TEM images of LDPE, HDPE, PP, etc. have been obtained by using RuO_4 staining agent. The first report of ruthenium staining of saturated polyolefin diblock copolymers (PE-*b*-PEP and PE-*b*-PEE) was by Khandpur *et al.*.[42] The contrast produced by using RuO_4 is believed to be, at least in part, a result of the differences in transport properties of RuO_4 in the rubbery domains versus the semicrystalline domains. However, based on the difference of mobility of RuO_4 in crystalline and amorphous region, we should also expect contrast between crystalline polyethylene and amorphous polyethylene within microphase separated semicrystalline domains. While good contrast between the amorphous block and semicrystalline PE block was observed by Khandpur *et al.*, the difference between amorphous and crystalline polyethylene was not resolved.

In this report, we use ruthenium trichloride ($RuCl_3$) in sodium hypochlorite (NaClO) to stain the amorphous domains in PE-*b*-*a*PP, a saturated polyolefin diblock copolymer. The morphological behavior of PE-*b*-*a*PP diblocks and their blends with *a*PP have been studied previously by Sakurai *et al.*.[25] TEM images were obtained for both block copolymers and their blends with *a*PP without employing any staining agent. Contrast was from differences in density between the two domain materials as well as due to diffraction from the crystalline regions. Although microphase separated morphology could be observed, the difference between crystalline polyethylene and amorphous polyethylene could not be resolved.

The application of $RuCl_3$/NaClO to stain polyolefins has been reported previously by Montezinos *et al.*.[90] The systems they studied were mainly commercial polyolefins and blends. By using this staining agent for semicrystalline polyolefin diblock copolymers, we now can not only observe the morphology due to microphase separation, but also the crystalline morphology of polyethylene crystallites within polyethylene nanometer scale domains. To the best of our knowledge, this is the first visualization of polymer crystallites within a confined region defined by microphase separation. Electron diffraction patterns were also obtained from local regions of the specimen. Combining TEM imaging and ED, the orientation of the crystalline PE lamella with respect the interfaces of the PE lamellar domains of the block copolymer morphology can be investigated.

2.3 Experimental

PE-*b*-*a*PP used in this research was synthesized via hydrogenation from its precursor, poly(1,4-butadiene)-b-poly(1,4-3-methyl-1-pentadiene), which was synthesized via sequential anionic polymerization. PE homopolymer used in this study was also obtained by hydrogenation of anionically synthesized polybutadiene. Detailed information on the synthesis as well as characterization by ^{1}H NMR ^{13}C NMR and GPC has been presented previously.[24,91] The polyethylene chains in both block copolymers and homopolymers had about 5% ethyl branching due to inevitable 1-2 additions of butadiene. The molecular weight of the diblock copolymer used was 100,000 g/mol (45,000 g/mol for PE and 55,000 g/mol for *a*PP) and its polydispersity was 1.06. The molecular weight of the PE homopolymer was 20,400 g/mol, and its polydispersity was

1.03. The melting temperature, T_m, for the crystallites in the polyethylene block was determined by DSC to be 108°C and the T_g for atactic polypropylene was about 0 °C.

Diblock copolymer and PE homopolymer were blended by co-dissolving both polymers in hot xylene. The solvent was slowly evaporated at room temperature over a period of one week. The resulting blend was then completely dried in a vacuum oven. Both the diblock copolymer and its blend with polyethylene homopolymer were shear-aligned in the melt-state by application of an elongational flow field in a channel die, as illustrated in Figure 2.1. The details of this procedure were given previously.[25,92] The samples were then melt annealed at 150°C for 1 day. After annealing, the samples were subjected to crystallization under different conditions. To investigate the effect of crystallization temperature on the morphology, a small amount of sample were first melted at 150°C and then quickly quenched to desired crystallization temperature.

In order to prepare samples for TEM imaging, the first step was to cut a thick slice about 1mmx1mmx5mm from the bulk material. This was accomplished with a Reichert Ultracut cryomicrotome using a glass knife at –110°C. The thick section was then stained by exposure to the vapor generated from 1ml of freshly prepared 2wt% $RuCl_3$/NaClO in water for 3 hours at room temperature. Longer staining provides no advantage as the staining reagent loses it efficiency over time and the heavily stained outer parts of the bulk sample prevent further penetration of the staining reagent. The stained bulk samples became completely black. They were then microtomed with a diamond knife at room temperature in order to obtain ultra thin (about 40 nm) sections for TEM. The microtome cutting speed was about 0.2mm/s. The sections were collected

on 400 mesh copper grids. The initial preparation of a thick microtomed section was necessary since the staining reagent would only penetrate the outer several micrometers. The first few microns of the sample are most effectively stained.

TEM and electron diffraction experiments were conducted on a JEOL 2000 FX-II. The diffraction camera length was calibrated by using an internal gold standard on some of the grids observed. The magnification of TEM imaging was calibrated using etched gratings of standard dimensions. The Ruthenium staining agent not only provides TEM imaging contrast to the sample, it also helps to stabilize the PE crystallites in the electron beam of the TEM since the surrounding amorphous regions become heavily crosslinked. This crosslinking around the periphery of the crystallites makes it more difficult for them to melt as they are heated by exposure to the beam. However, the PE crystallites are still beam sensitive and the sharp diffraction patterns in electron diffraction will disappear in seconds.

2.4 Results

2.4.1 Morphology of Solution Cast Samples

Figure 2.2 is a TEM micrograph for samples solution cast below the T_m of the PE block from a toluene solution. In this case, the crystallization of PE occurred from a homogeneous polymer solution prior to microphase separation. The individual polyethylene crystalline lamellae can be clearly seen from the micrograph, however, no clear cut microphase separation between the PE and the *a*PP domain can be observed. The morphology shows a typical polymer crystalline structure with no well defined microphase separation.

2.4.2 Morphology of Quenched Diblock Copolymer and its Blends with PE Homopolymers

Figure 2.3 is a TEM micrograph showing the semicrystalline morphology of the pure polyethylene homopolymer. This is the same PE homopolymer used in the blends with the PE-*b*-*a*PP diblock. It was subjected to the same processing conditions as the diblock copolymer. A loosely developed spherulitic structure is observed in the pure PE with clustering of long PE crystalline lamella which appears ribbon-like in the cross sectioned image. Clearly the PE lamella is very long (on the order of a micrometer) compared to their thickness (on the order of 100 Å). This estimate of the aspect ratio of the lamella is very rough since the sample is a thin section with a thickness that is much smaller than the lamellar length. What is actually observed is a randomly selected cut through the sample. If anything, however, the actual lamellar lateral dimensions are larger than what is observed in the TEM image.

Figure 2.4 shows a TEM micrograph of the PE-*b*-*a*PP diblock. The sample has a block copolymer microphase separated lamellar morphology with a repeat distance of about 74 nm and is shown to be well aligned. Fast quenching does preserve the morphology formed in the melt-state. The *a*PP phase appears dark due to preferential staining by the ruthenium reagent. The lighter layers are less heavily stained polyethylene lamellar domains. The moderate amount of variation in *a*PP domain thickness is unusual when compared to common amorphous-amorphous diblock copolymers such as poly(styrene-b-isoprene). Closer examination reveals that the lighter PE layers contain short sections of crystalline lamellae that appear to be randomly oriented. Figure 2.5b shows electron diffraction from this material in which the PE 110

and 200 reflections are clearly visible as rings. Figure 2.5a shows the region inside the selected area aperture of TEM from which this electron diffraction pattern was taken. Clearly the larger length scale block copolymer lamellar morphology is well aligned over this entire region. Thus the fact that the crystalline PE diffraction produces unoriented rings is an indication that there is no preferential alignment of the PE crystalline lamellae within the PE domains, i.e. the PE-PP interface produces no aligning effect on the crystallites. A schematic of the morphology is shown in Figure 2.5c. This random orientation is consistent with previous results from two-dimensional SAXS and WAXS measurements on PE-*b*-*a*PP blends with *a*PP homopolymer,[25] but different from the results observed in some other systems.[8,17]

Figure 2.6 shows TEM micrographs of a blend between PE-*b*-*a*PP and PE homopolymer with an overall PE volume fraction (including PE blocks of the diblock and PE homopolymer) of 65%. The sample was also shear-aligned and quenched in liquid nitrogen. Figure 2.6a and 2.6b are images from two microtoming directions (perpendicular to the x- and y- directions as shown in Figure 2.1. The sample was found to be predominantly lamellar, but small regions of co-existing cylinder morphology are visible in Figure 2.6a. In these cylinder regions the PE is in the matrix phase, and randomly oriented, crystalline PE lamellae are visible. The darker regions in these two micrographs are heavily stained *a*PP, while the lighter regions contain both PE blocks from the copolymer and the PE homopolymer. The PE crystallites appear to once again be randomly oriented within the PE domains. This observation is also born out by electron diffraction (not shown) similar to Figure 2.5.

Comparing Figure 2.3 with Figure 2.4 and Figure 2.6, the polyethylene crystalline lamellae, as observed in the diblock copolymer and its blends, are much shorter (in dimension perpendicular to polyethylene chain stem) than those observed in homopolymer. This effect is clearly due to confinement of the PE crystallization within the nanometer scale microphase separated PE domains. Since the PE crystallites grow with random orientations, most orientations will allow them only a small amount of lateral growth space before they impinge on the boundaries with the *a*PP domains.

2.4.3 Crystallization Temperature Dependent Morphology

To further investigate the effect of T_c on PE crystallization in PE-b-aPP block copolymers, the shear-aligned samples were crystallized at different temperatures in DSC instruments and studied by TEM and electron diffraction. Shown in Figure 2.7 - Figure 2.9 are TEM micrographs for samples crystallized at different temperatures.

It is found that for crystallization temperature at 20°C or lower, the morphology is very similar to that of quenched samples. The PE block is found to crystallize within in the confined space defined by microphase separation and the PE crystalline chains orient randomly within the PE microdomains.

For samples crystallized at 50°C (Figure 2.7), although on the large length scale, the alternating lamellar morphology due to microphase separation is still present, close examination (as shown in the enlarged inset) reveals that there is extensive breakthrough of PE crystalline lamellae outside the confinement of microdomain confinement. Electron diffraction results indicate that the PE crystalline chains do not show preferential alignment with respect to the microdomain interface.

Increasing the crystallization temperature to 80°C (Figure 2.8), unlike the sample crystallized around 50°C, the PE crystallites again appeared to be mainly contained within the microphase separated domains. More interestingly, they start to show some kind of orientation within the lamellar microdomain.

Further increasing the crystallization temperature to 95°C, the alternating microphase separated lamellar morphology is still present. In addition, the PE crystalline lamellae are observed to be mainly located inside the microdomains (Figure 2.9). Nonetheless the PE crystalline lamellae appear to have a preferential alignment in the microdomain as indicated by the formation of long and thin crystalline lamellae along the direction of microdomain interface, as clearly shown from the enlarged inset in Figure 2.9.

This observation is further proved by a combined study of electron diffraction and TEM imaging as shown in Figure 2.10a and Figure 2.10b. The 110, 200 and 020 reflections can be clearly seen. The 020 reflection is observed to be in the same orientation of microphase separated lamellae. Comparing the electron diffraction pattern to that of the enlarged inset in Figure 2.10, it clearly indicates that the 020 reflection is along the growth axis of the PE crystallites.

The orientation of the PE crystallites within the microdomain requires more discussion. Although the diffraction pattern observed appears to be the same as those reported in the literature where the PE crystalline lamellae were determined to orient

parallel to the microdomain interface.7,9. The same diffraction pattern could also be interpreted as sphero-disk like orientation with b- axis perpendicular to lamellar normal with free rotation of c- axis around b- axis.93,94 Shown in

Figure 2.11is the X-ray pole figure analysis of the above two situations. Both kinds of orientation will results in similar diffraction patterns. In order to differentiate between the two, it is necessary to obtain direct information on the orientation of c-axis. However, the 002 reflection of PE is very weak and hence difficult to resolve in electron diffraction. In addition, in the current study, the orientation of the PE crystallites is limited by the microphase separated morphology whose orientation is not perfect. This imposes additional difficulties in differentiating the two kind of orientation based on diffraction results alone. However, as shown in the TEM micrograph, there are many long crystalline lamellae whose orientation seems to be perpendicular to the microdomain interface. As a result, it suggests that at least part of the PE crystalline chains is oriented perpendicular to the microdomain interface. Combining this information with the electron diffraction pattern, the results indicate that the chain axis of PE crystallites have a free rotation along its b- axis. Only the portion that orients perpendicularly to the microdomain interface can be clearly observed in the TEM micrograph. Consequently, the orientation of PE inside the microdomain is more close to the one shown in

Figure 2.11b. This conclusion is further supported by TEM tilting experiments as shown in Figure 2.12. A schematic of the morphology is shown in Figure 2.10c.

From our current results, it suggests that the PE crystallization in block copolymers with a low T_g component may be separated into three regimes. 1) at low T_c, the PE crystalline lamellae are confined within the microdomain and have no preferential

alignment; 2) at intermediate T_c, extensive break through of the crystalline lamellae outside the confinement can be observed; 3) at high T_c, the PE crystalline lamellae again are located mainly inside the microdomain with preferential alignment of the PE crystalline lamellae inside microdomains.

2.4.4 Fabrication of Photonic Band Gap Crystals via Crystalline / Amorphous Block Copolymer Self Assembly

A natural example of photonic band gap is the Australian Opal. Recently, there are increasing interests in exploring new method to fabricate photonic band gap crystals because they have the potential in many applications such as optical switch and optical communication.[95-97]

Block copolymers with molecular weight of 100,000g/mol will typical have microdomain spacing on the order of 80-100 nm. In order to make photonic band gap crystals in the visible light range, it is necessary to have periodic spacing of about 400 nm or up. Block copolymers with higher molecular weight are much harder to synthesize. In addition, high MW block copolymers have much slower phase separation kinetics and very high viscosity. It is hard to achieve well order morphology with long range order using high MW block copolymers. The key point in using block copolymer as photonic band gap crystals is to achieve large spacing yet still maintain well order morphology with exceptional long range order.

The crystalline block copolymers have much better solvent resistance than typical amorphous block copolymer. This advantage over traditional block copolymers can be

used to make photonic band gap crystals with much easier processing and much better versatility. PE-*b*-aPP diblock copolymer was first shear aligned in the melt to achieve a well ordered morphology with long range order. The low Tg of PE and aPP permit fast solvent diffusion. PE-*b*-aPP diblock copolymers could be swollen by an organic solvent. Because of the improved solvent resistance, the crystalline diblock copolymers will not dissolve in the solvent but only to a swollen state. If a typical glassy / rubbery block copolymer (such as PS-b-PIP) is used, the T_g of PS will be reduced so much that the specimen will eventually become soluble. The swollen PE-b-aPP specimen showed different colors depending on the extent of swelling. To prove of idea, the diblock copolymer sample was swollen by low molecular weight aliphatic oil. As shown in Figure 2.13, the resulting sample showed an iridescent blue color indicating that it was possible to use this method to prepare photonic band gap materials. If the organic solvent is a monomer, such as myrcene, the entire sample may be exposed to UV radiation or heat to polymerize the monomer inside the microdomains. The structure will be fixed by this reaction and a stable photonic band gap crystal is obtained.

This current method has several advantages over using non-crystalline block copolymer / homopolymer blends. (1) The traditional method involves blending and solvent casting of diblock copolymers with two different low molecular weight homopolymers to increase the total lamellar spacing. However, only very limited amount of homopolymer can be added. Otherwise, the system will become disordered. The current method overcomes this problem because the morphology is fixed by polymer crystallites inside one of the microdomains and swelling by solvent could not change the morphology. (2) Because only limited total amount of homopolymer can be introduced

into the system using amorphous diblock copolymers, the increase in lamellar spacing is very limited. Consequently, relatively high molecule weight block copolymers have to be used (MW~800,000g/mol total). They are much difficult to synthesize and have slower kinetics. The current method overcomes this problem because the crystalline - amorphous block copolymers can be swollen significantly by solvent. Samples with MW~100,000-200,000g/mol total will be enough to cover the whole visible light range. (3) The current method is also much better in preparing specimen with exceptionally well long range order, which is crucial for photonic crystal applications. It is because that the sample can be aligned with ease using different method (shear align, roll casting etc.) before being swollen by solvent. (4) Using the traditional method, it is possible to fabricate one dimensional photonic band gap crystals from block copolymers exhibiting lamellar morphology. However, it is much difficult to make two dimensional, or three dimensional photonic band gap crystals. Blending too much homopolymers in block copolymers forming cylindrical or spherical morphology will usually result in a disordered system. However, this problem is overcome by current method because the morphology desired is fixed by crystallinity and the solvent added only increase the domain size without changing the structure.

2.5 Discussion

Because of the crystallinity involved, the morphology formation of crystalline block copolymers is more complex as compared to amorphous block copolymers. In addition to χN and ϕ, which dictates the morphology in the melt state, the mobility of the

amorphous block (T_g), the melting temperature of the crystalline block (T_m) and the crystallization condition involved (T_c) are all very important.

The growth of a crystallite is strongly affected by the mobility of the chains. In the case of PE-*b*-aPP block copolymer, it will be dominated by the mobility of the amorphous *a*PP block. In addition, the nucleation density is strongly affected by T_c and its relationship with T_m. As a result, we suggest that the observed different regimes of morphology formation may be explained by a modified crystallization growth rate equation.

$$\dot{\gamma} = \dot{\gamma}_o \exp\left[-\left(\Delta E^* + \Delta F^*\right)/RT\right]$$

where γ corresponds to the crystallization growth rate; ΔE* corresponds to the critical free energy of crystallization and is from the original Hoffman-Lauritzen theory and ΔF* corresponds to the activation energy for molecular transport and is a version of the well known WLF equation.

$$\Delta E^* = \frac{4b\sigma\sigma_L T_m^o}{\Delta h_f\left(T_m^o - T\right)} \qquad \Delta F^* = \frac{2080^* RT}{\left(T - T_g + 51.6\right)}$$

All the parameter in this equation can be obtained either from literature or from experimental data.[98] The T_m^o corresponds to the equilibrium melt temperature of PE homopolymers and the T_g corresponds to the glass transition temperature of the *a*PP block, which is determined as 0°C. As a result, we can make a plot of activation energy *vs*. the crystallization temperature, which is shown in Figure 2.14.

As shown in the plot, ΔE* increases monotonically with increasing crystallization temperature indicating that at higher T_c there is less driving force for crystallization to

proceed. ΔF^*, on the other hand, decreases significantly with increasing T_c indicative of increasing degree of chain mobility at higher temperatures. Also shown in Figure 2.14 is the sum of ΔE^* and ΔF^* which shows a minimum around temperature 50-70°C. This coincides with the temperature regime where extensive breakthrough of crystalline lamellae outside microdomain confinement is observed. Within this temperature regime, crystallization of PE block encounters the smallest amount of activation energy and as a result, has the highest degree of freedom to proceed. At much lower temperature, the mobility of amorphous *a*PP block is limited whereas the nucleation density of the PE block is high. As a result, multiple nuclei crystallize simultaneously inside the confined microdomain resulting in confined crystallization with random crystalline chain orientation. At much higher temperature, the nucleation density is very low yet chain diffusion to the crystallization front is fast. Consequently, there is only few crystallites propagating at the same time and they proceed through the confined space defined by microphase separation.

2.6 Conclusions

Our results demonstrate that by rapid quenching it is possible to preserve the morphology formed in the microphase separated block copolymer melt state as the PE block crystallizes. This is the case even for blends with polyethylene as the major component. $RuCl_3$/NaClO provided excellent staining contrast for TEM imaging between *a*PP and PE microphase separated domains, and between amorphous PE and PE crystalline lamellae within the PE microphase separated domains. The contrast between amorphous PP and amorphous PE region is likely due to a difference in their tendency

toward reaction with ruthenium reagent. *a*PP is more reactive as it has tertiary protons which are more easily abstracted. The contrast between crystalline PE and amorphous PE regions is due to a difference between the rates of transport of the ruthenium stain in amorphous and crystalline regions. Coupling electron diffraction with TEM imaging, the PE crystalline lamella orientation within the PE microphase separated domains can also be determined.

The PE-*b*-aPP diblock copolymers exhibit a path dependent morphology formation. Depending on the crystallization conditions, up to four different morphologies can be observed. (1) Crystallization from homogeneous melt results in formation of crystalline polymer morphology with no well defined microphase separation. (2) Crystallization from melt microphase separated morphology at low temperature results in confined crystallization with random crystalline chain orientation. (3) At intermediate T_c, extensive breakthrough of crystalline lamellae outside the microdomain confinement can be observed. (4) Finally, at high T_c, crystallization is again mainly contained within the confined space yet with preferential crystalline chain orientation. The observed phenomena may be explained qualitatively based on a modified crystal growth rate equation. The above results provide guidelines for processing crystalline amorphous block copolymers to obtain desired morphology.

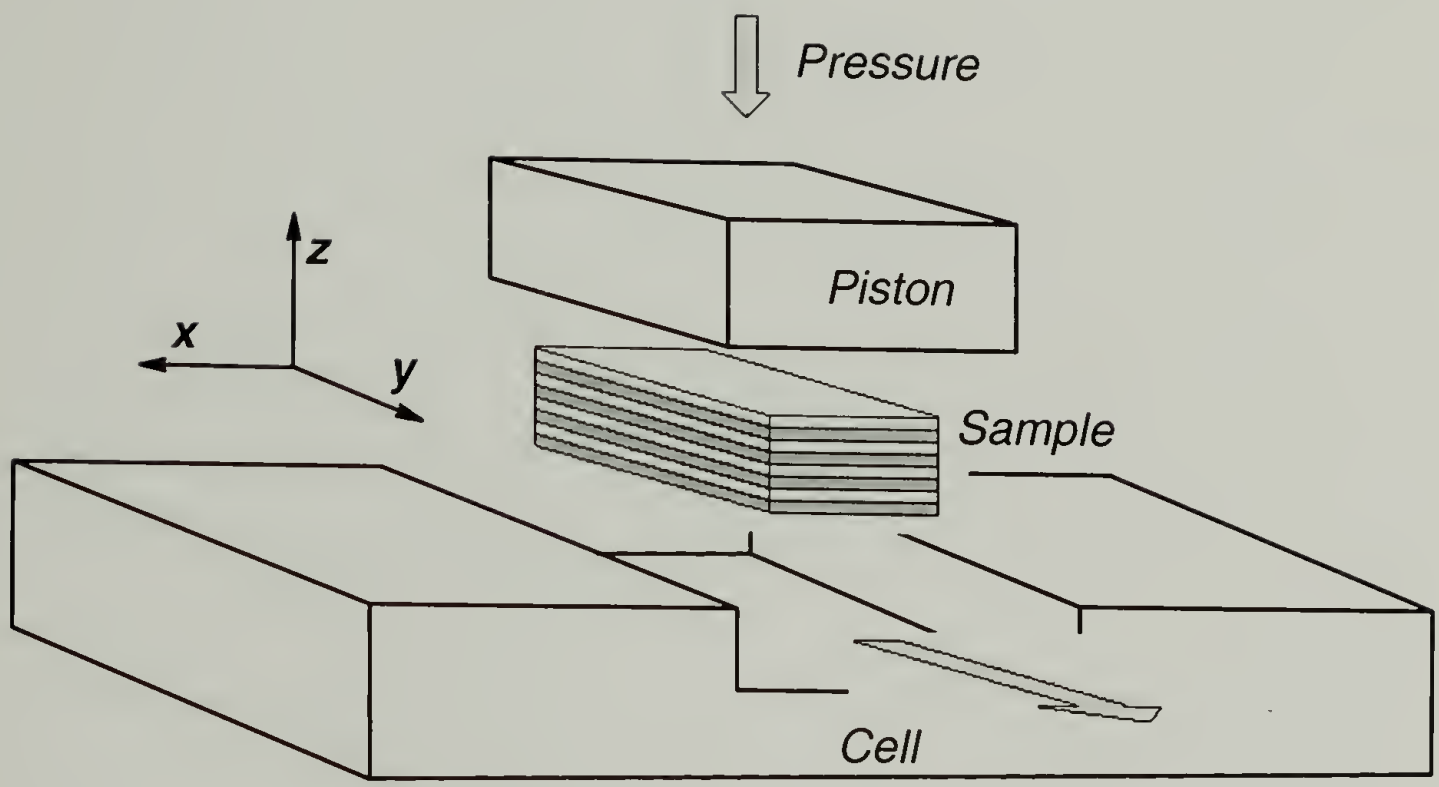

Figure 2.1: Shear cell for orienting macroscopically aligned block copolymer specimen.

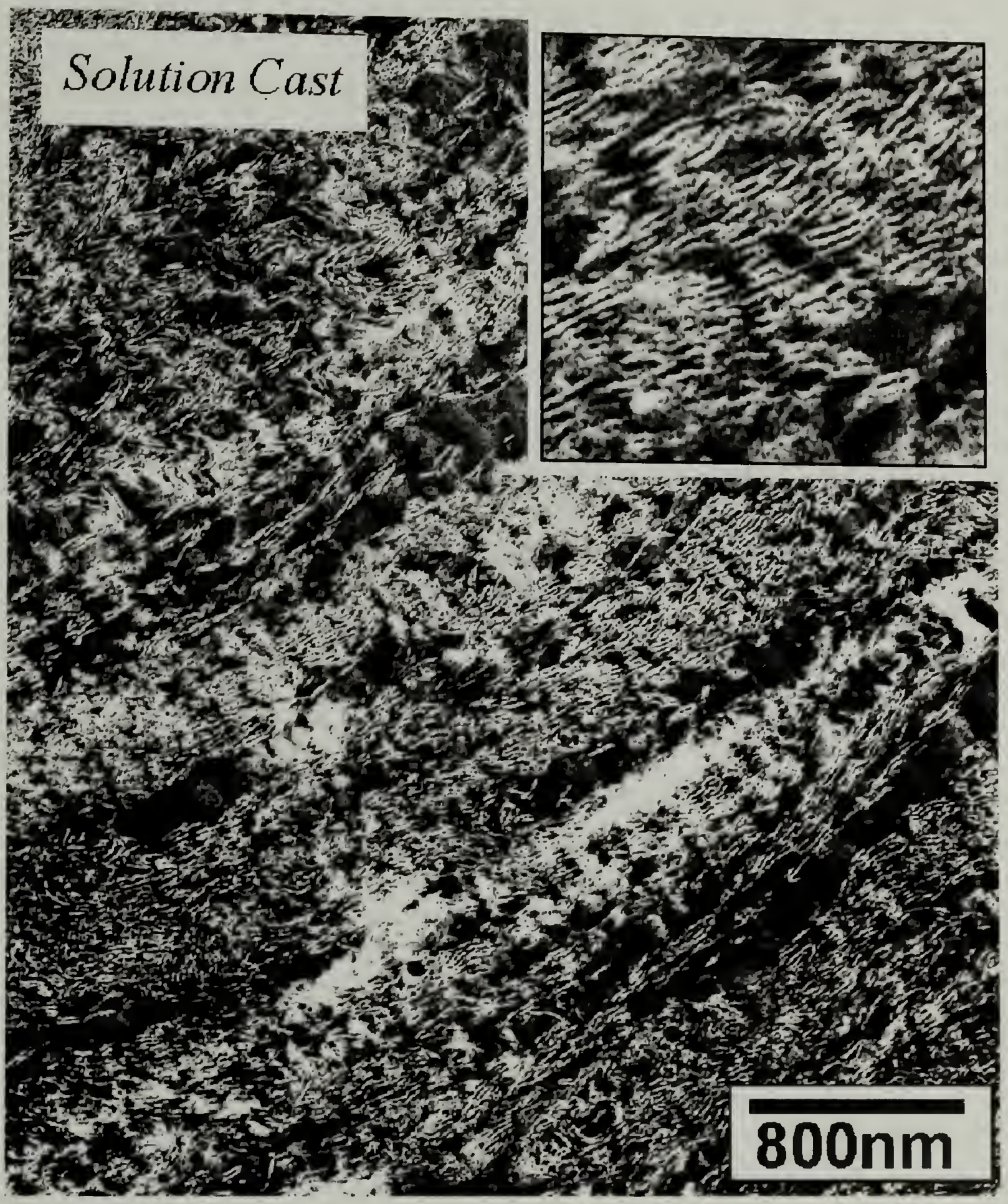

Figure 2.2: TEM micrograph of solution cast PE-*b*-aPP diblock copolymer samples.

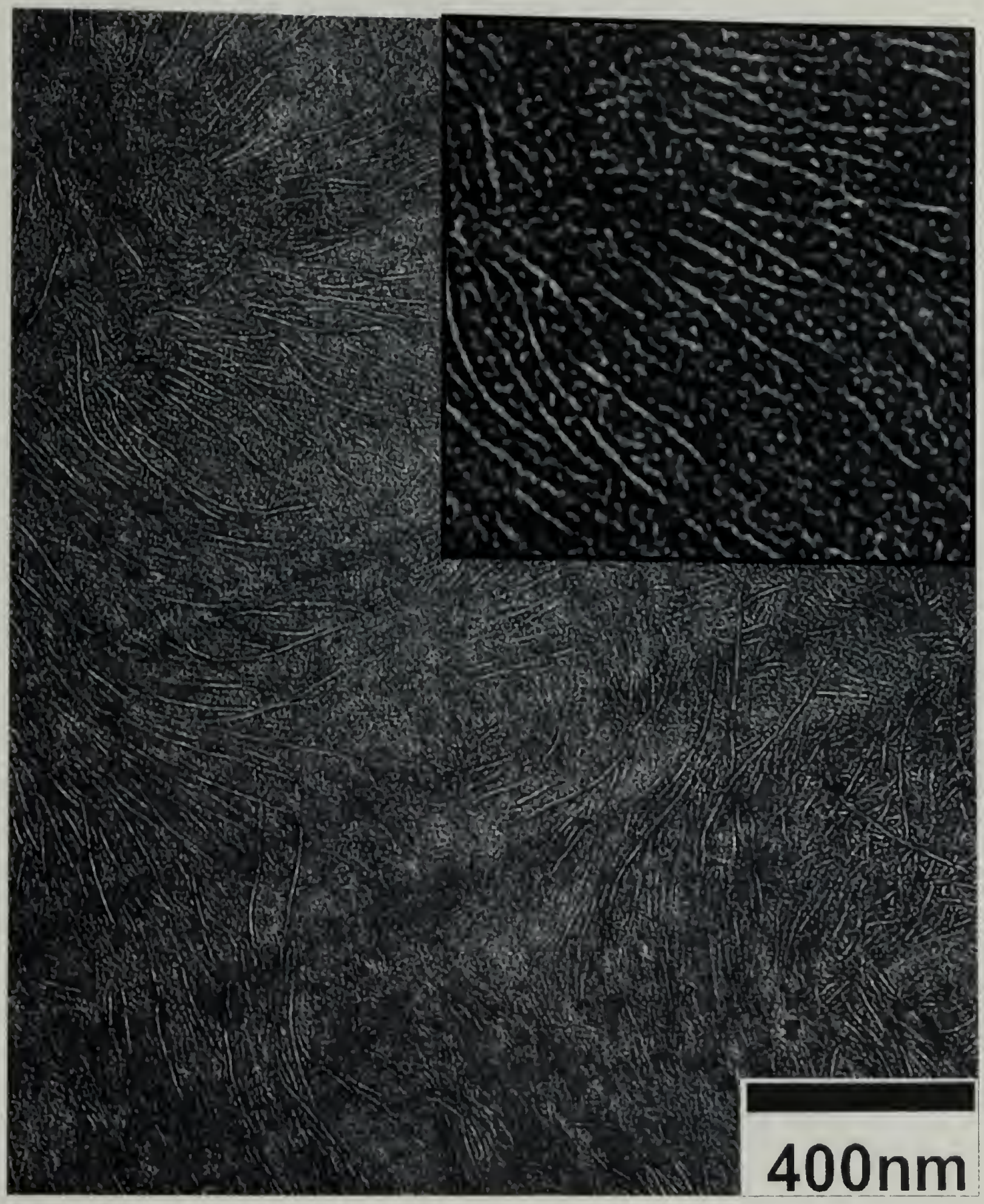

Figure 2.3: TEM micrograph of LDPE (hydrogenated PBD).

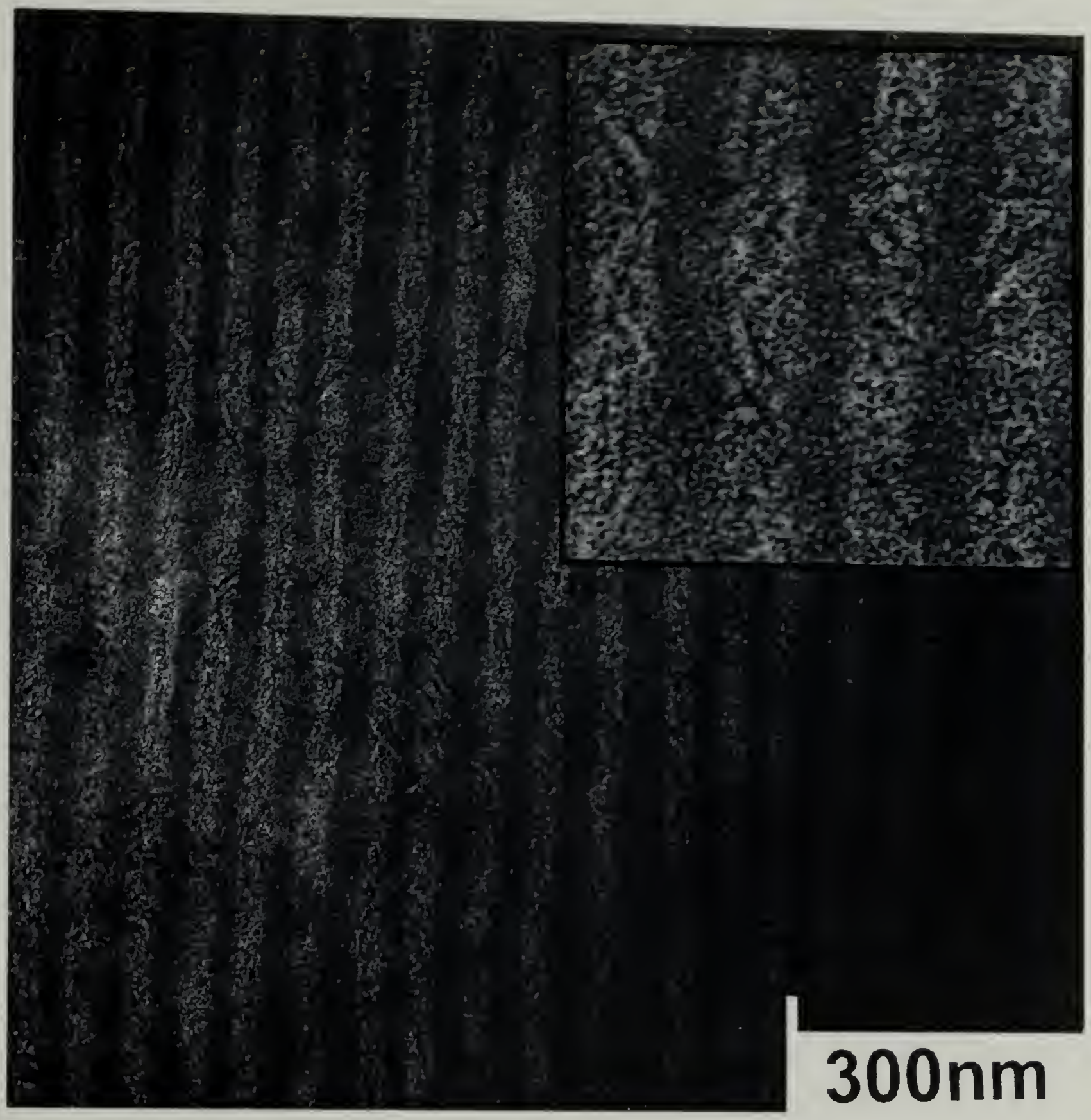

Figure 2.4: TEM micrograph of PE-*b*-aPP diblock copolymer quenched in liquid nitrogen from melt state.

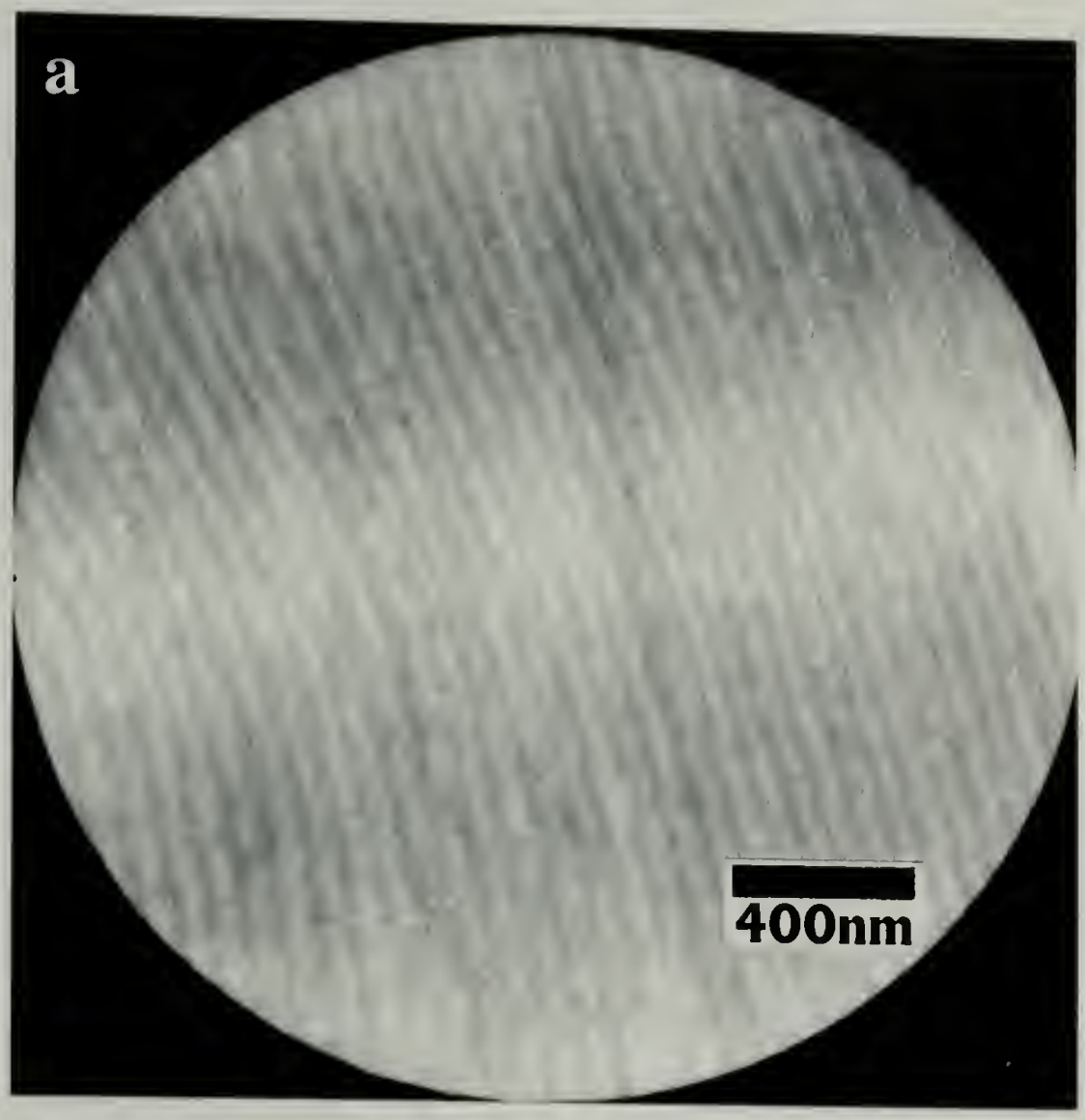

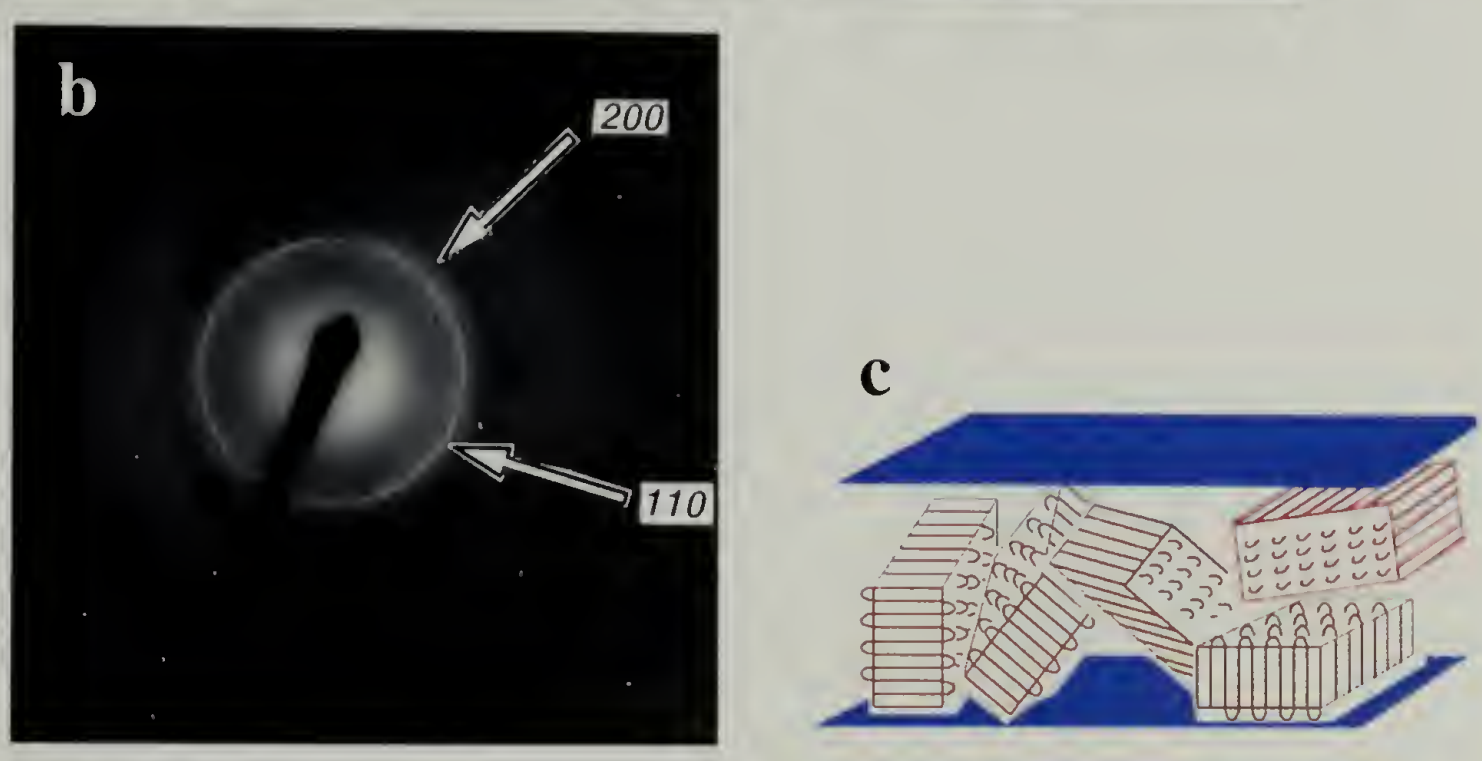

Figure 2.5: PE crystalline orientation inside microdomain for quenched samples.

a) TEM Micrograph inside the selected area aperture

b) Electron diffraction pattern

c) Schematic of PE crystalline chain orientation

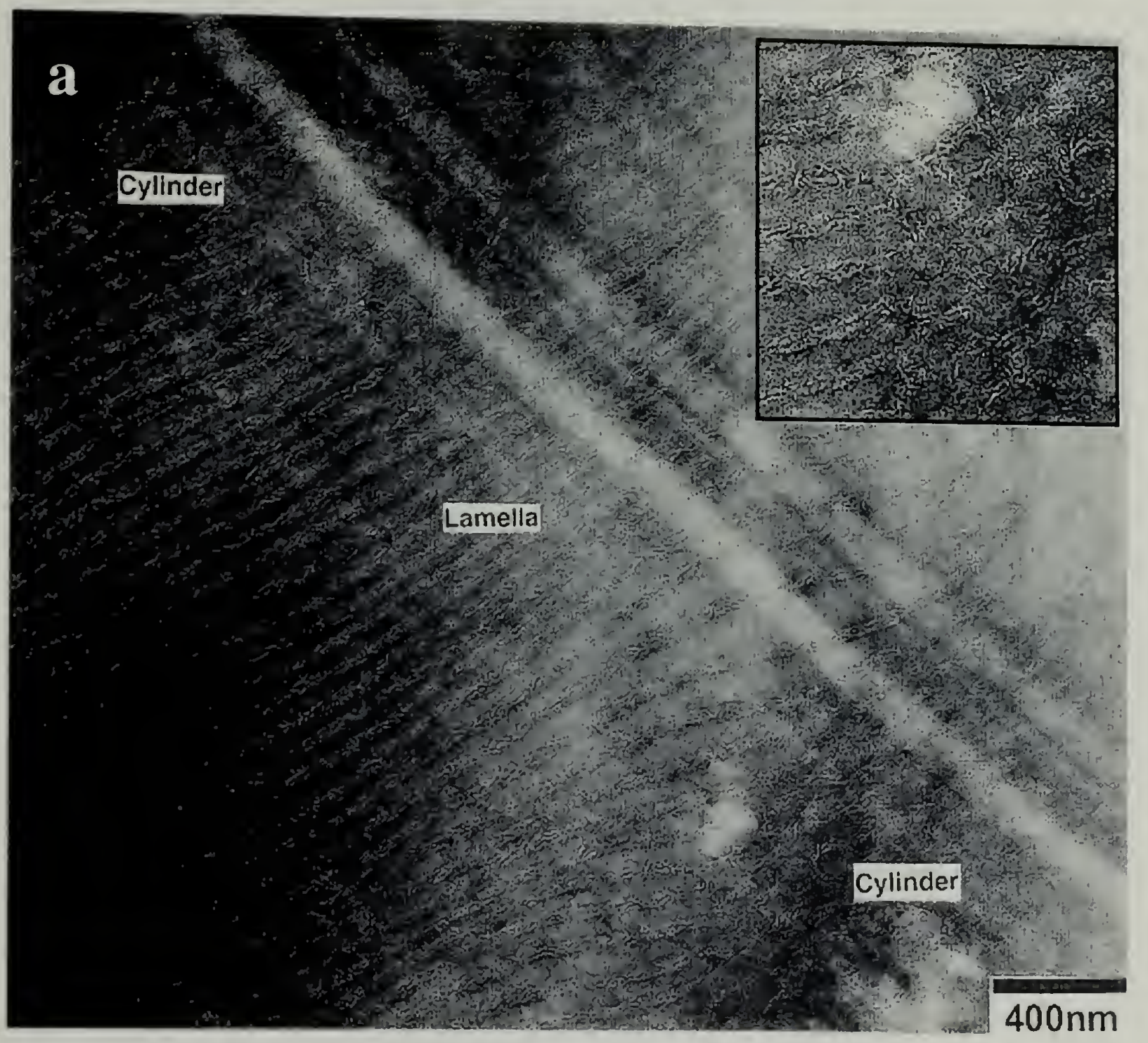

Figure 2.6: TEM micrograph of PE-b-aPP / PE blends. Sample was quenched from melt state. a) Microtoming direction parallel to x- axis; b) Microtoming direction parallel to y- axis

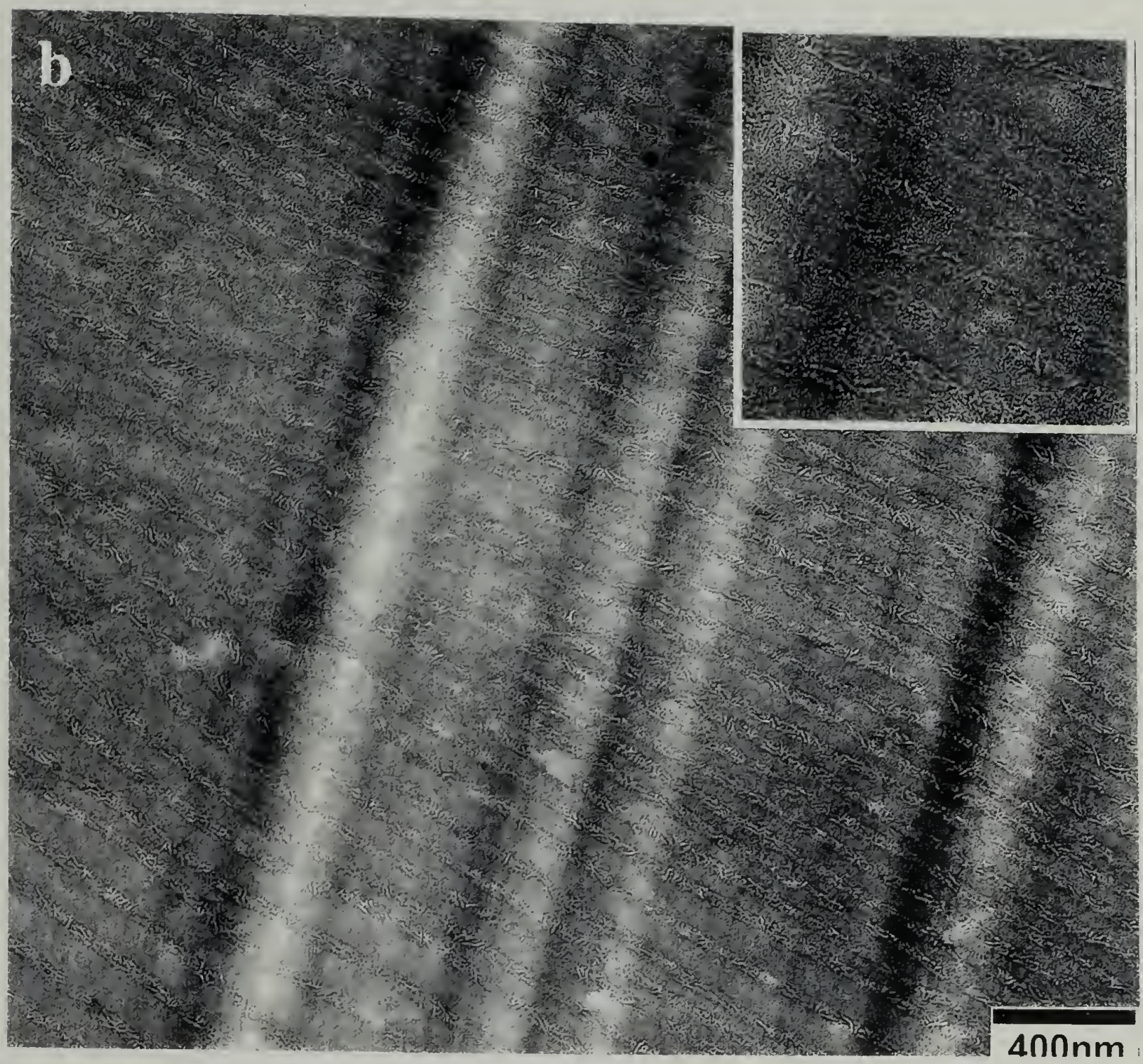
b
400nm

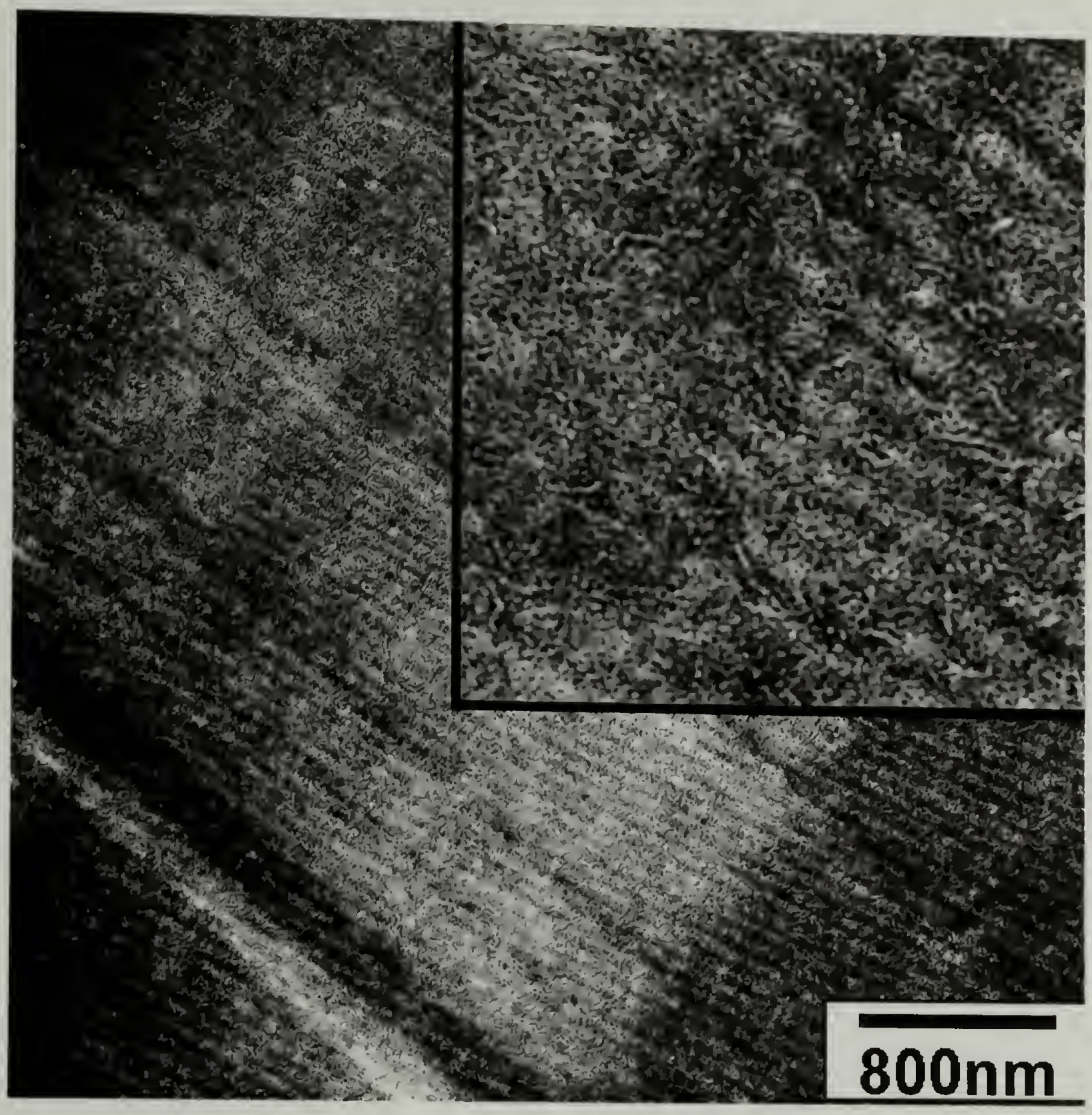

Figure 2.7: TEM micrograph for PE-*b*-aPP diblock copolymers crystallized at 50°C.

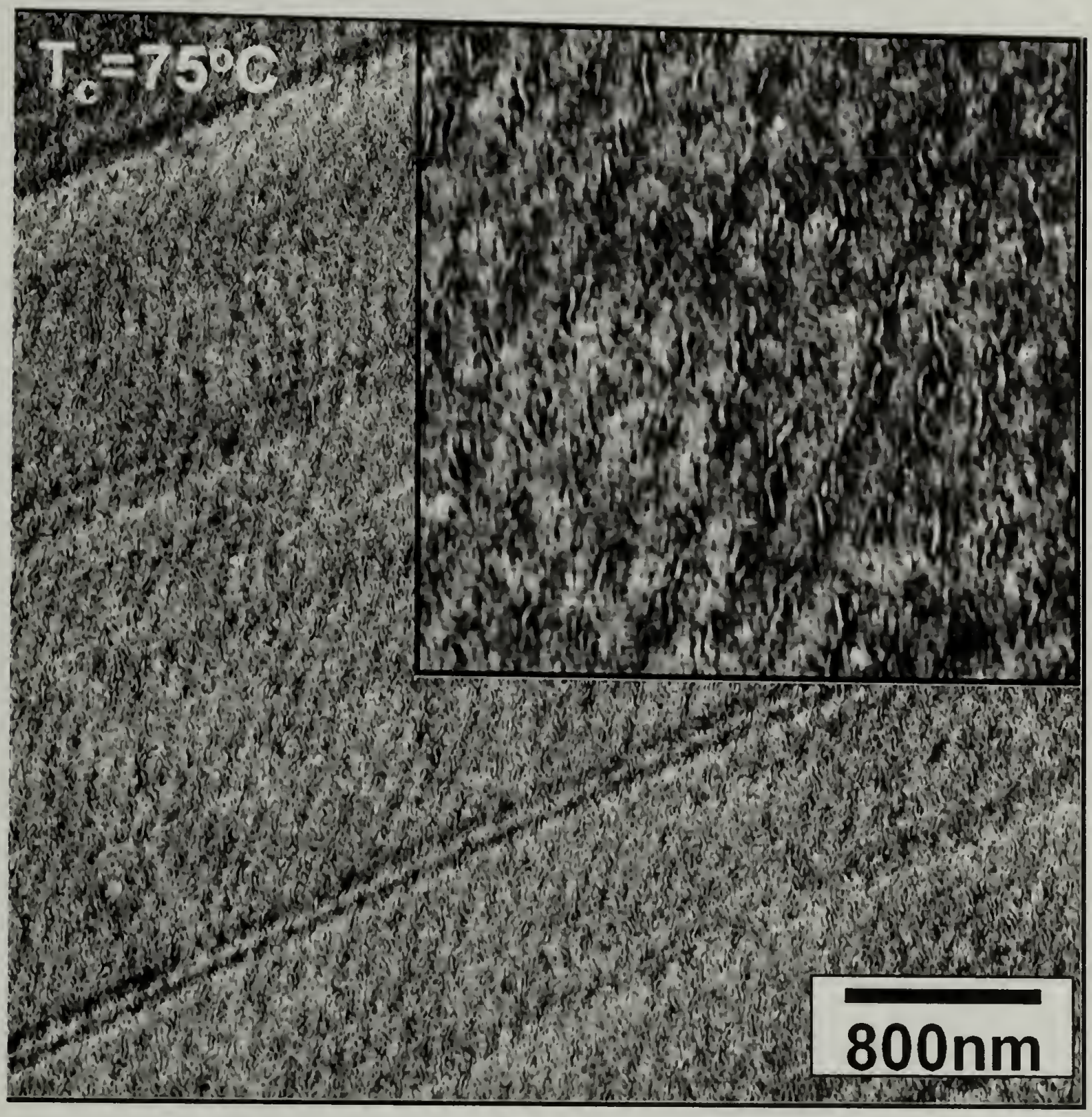

Figure 2.8: TEM micrograph for PE-*b*-aPP diblock copolymers crystallized at 75°C.

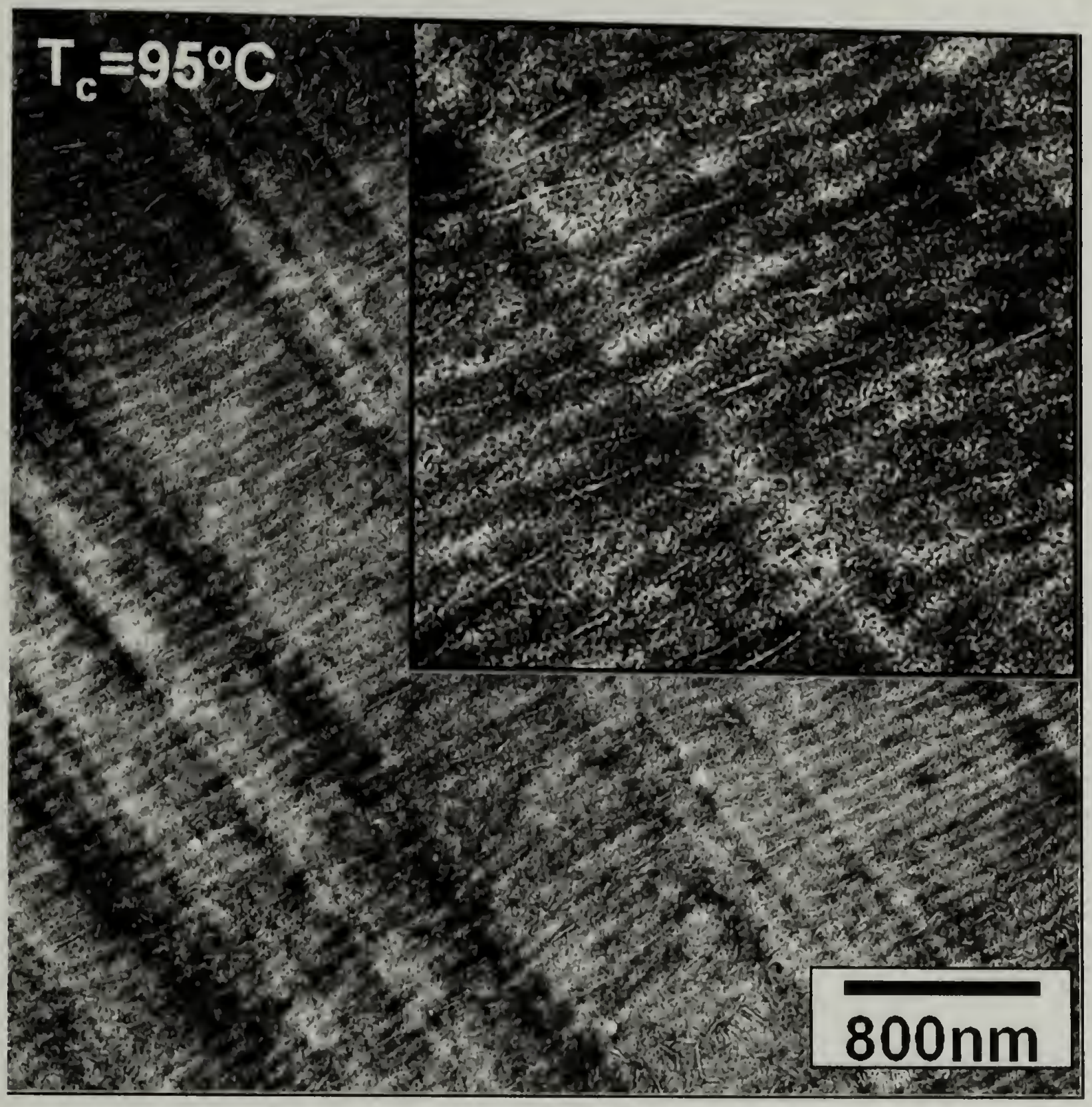

Figure 2.9: TEM micrograph for PE-*b*-aPP diblock copolymers crystallized at 95°C.

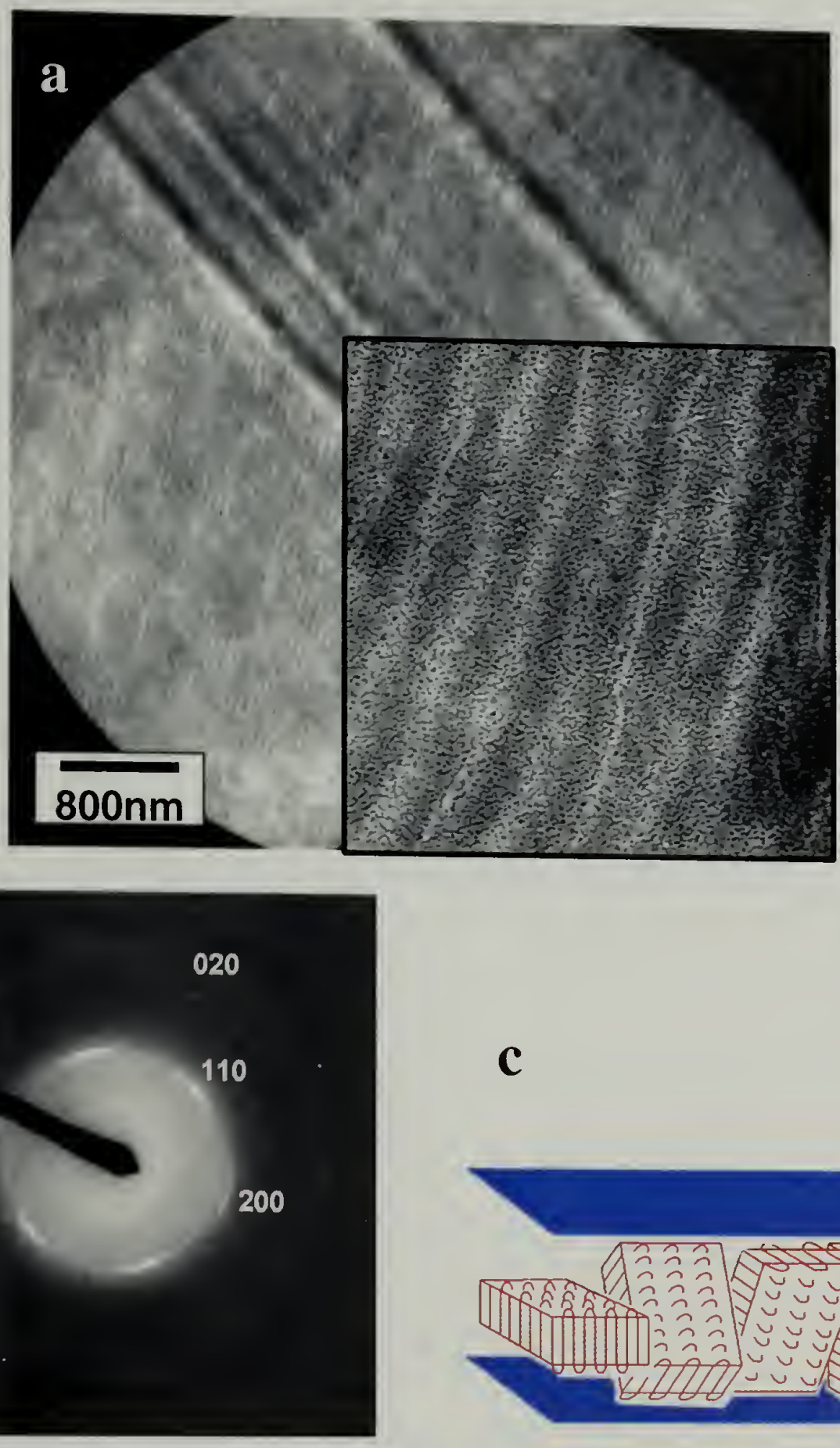

Figure 2.10: PE crystalline orientation inside microdomain for samples crystallized at 95°C. a) TEM Micrograph inside the selected area aperture; b) Electron diffraction pattern; c) Schematic of PE crystalline chain orientation.

a:

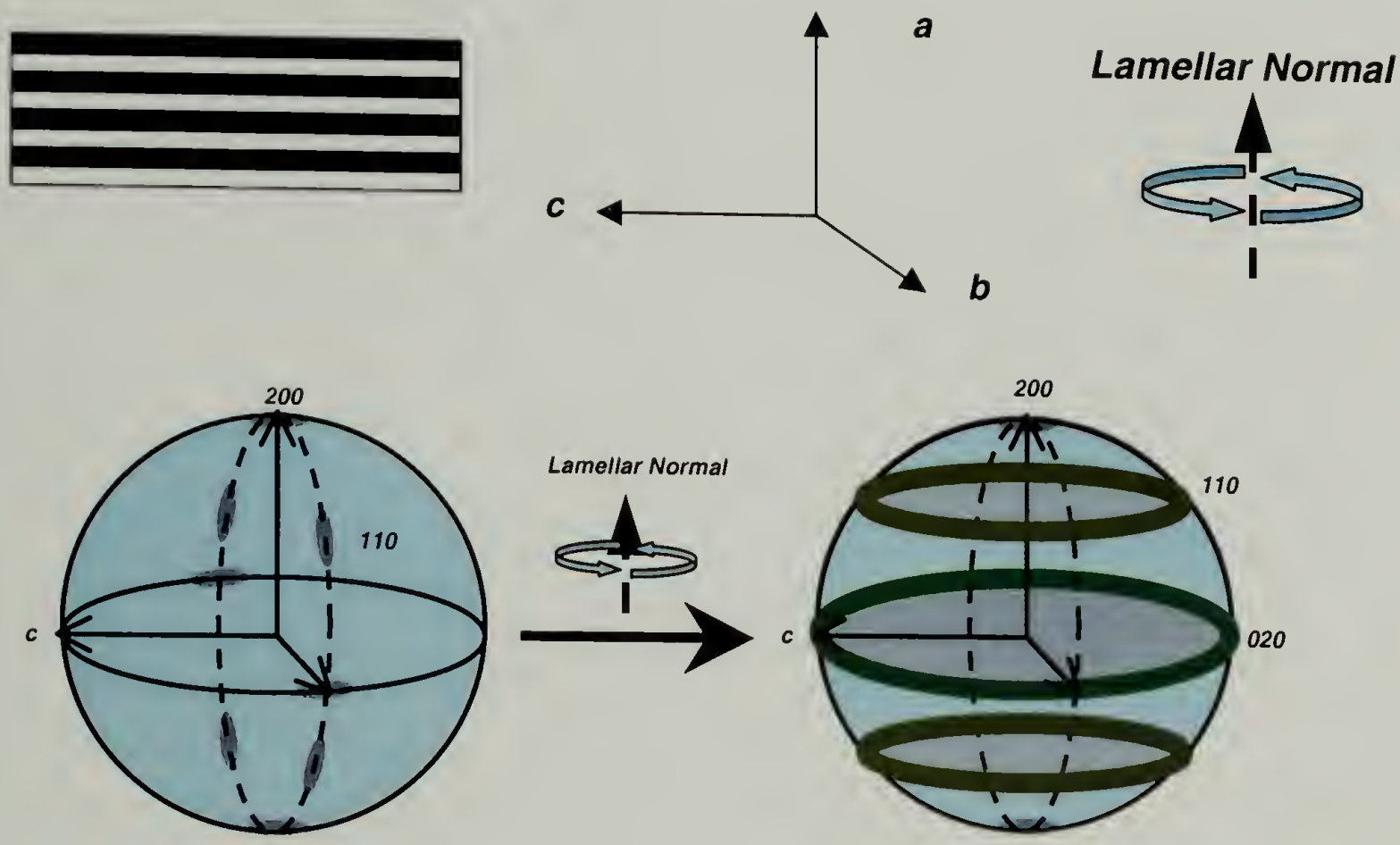

Figure 2.11: X-ray pole figure analysis of PE orientation. a) c- axis oriented parallel to the microdomain interface; b) b- axis oriented parallel to the microdomain interface with free rotation along b- axis (spherodisk orientation)

b:

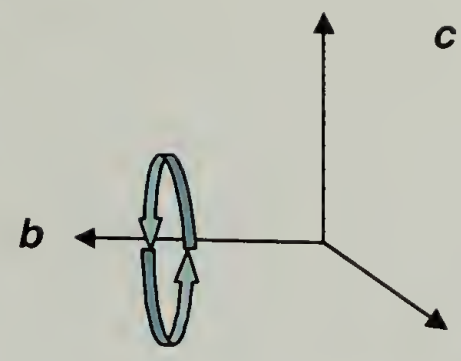
c
b
a

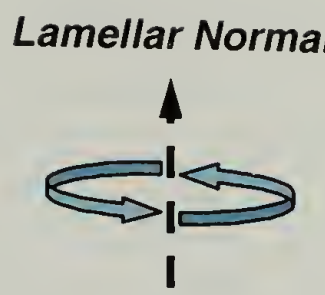
Lamellar Normal

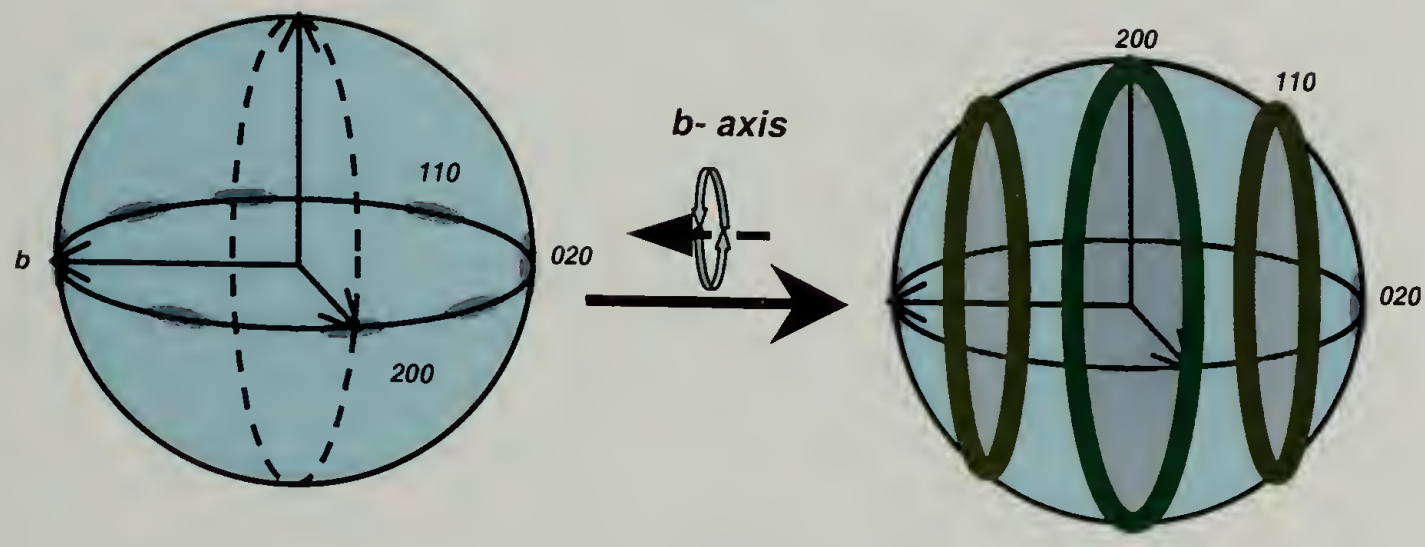
b
110
020
200
b- axis
200
110
020

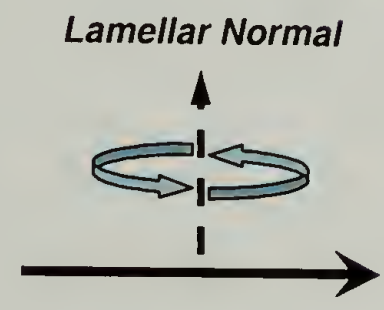
Lamellar Normal


110
higher intensity
200
higher intensity
020

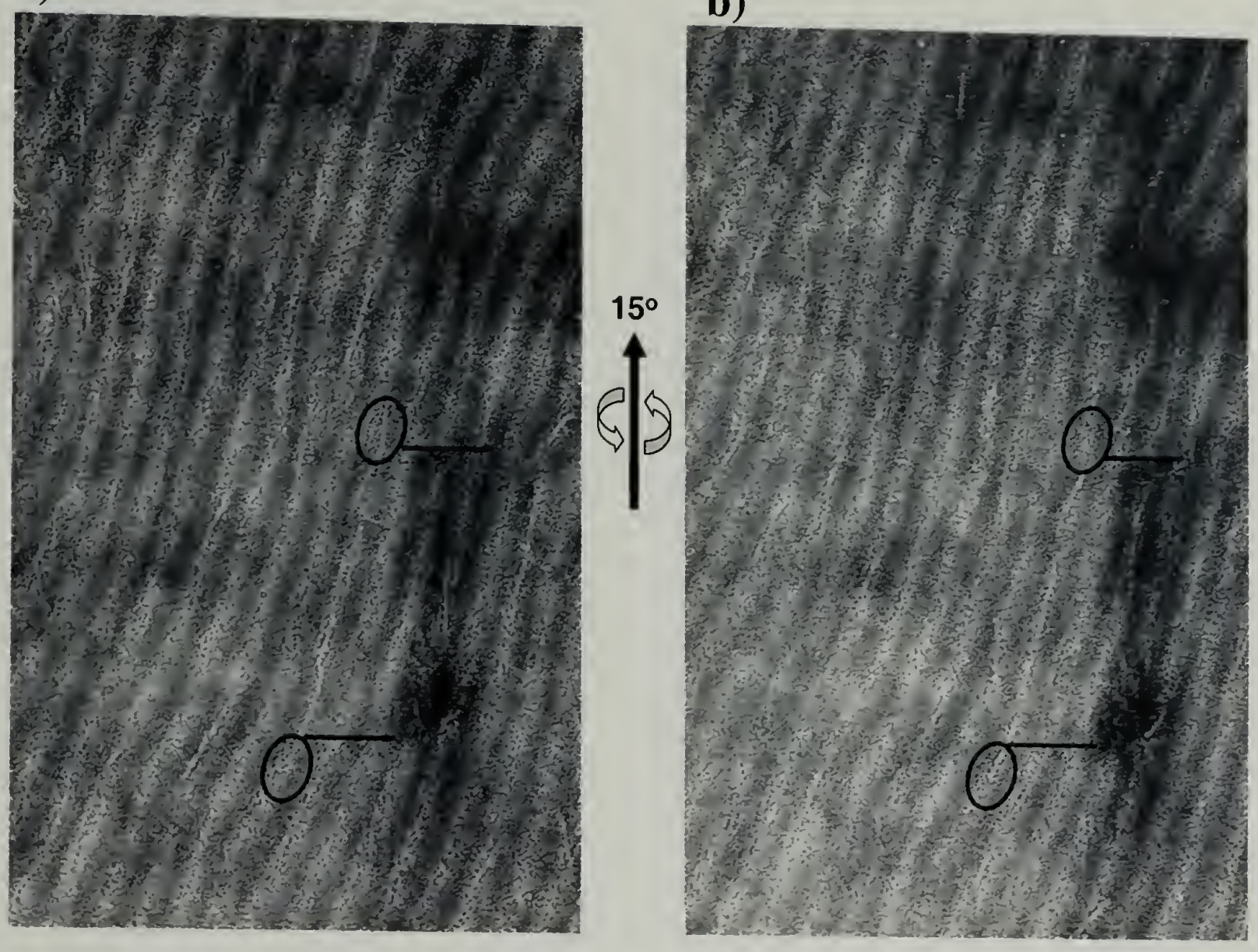

Figure 2.12: TEM micrographs of PE-b-aPP crystallized at 90°C at different tilt angles.

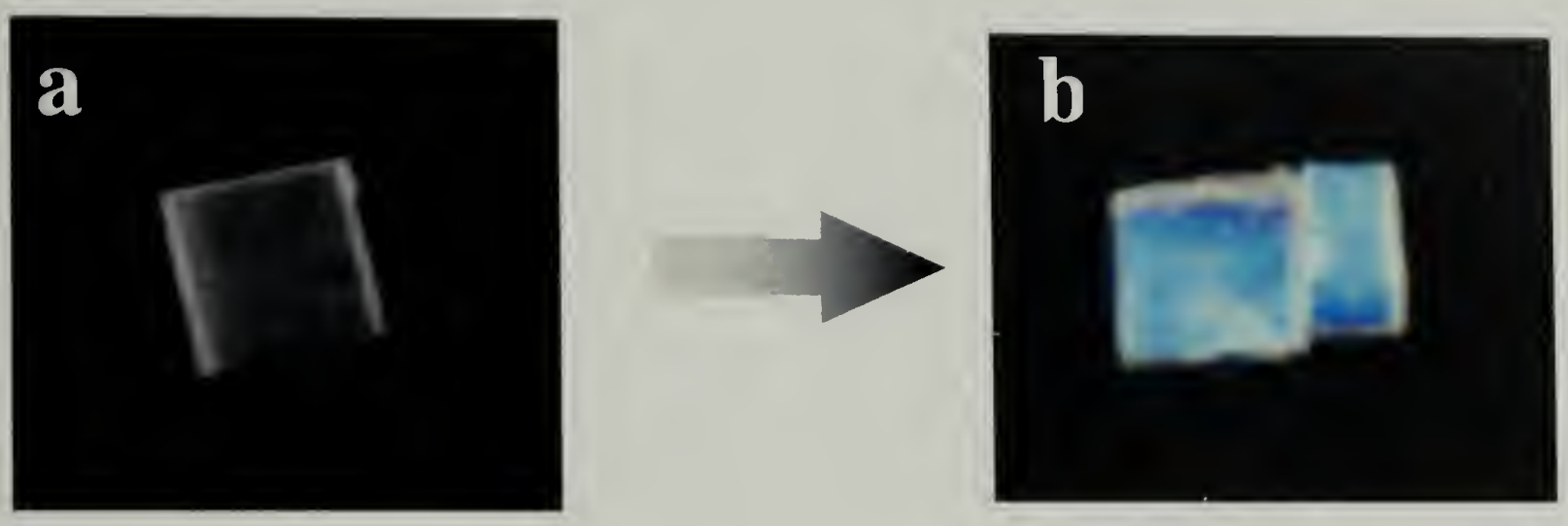

Figure 2.13: Photonic band gap crystal formed by swelling PE-b-aPP diblock copolymers.

a) Shear aligned PE-b-aPP diblock copolymer

b) After swollen by low molecular weight aliphatic oil

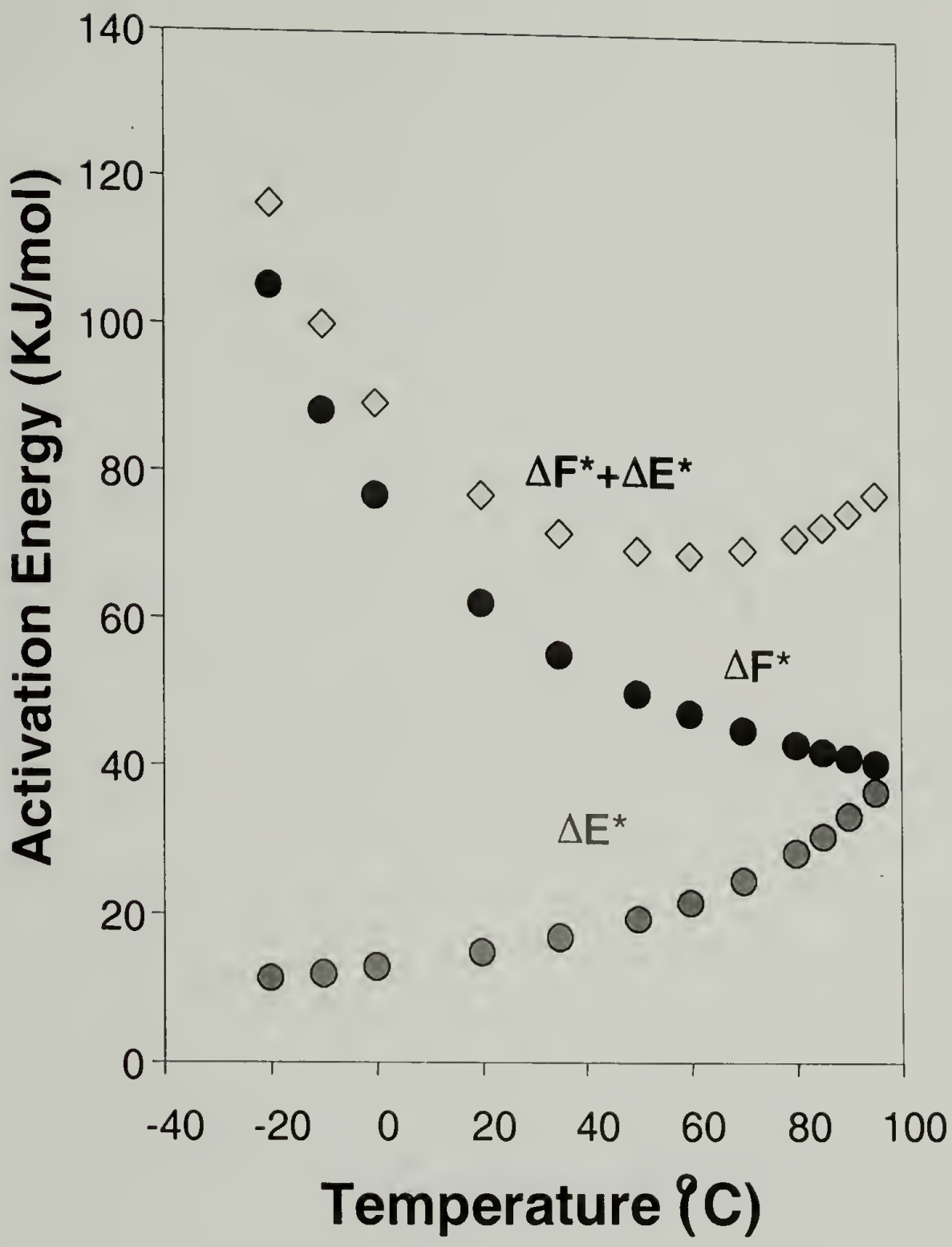

Figure 2.14: Plot of activation energy vs. crystallization temperature for PE-*b*-aPP diblock copolymers.

CHAPTER 3

MORPHOLOGY OF POLY(ETHYLENE OXIDE) CONTAINING CRYSTALLINE-AMORPHOUS BLOCK COPOLYMERS AND ITS BLENDS WITH HOMOPOLYMERS

3.1 Abstract

The bulk morphology of a crystalline / amorphous diblock copolymer under different thermal conditions was studied. The diblock copolymer, poly(ethylene oxide)-*b*-1,4 polybutadiene), forms a microphase separated lamellar morphology in the molten state. For samples crystallized within the range of 20°C to 50°C, TEM coupled with electron diffraction revealed a microphase separated, alternating lamellar morphology with the PEO crystalline chains oriented perpendicular to the interface between the PEO and PBD domains. A significant increase in the microphase separated, lamellar domain spacing was observed upon crystallization. On the length scale of tens of microns, as probed by polarizing optical microscopy, a non-spherulitic crystalline texture (with the absence of the Maltese-cross), corresponding to the microphase separated lamellar grain morphology, was observed. In contrast to the integral chain folding observed in PEO homopolymer, the increase in PEO lamellar thickness with decreasing undercooling is continuous in the block copolymer. In addition, the equilibrium melting temperature and lamellar spacing were determined.

3.2 Introduction

The morphology of a crystalline/amorphous diblock copolymer poly(ethylene oxide)-*b*-poly(1,4-butadiene) P(EO-*b*-BD) was investigated. Theoretical predictions concerning the morphology of crystalline/amorphous block copolymers have been developed by DiMarzio and coworkers[2], Whitmore and Noolandi[3], and Vilgis and Halperin[4] assuming that a thermodynamic equilibrium state can be achieved. The model, shown in Figure 1.1, assumes a structure of alternating crystalline and amorphous layers. In the crystalline layers there is regular chain folding with the chain stems oriented perpendicular to the interface with the amorphous domains.

Experimental results,[6,7,9-11,14,17,18,22,25,30,32,33,37,38,72,99,100] however, indicated significant deviation from the theoretical model. The morphology of diblock copolymers containing crystallizable blocks was found to be significantly influenced by the crystallization conditions. Depending upon the thermal history and the material properties, either a spherulitic morphology dominated by crystallization or a block copolymer morphology confining the crystalline block into nano scale domains can be formed.[6,17,25] The morphology was thus heavily influenced by kinetics, similar to the case of semi-crystalline homopolymers. The parameters controlling the kinetics of the system and thus the morphology formed include the glass transition temperature of the amorphous block, the block copolymer order-disorder transition temperature and the crystallization temperature.[17,25,37]

For many of the previously studied systems, the domain spacing of lamellar diblock copolymers due to microphase separation is larger than the thickness of chain folded

crystallites which grow inside the microphase separated layers.[6,9,17,25,100] Therefore, constraints of the pre-existing microphase-separated morphology do not limit chain folded crystallite thickness and have only a modest effect on crystallite orientation.

On the other hand, the poly((ethylene oxide)-*b*-butadiene) (P(EO-*b*-BD)) diblock copolymers studied in this report have a smaller lamellar domain size in the microphase separated amorphous state than the crystalline lamellar long period of PEO homopolymers with similar molecular weight. In addition, it is well know that low molecular weight PEO homopolymer crystals have a characteristic preference for integral chain-folding.[48,57,64] In our previous work,[101,102] we studied the morphological evolution and the influence of dimensional constraint on lamellar domain spacing in thin films of the same P(EO-*b*-BD) material and found, *via* atomic force microscopy (AFM) and interference optical microscopy, a gradual increase of the melting temperatures and domain spacing with decreasing degree of undercooling. Similar results on P(EO-*b*-hydrogenated 1,2-butadiene) diblock thin films have been reported by Reiter and coworkers.[103] Our thin film results differed from normal low molecular weight PEO crystallization where changes of T_m and crystal long period occurred in discrete steps due to the preference for integral chain folding. Here the study of the effects of microphase separated confinement upon PEO block crystallization is extended to bulk morphologies of the P(EO-*b*-BD) system.

3.3 Experimental

P(EO-*b*-BD) was obtained from Polymer Source Inc. It was synthesized via sequential anionic polymerization where polybutadiene (PBD) was polymerized first in

cyclohexane. The PBD block has about 69% 1,4 *trans* structure, 25% 1,4 *cis* and about 6% 1,2 structure. The molecular weights and molecular weight distributions of PBD and diblock copolymer were characterized by GPC calibrated with PBD standards. The molecular weight for the PBD block was 5,000 g/mol. The molecular weight for the PEO block was calculated from ^{1}H NMR based on the mole ratio of PBD and PEO blocks and was found to be 5,600 g/mol. The polydispersity of the diblock copolymer was 1.04. The χN of our system at 80°C was estimated to be about 70, indicating a relatively strong degree of segregation in the melt state. The density of PBD is 0.94 g/mol,[104] and the densities of crystalline and amorphous PEO are 1.13 and 1.03 g/mol respectively.[104] These densities allow the calculation of a PEO volume fraction of 51% in the melt state, and 48% when crystallized to the degree (88%) indicated by DSC results. The thermal stability of P(EO-*b*-BD) was examined by thermogravimetric analysis (TGA). The sample was held at 150°C in air for one hour, and no weight loss was observed. GPC results on the material used in this TGA experiment indicated a slight increase of polydispersity to 1.13. The experiments reported here did not expose the sample to temperatures greater than 90°C and generally protected the sample from exposure to air. Thus the copolymer is thermally stable under current experimental conditions without noticeable degradation. To avoid absorption of moisture by PEO, samples were dried under vacuum at 50°C prior to use and all the samples were stored under vacuum.

The diblock copolymer was dissolved in toluene and solution cast for a period of one week to produce films approximately 1 mm thick. The samples were annealed in a vacuum oven for 2 days, at 90°C, and then subjected to different thermal treatments in a DSC instrument. Differential thermal analyses were carried out in a Perkin Elmer DSC-

7 equipped with liquid nitrogen cooling. Isothermal crystallization experiments were conducted by heating the sample up to 80°C and then quickly quenching to the desired crystallization temperature at the maximum speed (-150°C / min) that can be achieved by the instrument. For experiments using self-seeding methods, the procedures were similar to those described by Kovacs *et al.*[48] The quantity of the diblock copolymer used in each DSC measurement was 0.8 mg or less. The instrument was calibrated with indium(T_m = 156.6°C) and eicosane(T_m = 36.44°C) at the experimental heating rate of 1.0°C/min on a daily bases. The reproducibility of the melting temperature measured by DSC for identical runs on the same sample was found to be better than 0.1°C, while for different samples it is better than 0.2°C.

SAXS data were collected at the Advanced Polymers Beamline (X27C), located at the National Synchrotron Light Source at Brookhaven National Labs (BNL), Upton, NY. Two-dimensional scattering patterns were collected on Fujitsu image plates, then read by a Fujitsu BAS 2000 image plate reader. Custom software at BNL was used to subtract background noise and perform circular averaging. Data were collected for a wavelength of 1.307 Å and a camera length of 1510 mm. SAXS measurements of long periods of samples crystallized at various temperatures were all conducted at room temperature (25°C). The difference in domain spacing between the crystallization temperature and the lower temperature at which SAXS was run, due to changes in amorphous domain chain conformations, will be very slight.

Samples for optical microscopy were prepared by evaporating 7% toluene solutions of the block copolymer onto a glass cover-slide, yielding films approximately 10-100μm

thick. Experiments were conducted using an Olympus BX60F3 optical microscope under cross-polar conditions. Two Mettler FP80 hot stages were used. Samples were held in the melt at 80°C on one stage and then rapidly transferred to the second stage which was preset to the desired crystallization temperature.

TEM and electron diffraction experiments were conducted on a JEOL 2000 FX-II instrument. The diffraction camera length was calibrated by using an internal gold standard on some of the grids observed. To prepare specimens for TEM, a small piece of copolymer sample was microtomed using a Leica Ultracut Cryomicrotome with a diamond knife at −110°C to obtain ultra thin (about 40nm) sections. No solvent or water was used in microtoming and collecting the specimen in order to minimize moisture absorption by the PEO. The thin sections were stained by OsO_4 and observed under TEM. While OsO_4 stains both PBD and PEO, it stains PBD more heavily due to the lack of crystallinity and the presence of unsaturation. Due to the possibility that OsO_4 may disrupt the crystallinity of the PEO block, electron diffraction experiments were conducted on unstained specimens.

3.4 Results

3.4.1 TEM and Electron Microscopy Study

Figure 3.1 and Figure 3.2 shows TEM micrographs of P(EO-*b*-BD) block copolymer that was annealed in the melt at 90°C and then crystallized at 30°C. The darker regions are PBD domains that were preferentially stained with OsO_4, while the lighter regions are crystalline PEO domains. It is obvious that the diblock copolymer adopts an alternating lamellar morphology with PEO crystals confined between

amorphous PBD layers. WAXS results (not shown) indicated that the PEO in the diblock copolymer had the same monoclinic crystalline structure as formed by PEO homopolymer. As shown in Figure 3.1, the sample has good long-range order. However, as shown in Figure 3.2, it does display typical block copolymer grain structures,[105,106] suggesting that PEO crystallization occurs within the confinement provided by the pre-existing microphase separated morphology.

The orientation of the PEO crystallites inside the nano-scale domains is determined by TEM and electron diffraction. Figure 3.3a is an indexed electron diffraction pattern of P(EO-*b*-BD), taken from the region inside the selected area aperture, shown in Figure 3.3b. The results shown here are from a sample crystallized at 34°C. However, similar behavior was observed for all samples within the temperature range examined (20-50°C). In order to avoid damage to the crystalline structure due to staining, the samples for electron diffraction were not stained. Consequently, the image contrast in Figure 3.3b is from diffraction contrast and mass thickness contrast arising from the density difference between the crystalline PEO and the amorphous PBD. This contrast is opposite to that of the stained specimens, *i.e.* dark regions are now PEO domains while the bright regions are PBD domains. Overall, the contrast is much weaker than in the stained samples and disappears within seconds of electron beam exposure. From Figure 3.3b, the lamellae inside the selected area aperture are observed to all be oriented in approximately the same direction. The diffraction arising from this area (Figure 3.3a) indicates uniaxial orientation of crystallites with the PEO chain axis perpendicular to the microphase separated lamellar domains. The *120* reflections are oriented parallel to the lamellar layers in the image, indicating that the *[001]* crystallographic direction which is also the

chain axis is perpendicular to the layers. The three, labeled reflections do not exist in a single planar section through the reciprocal lattice. These reflections intersect the Ewald sphere at the spacings and geometry shown if the PEO reciprocal lattice is rotated around the *[001]* direction, indicating that the material possesses a fiber-like polycrystalline texture. Generally, the structure of the P(EO-*b*-BD) diblock is similar to that illustrated in Figure 1.1.

In thin film study, as will be discussed in Chapter 5, we observed perfect three dimensional crystallographic registry between adjacent lamellar layers of P(EO-*b*-BD) block copolymers in thin films containing about 6 or 7 lamellar repeats.[101,102] Our results for bulk samples indicate only uniaxial alignment of the chain axis normal to the lamellar domains but with rotational disorder of the PEO crystallites around this chain axis direction. The TEM micrographs in Figure 3.3b show that the orientation of the microphase separated lamellae is not perfect. The selected area aperture is about 2.5μm in diameter and thus the diffraction pattern is collected over a range of lamellar orientations, resulting in the arcing of the reflections observed in Figure 3.3a. The fact that we are also collecting diffraction data over more than 100 lamellar repeats makes it much less likely that any more highly aligned relationships between adjacent crystalline PEO layers will be detected in the bulk even if such alignments do exist locally within the sample.

3.4.2 Block Copolymer Crystalline Super Structures

To investigate the crystalline morphology of P(EO-*b*-BD) on the length scale of tens and hundreds of microns, sample films were studied by optical microscopy under cross-polar conditions, as shown in Figure 3.4. The sample was first melted at 80°C and

then crystallized isothermally at various temperatures. Figure 3.4a was taken while the crystallites were still growing at 45°C. The dark regions correspond to block copolymer in the molten state. The textured bright region contains crystalline PEO and appears to grow from a nucleus located at the center. The lack of any observable texture in the molten region is due to a lack of contrast between PBD and amorphous PEO blocks. Crystallization of PEO in P(EO-*b*-BD) increases the refractive index of the PEO domains and consequently changes the birefringence of the system so that the underlying block copolymer morphology can be seen. Figure 3.4b shows an enlargement of the texture in the crystalline region, which is due to the grain structures of the microphase separated block copolymers. Optical images with the same essential features have been reported by Balsara and coworkers[107] in fully amorphous poly(isoprene-*b*-styrene) diblock copolymers.

The bright regions in Figure 3.4 are grains whose optical axes are oriented at approximately ±45° to the polarizers. These images indicate that the size of the grains of the microphase separated block copolymer morphology is about 5 to 20 μm. Figure 3.4a indicates that the region of PEO crystallization originating from a single nucleus can be 500μm or larger in diameter. Thus the growth of crystallites is found to propagate across grain boundaries and to encompass many differently oriented grains. This is possible due to the grain boundary morphologies in microphase separated lamellar systems which provide for continuity of domain structure across the boundaries.[105,106,108-110]

The crystalline region in Figure 3.4 does not show the characteristic Maltese cross, typical of spherulitic textures, such as those formed by PEO homopolymer. Similar lack

of the Maltese cross pattern has been previously reported by Wittmann *et al.* in the study of poly(ethylene oxide-*b*-styrene) (P(EO-*b*-S)) block copolymers,[31] where it was termed *pseudomorphosis*. Psudomorphosis is a term originally meant to describe crystallization confined within a pre-existing liquid crystalline texture.[111] We conducted similar optical microscopy studies on P(EO-*b*-BD) samples crystallized at temperatures ranging from 20°C to 50°C. The effect of crystallization temperature on block copolymer grain structure is beyond the scope of the current paper, but the results observed at all temperatures were qualitatively similar to those reported here.

3.4.3 Effect of Crystallization on Lamellar Grain Size

For crystalline homopolymer, crystallization at different temperature can yield different crystalline super structures.[112] The crystallization temperature has a profound effect on the crystalline morphology and spherulite size and shape. In the case of P(EO-*b*-BD) crystalline / amorphous block copolymers, as mentioned in the previous section, crystalline super structure is significantly influenced by the microphase separated morphology formed in the melt state. However, it is also observed in this study that different crystallization temperature can result in variations in the morphology.

Shown in Figure 3.5 is the optical micrograph of P(EO-*b*-BD) diblock copolymers crystallized at 30°C and 50°C respectively. Both samples were solution cast onto glass slide followed by annealing at 90°C and then crystallization at different temperatures. The sample crystallized at 50°C has a much larger grain size than the sample crystallized at 30°C. This observation can be more clearly seen in the micrographs in Figure 3.6. The sample shown in Figure 3.6a was at first crystallized at 50°C followed by a temperature jump and remaining part of the sample was then crystallized at 30°C. The lamellar grain

size difference between the two crystallization temperatures can be clearly observed. The sample shown in Figure 3.6a was then melted at 90°C and re-crystallized at 30°C. The resulting morphology is shown in Figure 3.6b, which appears almost identical as Figure 3.6a.

3.4.4 Crystallization of PEO in P(EO-b-BD) Block copolymers

The crystallization characteristics of PEO in the block copolymer were investigated by DSC and SAXS. Results including T_m, ΔH, and domain spacing l of the samples crystallized at various temperatures (T_c) are summarized in Table 3.1. Figure 3.8 shows the DSC heating curves for the P(EO-*b*-BD) block copolymer crystallized isothermally between 30°C and 50°C. The DSC heating rate was 1°C/min. Crystallization temperatures of 52°C or higher do not produce observable crystallinity even after an extended period of time and with the use of self-seeding methods. ΔH was found to be essentially independent of T_c. Using the heat of fusion for an infinite, perfect PEO crystal (ΔH_f^o) obtained by Buckley and Kovacs[65] via extrapolation of experimental results on PEO homopolymer (188.9 J/g) the degree of crystallinity of PEO in P(EO-*b*-BD) was about 88%.

For isothermal crystallization below 44°C, the subsequent heating curves (Figure 3.8) show two melting endotherms. The first peak has an onset temperature at 52.2°C while the onset temperature of the second peak is at 54°C. The position of the second melting endotherm does not change noticeably as the crystallization temperatures vary from 34°C-42°C. This indicates that this higher temperature endotherm may correspond to a population of integrally folded crystallites. Figure 3.10 shows a series of heating

curves for samples all crystallized at 34°C but subject to different heating rates in the DSC. As the heating rate increases the ratio of the first peak to the second peak increases dramatically. Therefore it can be concluded that these higher melting crystallites were not formed during the initial crystallization process. Instead they result from thickening of the existing crystallites during heating in the DSC. At higher heating rates, there is less time for crystallite thickening, and the area under the higher melting peak decreases. With decreasing degree of undercooling, as shown in Figure 3.8, the intensity of the second melting peak decreased indicating less crystallite thickening.

Figure 3.9 shows SAXS data for the block copolymer in the molten and crystalline states. The samples were prepared in the DSC instrument at different isothermal crystallization temperatures. The lamellar long period in the melt at 80°C is 16.4nm. Figure 3.11 is a plot of experimentally measured P(EO-*b*-BD) lamellar repeat spacings (l) as a function of temperature (T) in the molten state. From the plot, l was found to scales as $T^{-0.35}$, which agrees closely with the theoretically predicted[1] scaling of $T^{-1/3}$. Taking this temperature effect into consideration, a hypothetical P(EO-*b*-BD) sample in the molten state at 34°C would have a domain spacing of 17.2 nm. The crystallization of the PEO blocks results in an increase in lamellar long period of about 4 nm over the lamellar spacing of the hypothetical amorphous system at 34°C. In the lamellar morphology, the thickness of the PEO crystalline lamellae can be calculated by multiplying the long period by the PEO volume fraction. The volume fraction of crystalline PEO in the block copolymer, considering 88% weight percent crystallinity, is about 48%. Therefore, the calculated PEO crystalline lamellar fold length, when crystallized at 34°C, is about 10.5nm. PEO homopolymer is known to crystallize in a 7_2 helical structure with a chain

axis repeat distance of 1.95 nm,[104] corresponding to 0.28 nm per monomer unit. Thus the fully extended, crystalline chain length of our 5600 g/mol PEO blocks is about 35.6 nm. Consequently, the PEO blocks crystallized at 34°C are folded to produce at least three chain stems per molecule.

For T_c higher than 46°C, a small shoulder appeared at higher T_m in the DSC melting curves shown in Figure 3.8. The SAXS data in Figure 3.9 shows a corresponding lower q shoulder on the Bragg peaks indicating a presence of a minority population of thicker crystallites in the samples crystallized at 46, 48, and 50°C. Both the T_m and the size of the crystals corresponding to these small shoulders increased with increasing T_c. This suggests another population of non-integral folded crystallites but with a slightly larger fold length. This phenomenon has been previously reported by Cheng and coworkers,[56] where it was suggested that it might be related to fluctuations in the fold length of the initial nuclei.

3.4.5 Morphology and Crystallization of P(EO-b-BD) / homopolymer blends

3.4.5.1 Block copolymer blends with polybutadiene homopolymers

To investigate the morphology and crystallization of PEO in block copolymer / homopolymer blends, blends with different PBD volume fraction were prepared.

The morphology of block copolymer / homo-polybutadiene will be discussed first. Shown in Figure 3.12 is the SAXS profile for blends with 58% PBD volume fraction but with different PBD homopolymer molecular weight. For comparison, the SAXS profile for the pure diblock copolymer was also shown. All the samples were crystallized at

30°C from the melt state. By blending homopolymer into the system, the lamellar spacing showed an apparent increase from 21.5 nm to 24.5 nm. On the other hand, blends with different PBD homopolymer molecular weights showed similar the lamellar spacing.

If crystallized at different temperatures, the blends were also found to exhibit a crystallization temperature dependent lamellar spacing. Shown in Figure 3.13 are the SAXS scattering profiles for blends with PBD 5k with 58% PBD volume fraction. Similar to the case of pure diblock copolymers, a monotonic increase in lamellar spacing was observed. The thickness of the PEO crystalline lamellae could be obtained by multiplying the volume fraction of the PEO block with the overall lamellar long period. The results are summarized in Figure 3.14. As discussed previously, the block copolymers adopted morphology similar to the schematic shown in Figure 1.1. In the case of blends with PBD homopolymers, if the homopolymer is able to penetrate into the microphase separated domain interface, as possible with noncrystalline block copolymer / homopolymer blends, we should observe a decrease in PEO crystalline lamellar thickness. However, in the present case, by blending PBD homopolymers into the system, the PEO crystalline lamellar thickness was almost unchanged as shown in Figure 3.14. The results suggested that in the crystalline state the PBD homopolymers were mainly located at the center of the PBD domain. Consequently, they did not affect the PEO crystalline lamellar thickness. A schematic of the morphology is shown in Figure 3.15.

By blending more PBD homopolymers into the system, the morphology in the melt state transformed from lamellar morphology to cylindrical morphology. Shown in Figure 3.16 is a series of DSC cooling thermogram of blends with different PBD homopolymer concentration. Samples with 58% and 64% PBD volume fraction exhibited lamellar morphology in the melt state, while sample with 72% PBD volume fraction showed cylindrical morphology in the melt state. When the morphology in the melt was lamella, blending in PBD homopolymers only resulted in a small decrease of crystallization temperature (less than 20°C). On the other hand, when the overall PBD block volume fraction increased to 72%, the system showed a dramatic decrease of PEO crystallization temperature, almost 60°C if compared with pure diblock polymers.

Shown in Figure 3.17 is SAXS profiles of the sample with 72% PBD volume fraction. It formed cylindrical morphology in the melt state as can be determined from the higher order reflections. Crystallization proceeded with a slight increase of first order scattering peak and decrease in intensity of higher order peaks. The resulting morphology might be a distorted cylinder. TEM study on this sample was unsuccessful because the sample contained significant amount of low molecular weight PBD homopolymers. It was basically a fluid at room temperature and was very difficult to maintain its shape as 40nm film on the grid.

3.4.5.2 Block copolymer blends with poly(ethylene oxide) homopolymers

Shown in Figure 3.18 are SAXS scattering profile for several blends with different PEO homopolymer volume fractions and molecular weight. For blends with 58% PEO volume fraction, the sample showed lamellar morphology in the solid state. The results

were further confirmed by TEM microscopy (Figure 3.19), where alternating lamellar morphology was observed. Interestingly, if compared with the pure diblock copolymer, the overall lamellar long periods were almost unchanged. However, the relative intensity of higher order reflections varied indicating that PEO homopolymers were effectively blended in which changed the relative volume fraction of the two microdomains. The results suggested that the system might have morphology similar to the schematic shown in Figure 1.6.

By blending more PEO homopolymers into the system, the morphology in the melt will also transform from lamella to cylinder. However, as shown in Figure 3.18, the blends with 72% PEO homopolymer volume fraction showed lamellar morphology in the solid state, indicating that PEO crystallization disrupted the original morphology in the melt and formed lamellar morphology driven by crystallization.

Shown in Figure 3.20 are several DSC thermograms of blends. Figure 3.20a is the DSC thermogram of PEO homopolymer with 3000g/mol molecular weight. It showed one melting peak around 58°C, which did not vary much with different crystallization temperature. Figure 3.20b is the DSC thermogram of PEO 3k / block copolymer blends with 58% PEO volume fraction. The melting endotherms of the blends showed a similar pattern as the pure diblock copolymer. The melting endotherm at 58°C, which corresponds to PEO 3k homopolymers, could not be observed indicating the PEO homopolymers were effectively blended with the block copolymers. Figure 3.20c is the DSC thermogram of blends with 72% PEO volume fraction. The results showed clearly two melting endotherms corresponding to the PEO in block copolymer and PEO

homopolymers respectively. The results suggested that at this volume fraction, the miscibility between the PEO in the block copolymer and the PEO homopolymer decreased.

3.5 Discussion

3.5.1 Effect of Crystallization on the Melt Microphase Separated Morphology

TEM observation of block copolymer grain structure and the absence of spherulitic texture in optical micrographs indicate that crystallization occurs within the confinement imposed by the pre-existing microphase separated morphology. Due to the flexibility of the amorphous PBD block in P(EO-*b*-BD), thickening of the PEO domains can occur upon crystallization without major disruption of the microphase separated lamellar organization. This behavior is in contrast to that of poly(ethylene oxide-*b*-styrene)[37,72] or poly(ethylene-*b*-styrene)[6,8] block copolymers, where the rigid PS domain prohibits any dimensional change of the morphology during crystallization.

For P(EO-b-BD) block copolymers, crystallization at higher temperature was observed to have slower growth kinetics. In this study, it was also found that higher crystallization temperature could coarsen the size of the microphase separated grains. Shown in Figure 3.5a and Figure 3.5b are a comparison between the samples crystallized at 30°C and 50°C respectively. The textures in both micrographs corresponded to the grain structures of microphase separated block copolymer and they had the same essential features. However, comparing Figure 3.5a and Figure 3.5b, crystallization at higher temperature resulted in an enlargement of the microphase separated block copolymer grain sizes. This effect could be more clearly seen in Figure 3.6. Figure 3.6a is a sample

film where it was first crystallized at 50°C (left region) and then a temperature jump was performed and the remaining part of the film was then crystallized at 30°C (right region). The difference in the average size of the textures could be clearly observed from this micrograph. More interestingly, shown in Figure 3.6b is the same sample which was completely melted at 90°C for 5 minutes after treatment used in Figure 3.6a and then re-crystallized at 30°C. Figure 3.6b is essentially identical to Figure 3.6a. The textures that existed before melting the sample were maintained even after a different thermal treatment.

Crystallization represented a strong external force to disturb the microphase separated morphology and it preferred to form straight crystalline lamellae consistent with the overall crystallite growth direction rather than winding through the channels predefined by microphase separation. Crystallization at higher temperatures was accompanied by thickening of lamellar spacings, slower growth kinetics while at the same time faster molecular transport, all of which resulted in stronger force to disturb the microphase separated morphology. On the length scale of tens to hundreds of microns, block copolymer grains were known to have a liquid crystalline like texture where directors could change continuously in three dimensions. In cases, there might not be rigid grain boundaries between microphase separated lamellae with different orientations. As a result, there were many grains that were not at acute angle, but simple distinguished themselves by astute Ω or chevron boundaries, which might be destroyed by crystallization at high temperature and resulted in the apparent coarsening of the grain sizes. This increase in the average grain size is a result of a competition between crystallization and microphase segregation.

For P(EO-b-BD) block copolymers, melting of the crystalline PEO does not result in a disordered state but a microphase separated morphology. Consequently, any disturbance to the morphology occurred during crystallization will be carried over to the melt state after melting of the crystallites. Larger grains are thermodynamically more stable than smaller grains because of smaller concentration of grain boundary defects. Once the large grain was formed, the effect was "permanent" even after melting. Subsequent crystallization would again be restricted by the morphology that already existed in the melt state due to microphase separation. If crystallized at a lower temperature (30°C), which did not involve much change in the average grain size, the "original" texture before the melting should be observed. This effect was clearly observed in Figure 3.6b and indicated that the melt microphase separated morphology truly acted as a template for crystallization.

An interesting ramification from the above observation would be that if the same sample was repeatedly crystallized at 50°C and melted at 80°C, we should observe an enlargement of the average grain size even more significant than those shown in b. A result of such an experiment was shown in Figure 3.7, where the sample was repeatedly crystallized at 50°C for several times. An irreversible change in the block copolymer grain sizes was observed. This result further proved the above arguments.

TEM and electron diffraction indicate that the model shown in Figure 1.1 is fairly representative of the P(EO-*b*-BD) structure. The amorphous PBD blocks and crystalline PEO blocks share a common interfacial area per chain. Increasing the thickness of the

crystalline lamellae will decrease the area per diblock at the P(EO-*b*-BD) interface and thus will cause stretching of the amorphous PBD chains. The interaction between an enthalpic driving force to minimize the fold surface energy and the entropic term from stretching of the amorphous chains will result in an equilibrium structure which has folded chain crystallites. This clearly differs from the equilibrium structure of homopolymers where the extended chain crystals are the most stable species. However, crystallization is heavily influenced by kinetics and the equilibrium state, often can not be achieved experimentally. However, analysis of a series of data taken at decreasing undercoolings, of the type presented here, can be used to estimate properties of the equilibrium structure.

3.5.2 Effect of Morphology on the Crystallization of PEO

The crystallization and melting behavior of PEO homopolymer have been extensively studied.[50,53,56,60,65,113] For low molecular weight PEO, crystallites with an integral number of folds are much more stable than non-integral folded crystallites, and thus non-integral folded chains will transform to integral folded crystals via isothermal thickening or thinning processes.[56,57] As a result, the DSC heating curves of low molecular weight PEO usually consist of multiple melting endotherms corresponding to different populations of PEO crystallites with different integral fold numbers.[65] Changing the undercooling results in stepwise changes in crystallite thickness from one integrally folded state to another, and in several distinctively different melting temperatures (T_m) as a function of different isothermal crystallization temperature (T_c).

In the present study, monotonically increasing melting temperatures with decreasing degrees of undercooling were observed, suggesting that the thickness of the

folded chain crystals changed continuously. The DSC results were consistent with the SAXS measurements, where a continuous increase in lamellar spacing with decreasing undercooling was observed. The T_m and long period are plotted vs. T_c in Figure 3.21. The results clearly indicate that for P(EO-*b*-BD) block copolymers that the PEO fold lengths and the corresponding melting temperatures are T_c dependent and that there does not appear to be a special preference for integral folding of PEO crystalline chains.

The equilibrium melting temperature (T_m^*) of a polymer can be estimated by the Hoffman-Weeks method.[112] Extrapolating the measured T_m *vs.* T_c curve to $T_m = T_c$, assuming a constant thickening ratio (β) with respect to the initial nuclei, results in $T_m^* \sim 54.8^oC$, which is much lower than the equilibrium melting temperature (64^oC) of 6000g/mol PEO homopolymer.[65] This method allows for some estimation of T_m^*. However, strictly speaking, the Hoffman-Weeks extrapolation is only suitable for homopolymers because it does not consider the entropic contribution of the amorphous block. In addition, using Hoffman-Weeks extrapolation we can not obtain the equilibrium lamellar spacing.

A thermodynamic analysis of the melting process of the P(EO-*b*-BD) block copolymers is carried out, which assumes equilibrium and thus equates the chemical potentials of the system in the molten and crystalline states at T_m. The Gibbs free energy in the crystalline state is the sum of the contributions from the interfacial energy between PEO and PBD, the conformational energy of the amorphous PBD chains, and the enthalpy and entropy changes on the formation of crystalline PEO. The Gibbs free energy in the melt is the sum of the contributions from the interfacial energy between

PEO and PBD in the molten state, and the conformational energies of amorphous PEO and PBD chains. Equating chemical potentials and simplifying, the following relationship between melting temperature (T_m) and morphological structure is obtained:

$$T_m = \frac{N_{PEO} \bullet \Delta H_f^o - \left(\frac{\tilde{v}_{PBD}}{L_{PBD}} \gamma_c - \frac{\tilde{v}_{PBD}}{l_{PBD}} \gamma_a \right)}{N_{PEO} \bullet \frac{\Delta H_f^o}{T_m^o(\infty)} + \left(\frac{\pi^2}{16} \left(\frac{L_{PBD}^2}{R_{PBD}^2} - \frac{l_{PBD}^2}{R_{PBD}^2} \right) - \frac{\pi^2}{16} \frac{l_{PEO}^2}{R_{PEO}^2} \right) \bullet R^*} \qquad \text{(Eq. 3.1)}$$

In this equation, for component i, N_i is the degree of polymerization, $\tilde{v}_i$ is the molar volume of segments, and R_i is the unperturbed chain dimension. The brush heights for component i in the crystalline and melt states are L_i and l_i respectively. The interfacial energies between the PEO and PBD in the crystalline and amorphous states are γ_c and γ_a respectively. The heat of fusion of a perfect, infinitely thick PEO homopolymer crystal is ΔH_f^o, and its melting temperature is $T_m^o(\infty)$. The universal gas constant is R^*. The difference between Equation 1 and the derivation of Ashman and Booth[27] is that Equation 1 applies to melting from a semicrystalline structure into a microphase separated state while the Ashman and Booth model melts into a homogenous, non-microphase separated state.

L_{PBD}, l_{PBD}, and l_{PEO}, were obtained from SAXS measurements of the lamellar long period and a knowledge of component volume fractions. The interfacial free energy in the melt state γ_a is estimated[36] to be about 1.7 kT/nm^2. The typical interfacial energy for fully amorphous, microphase separated block copolymers[110] such as poly(styrene-*b*-butadiene) is on the order of 1 kT/nm^2. The interfacial free energies in the crystalline state, γ_c are difficult to measure. However, Equation 1 can be fitted to an experimentally

determined plot of T_m vs L_{PEO} using γ_c as an adjustable parameter. The plot is shown in Figure 3.22. The solid line gives the fitted curve in the region were experimental data is available; this fitting provides an estimate of the interfacial energy in the crystalline state: $\gamma_c \approx 16\ kT/nm^2$. For comparision, the surface energy of homopolymer PEO crystallites in a PEO melt was reported to be 7.5 kT/nm^2 by Buckley and Kovacs.[65] The crystal/amorphous interfacial energy as obtained by Ashman and Booth[27] for a miscible PEO/PPO block copolymer system is about 4.4 kT/nm^2. Presumably, our value of γ_c is higher because it results from both the difference between crystalline and amorphous material and a difference in chemistry between PEO and PBD. Our results, considering the simplicity of the treatment, are in good agreement with previously reported data.

The dashed part of the curve in Figure 3.22 represents the theoretical model embodied in equation 1 with the interfacial energy parameters obtained by fitting the experimental data. This curve shows a maximum at $T_m = 57.7^oC$. This indicates that in a crystalline / amorphous block copolymer, if the crystalline lamellar thickness becomes longer than a limiting value (18.9 nm), the melting temperature of the structure is reduced as unfavorable stretching of the amorphous chains begins to dominate. Consequently, the maximum in T_m corresponds to the melting temperature of crystalline / amorphous block copolymers in their most stable state. Thus, the equilibrium thickness for the crystalline PEO block is about 18.9 nm. In addition, the equilibrium melting temperature of the P(EO-*b*-BD) studied in this report is estimated to be 57.7^oC which is a considerable depression relative to that of PEO homopolymer of the same molecular weight. SAXS results in Figure 3.11 indicate that the amorphous PBD chains are considerably more stretched when the PEO block is crystallized than when the PEO block is in the melt

state. Thus melting of PEO block of the copolymer will release entropic energy stored in the amorphous chain, further depressing the observed melting point. Consequently, the observed decrease of the P(EO-*b*-BD) melting point relative to PEO homopolymer results from both a reduction of the crystalline thickness and the entropy of stretched amorphous chains.

3.6 Conclusions

The morphology of a symmetric block copolymer P(EO-*b*-BD) was found via TEM and electron diffraction to consist of strictly alternating PEO and PBD layers with PEO crystalline chain oriented normal to the microphase separated domain interface. Optical microscopy indicated that the confinement of PEO by the microphase separated structure suppressed the formation of spherulitic texture during crystallization. The PEO block was found to have a high crystallinity, about 88%. Thus, the structure of this block copolymer in the solid state can be best described by the theoretical model proposed previously.[3,7] The crystallization of PEO in the diblocks results in non-integral folded crystallites and chain stretching energy in the amorphous blocks prevents the formation of extended chain PEO crystallites.

For P(EO-b-BD) block copolymer, the melt microphase separated morphology acted as a template for crystallization. Increasing the crystallization temperature resulted in an irreversible coarsening of the average microphase separated lamellar grain size. Achieving control over the block copolymer grain size is not an easy task to achieve. The current observation may provide means that allowed us to have some control over

the block copolymer grain sizes. This may enable us to study phenomena that may be related to block copolymer grain sizes.

By using the methods discussed in this paper, the melting temperature and structure information of equilibrium state of the P(EO-*b*-BD) studied can be obtained. This study proved that, for crystalline-amorphous diblock copolymers, a chain folded crystalline structure was formed at equilibrium state. Current study only utilized a single block copolymer of given molecular weight. In order to study the scaling behavior of the equilibrium state for these systems, for comparison to theory, this work would need to be extended to encompass a series of samples of varying molecular weights. The present work indicates that the P(EO-*b*-BD) system is a good model system in achieving such a task.

Table 3.1: Summary of DSC and SAXS results on P(EO-*b*-BD) block copolymer samples crystallized isothermally at various temperatures

T_c (°C)	T_m [a] (°C)	T_m [b] (°C)	ΔH (J/g)	L_o (nm)	L_{PEO} (nm)
34	52.1	52.7	165	21.5	10.3
38	52.2	52.8	163	21.6	10.4
40	52.4	52.9	162	-	-
42	52.6	53.1	165	22.4	10.8
44	52.8	53.4	165	-	-
46	53.0	53.6	167	23.2	11.1
48	53.3	53.8	169	23.8	11.4
49	53.5	54.1	167	-	-
50	53.7	54.3	169	24.9	12.0
51	53.9	54.6	167	-	-

T_c: isothermal crystallization temperature; T_m[a]: onset temperature of the primary melting peak; T_m[b]: peak temperature of the primary melting peak; ΔH: heat of fusion, normalized to the weight of PEO in the block copolymer; L_o: lamellar domain spacing measured by SAXS; L_{PEO}: PEO crystalline chain length calculated based on volume fraction and percentage crystallinity.

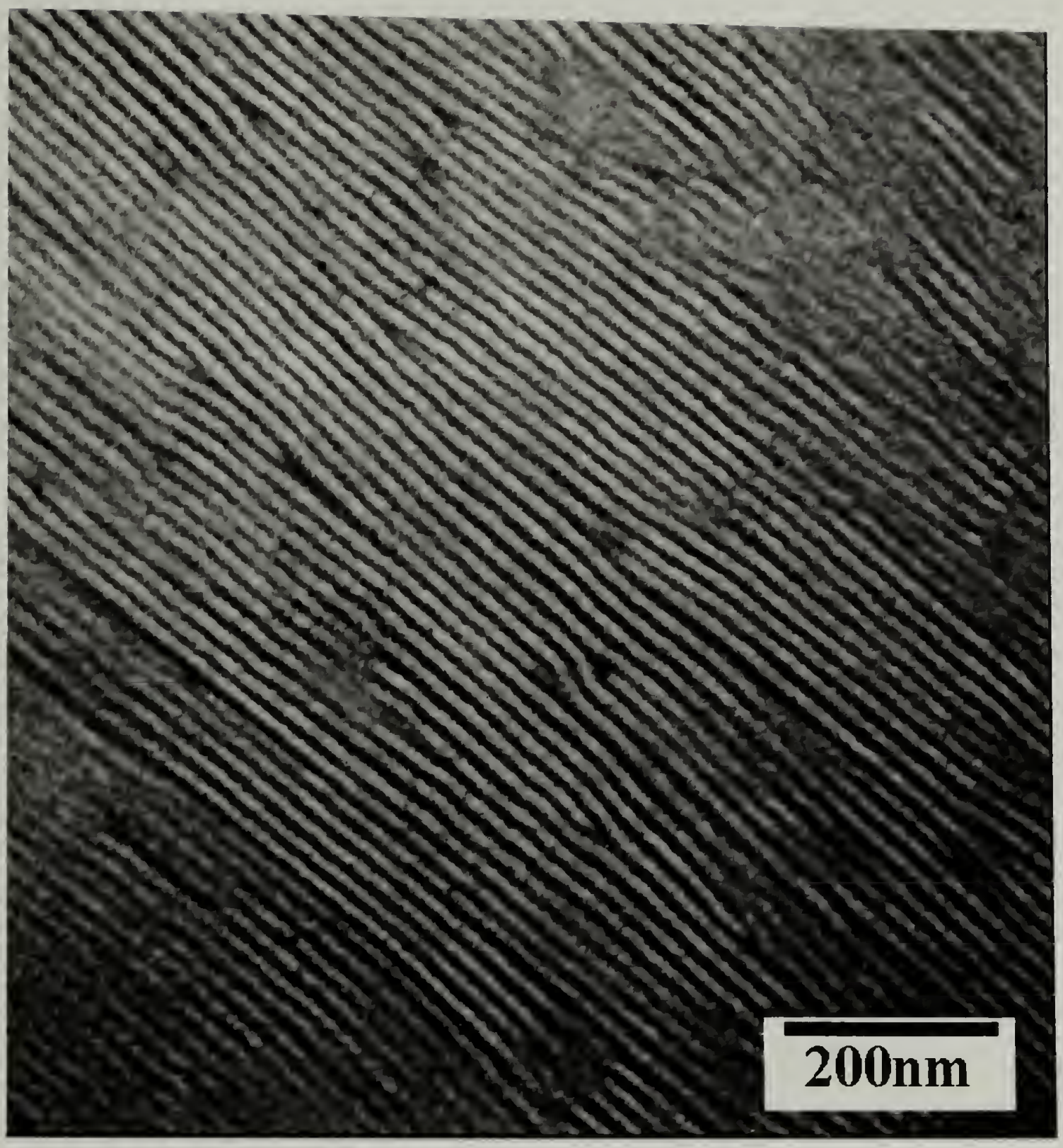

Figure 3.1: Morphology of P(EO-*b*-BD) diblock copolymers crystallized at 30°C showing lamellar morphology with good long range order.

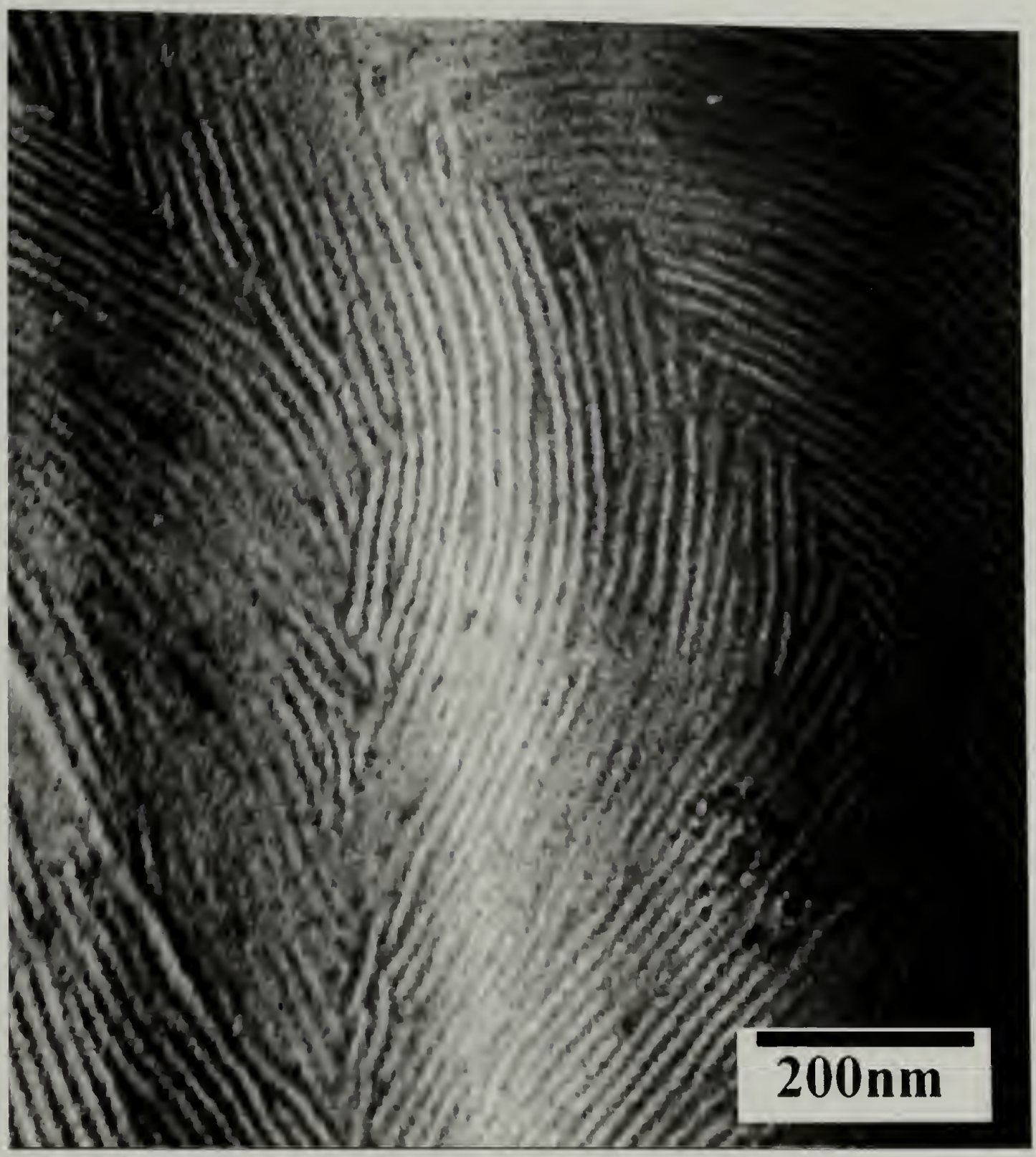

Figure 3.2: Morphology of P(EO-b-BD) diblock copolymers crystallized at 30°C showing typical block copolymer grain boundary structures

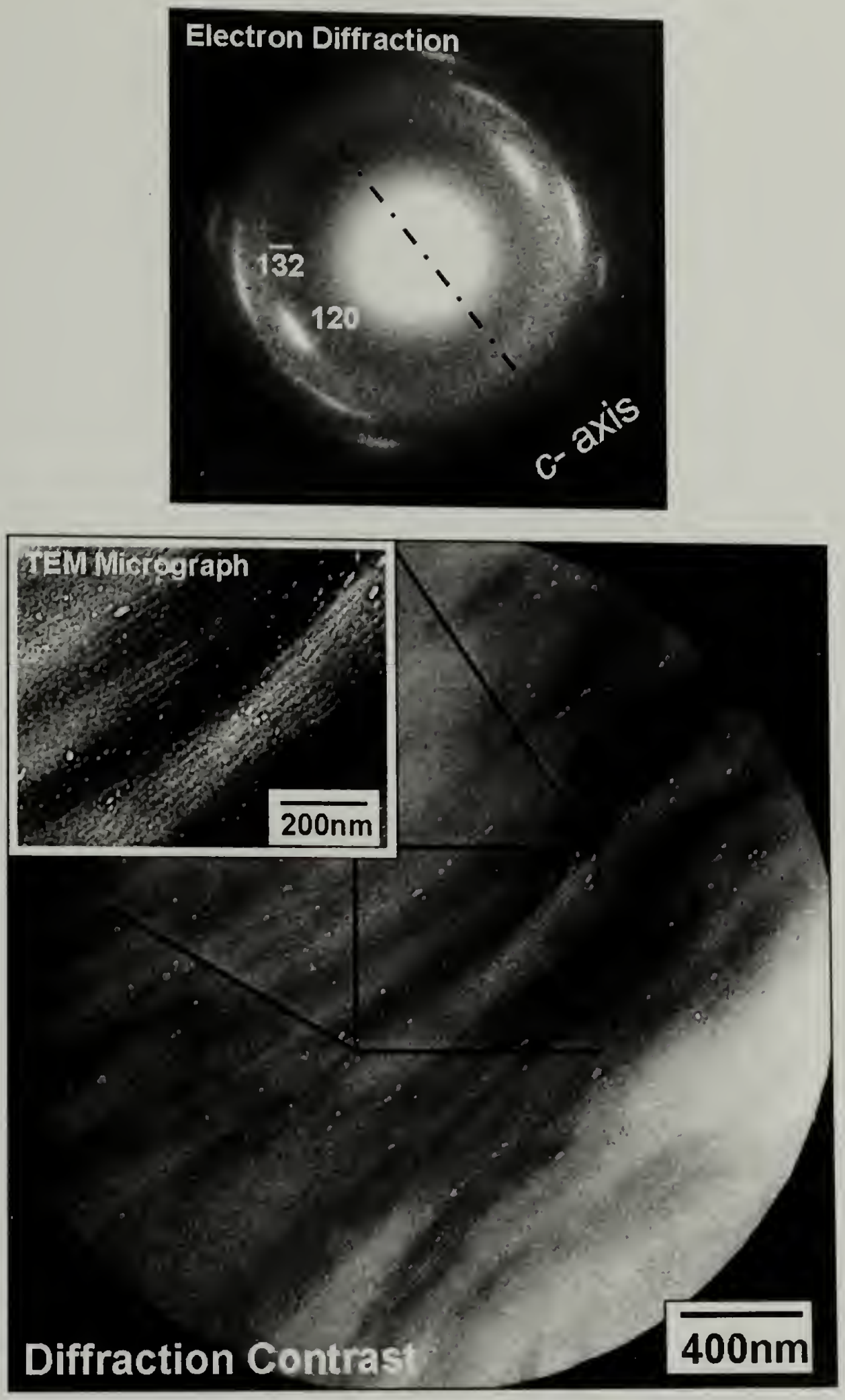

Figure 3.3: PEO Crystalline Orientation in P(EO-*b*-BD).

a) Electron Diffraction Pattern

b) TEM image taken inside the selected area aperture

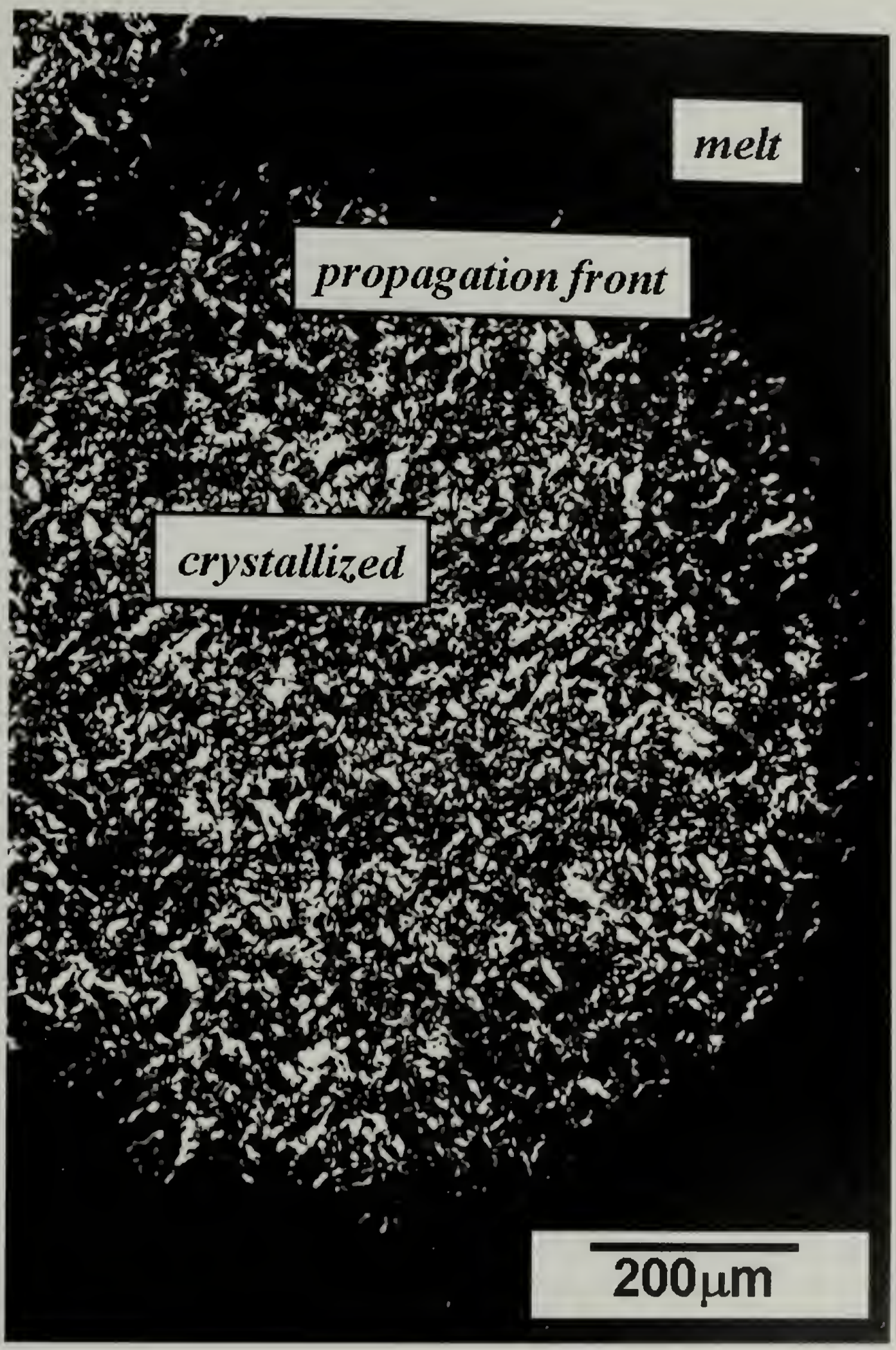

Figure 3.4: Optical micrograph under cross polar for P(EO-b-BD) diblock copolymers crystallizing at 45°C

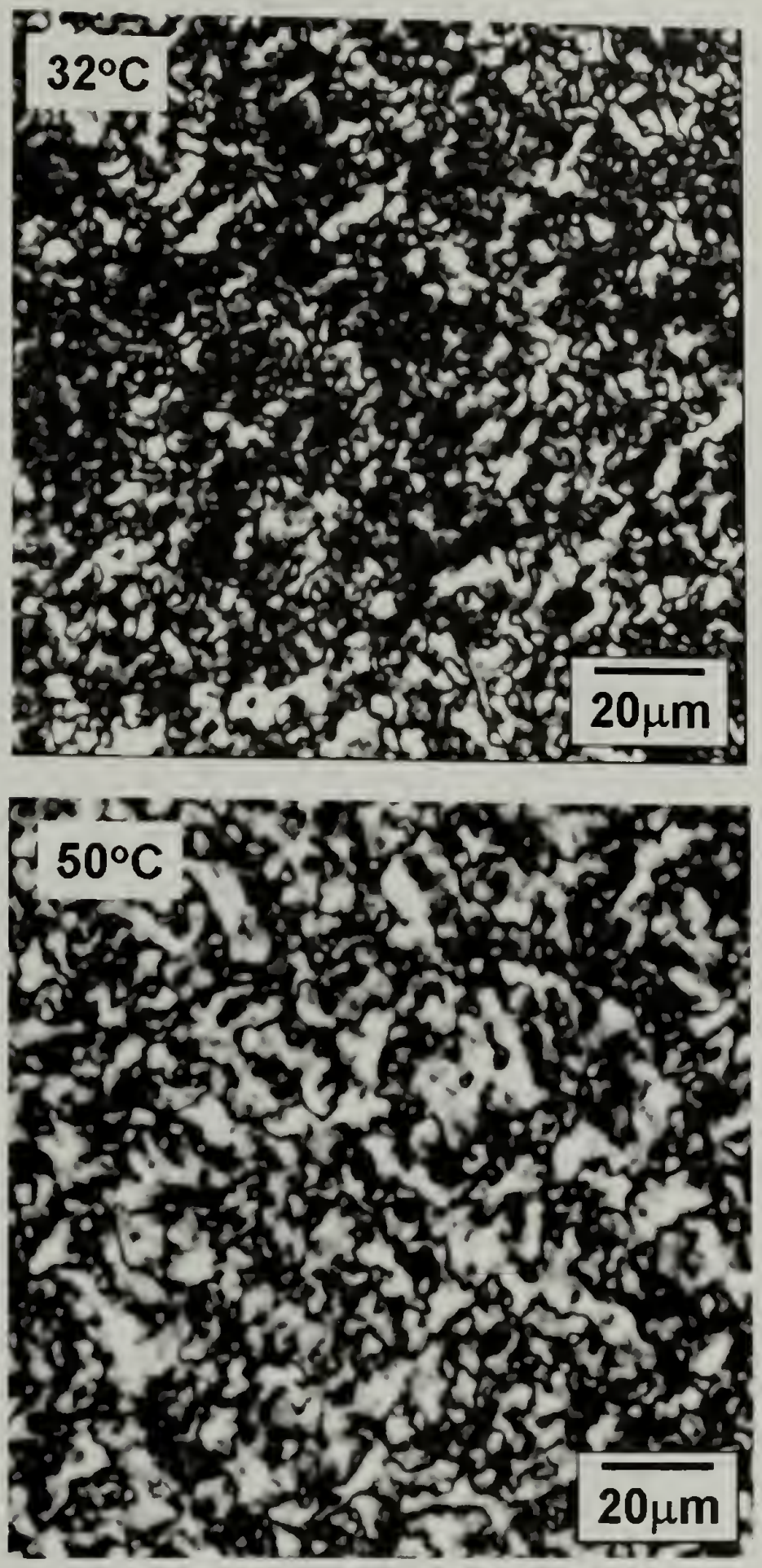

Figure 3.5: Effect of crystallization temperature on P(EO-b-BD) block copolymer grain sizes.

a) Crystallized at 32°C

b) Crystallized at 50°C

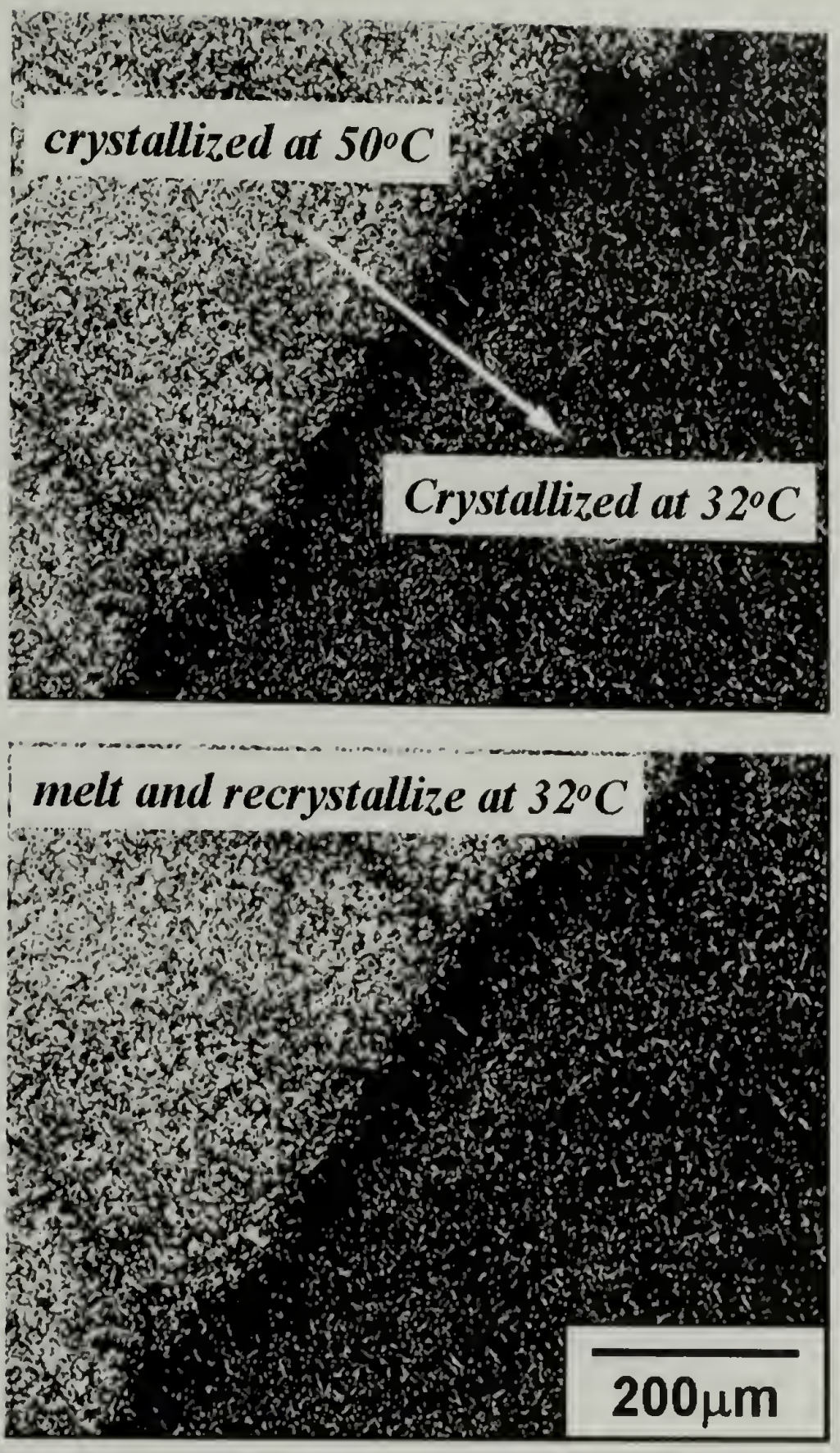

Figure 3.6: Effect of melt microphase separated morphology on the crystallization of PEO in block copolymers.

a) Sample was first crystallized at 50°C and then a quick temperature jump was performed at part of the sample was crystallized at 32°C.

b) Sample in (a) was melted completely and re-crystallized at 32°C again. The texture that was produced in the previous run was still maintained.

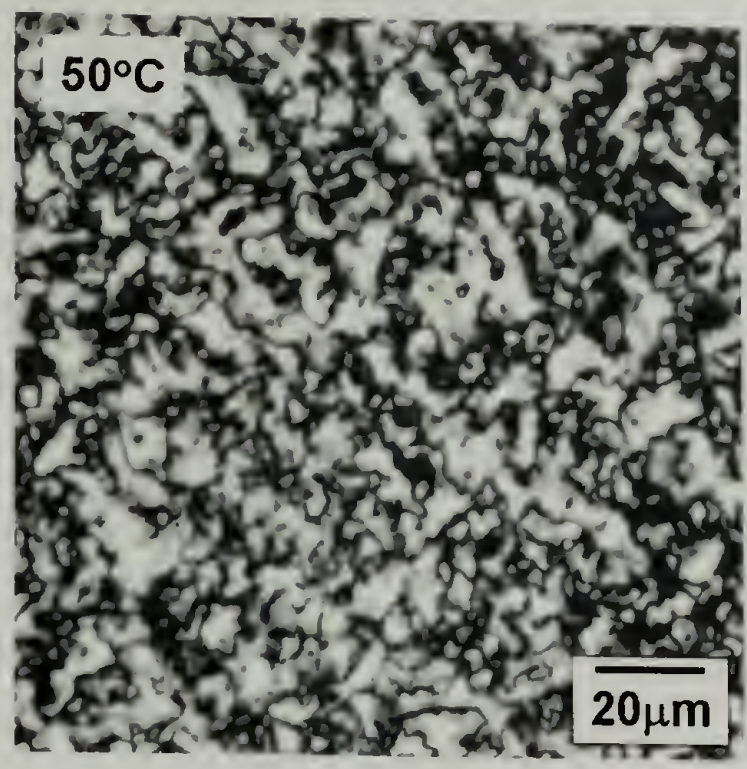

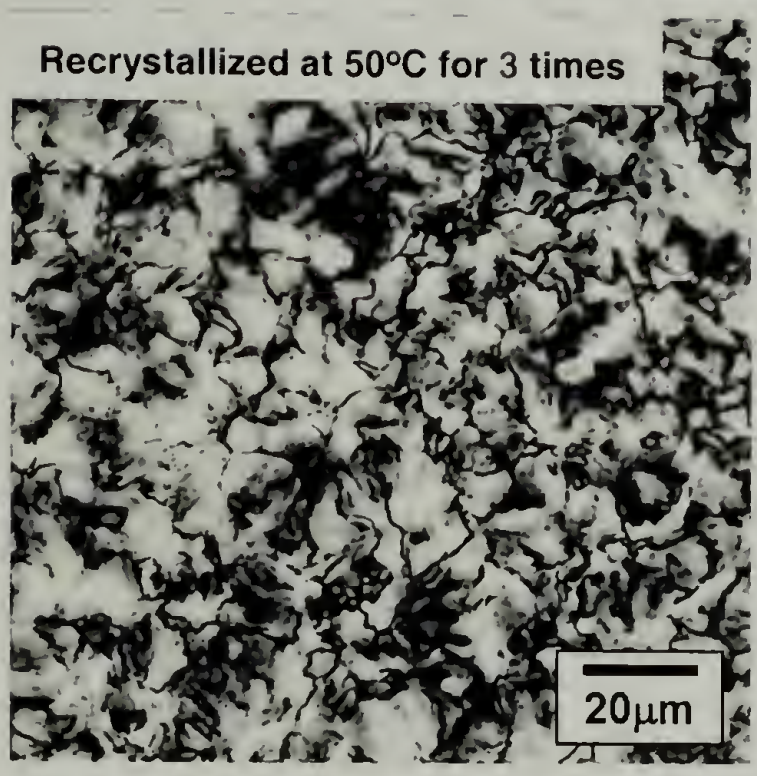

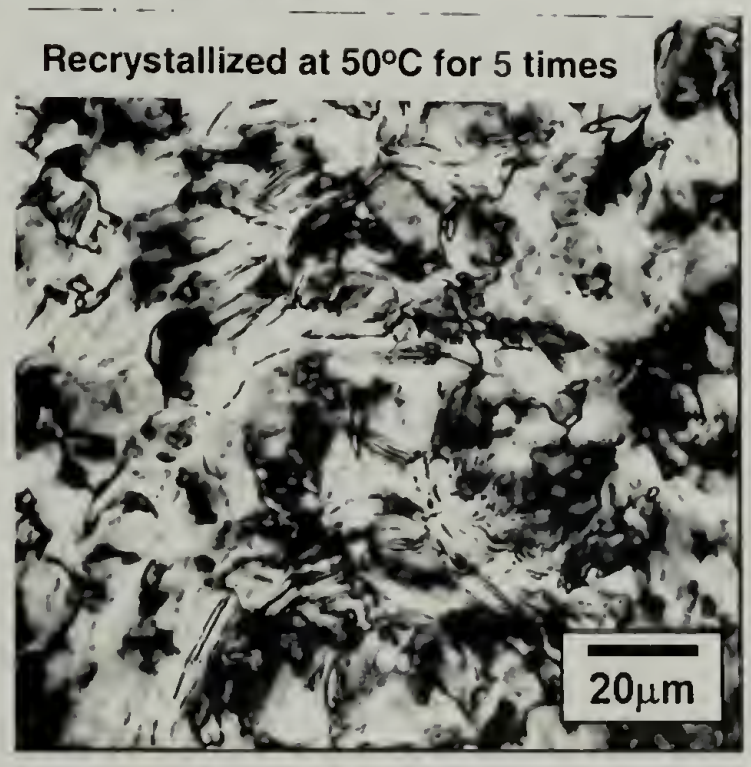

Figure 3.7: Irreversible change of crystalline texture with increasing numbers of recrystallization cycles.

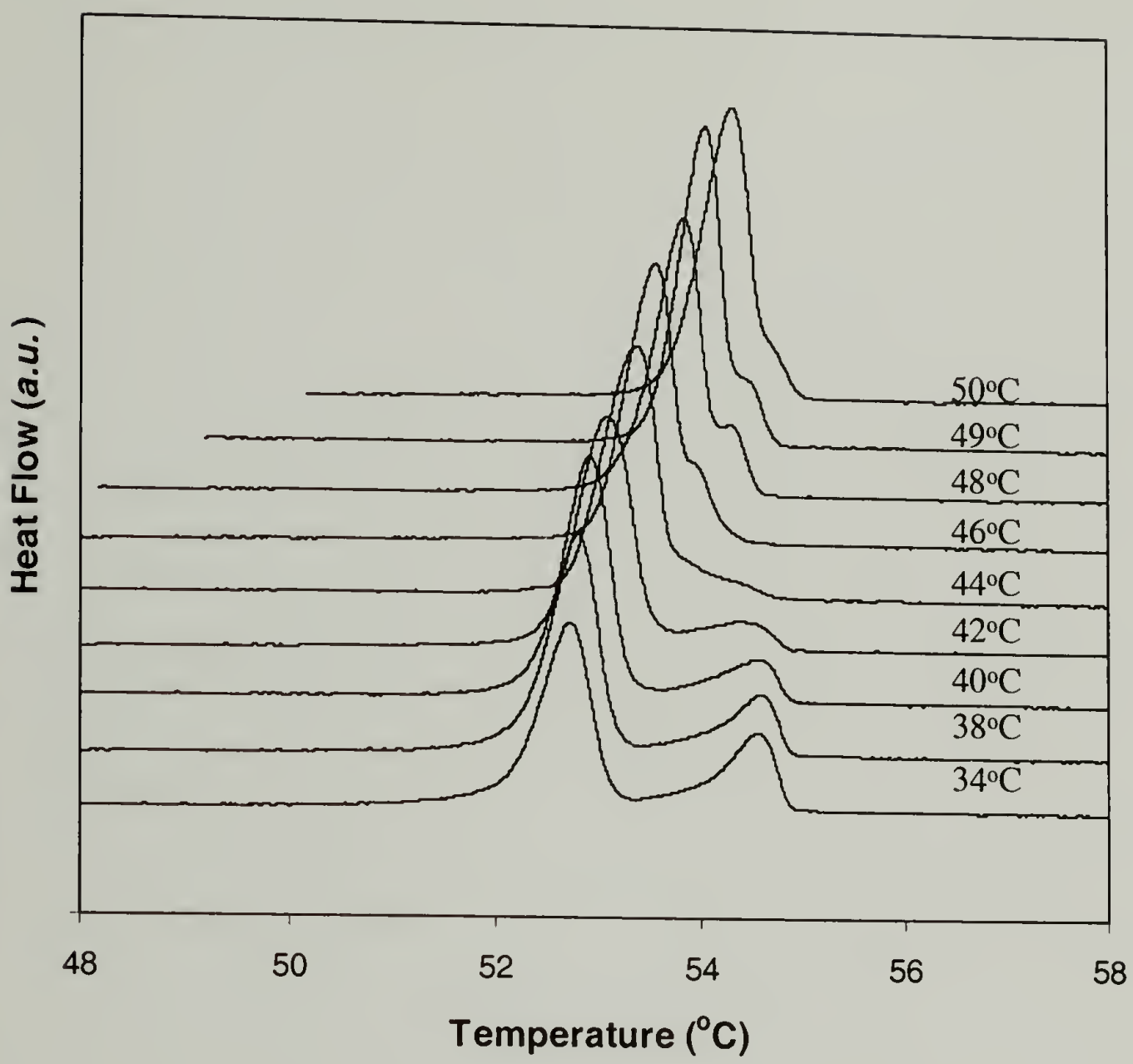

Figure 3.8: DSC melting endotherm for P(EO-*b*-BD) crystallized isothermally at different temperatures.

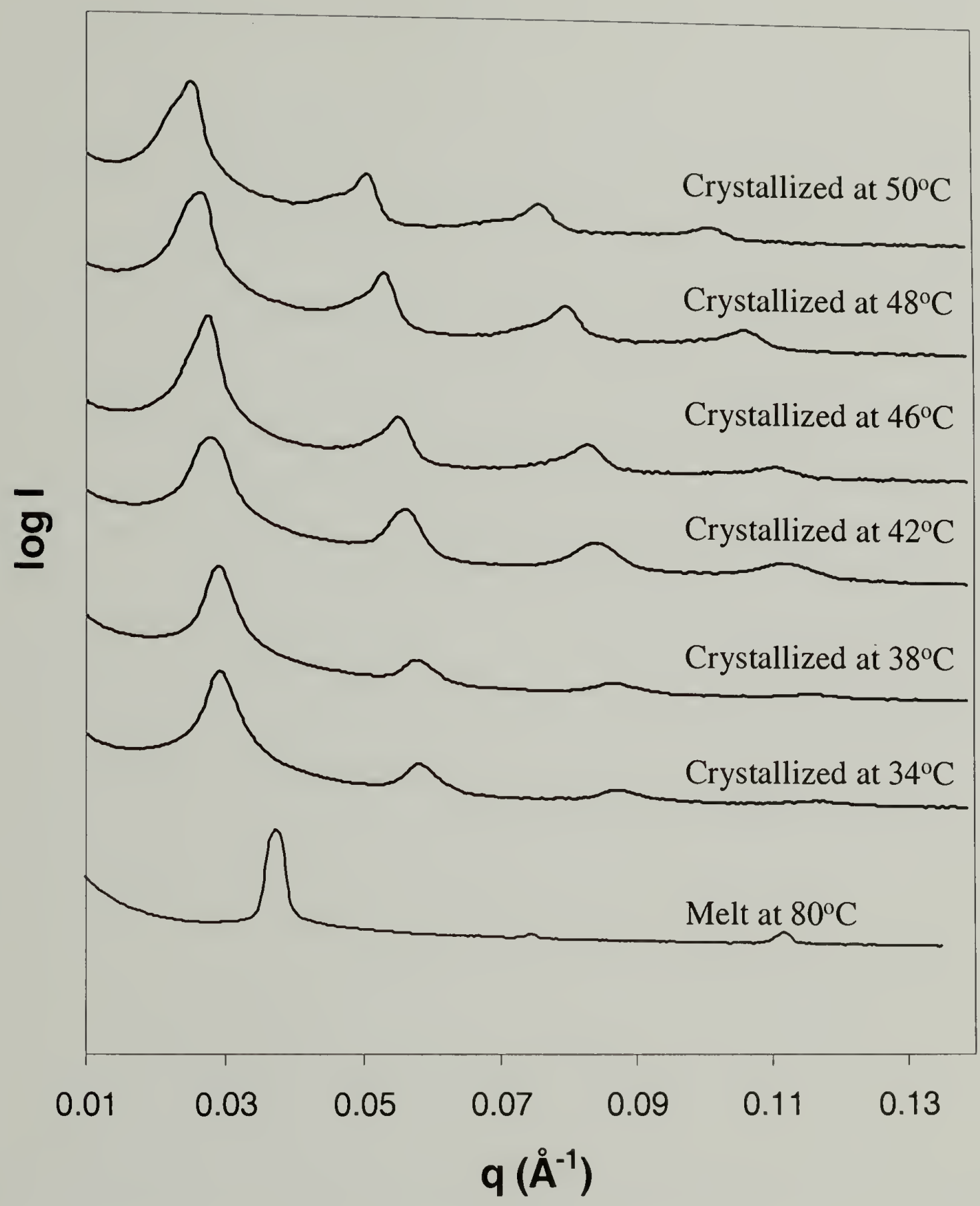

Figure 3.9: SAXS of P(EO-*b*-BD) in the melt and crystalline state

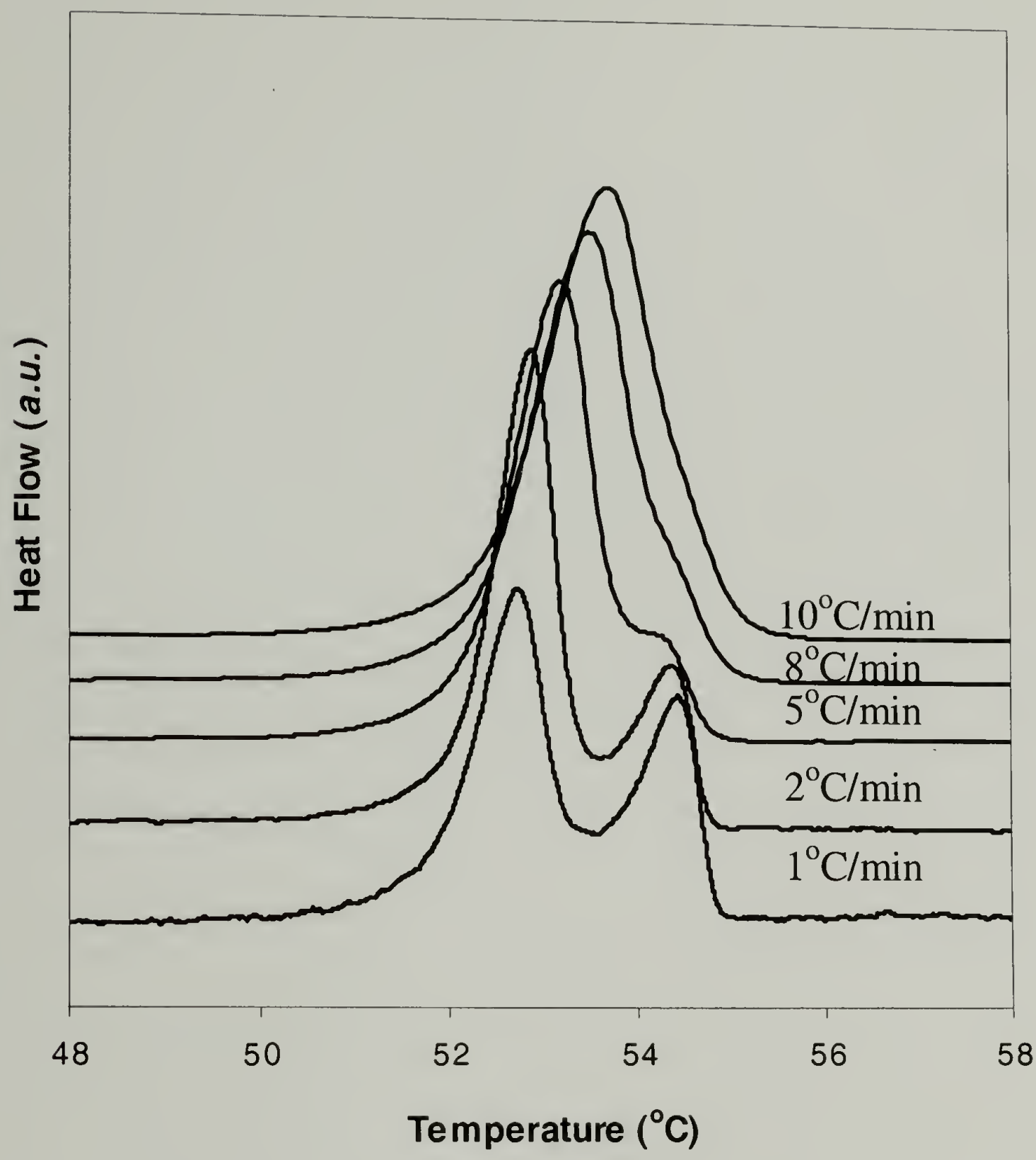

Figure 3.10: Effect of heating rate on the DSC melting endotherm of P(EO-b-BD) diblock copolymers.

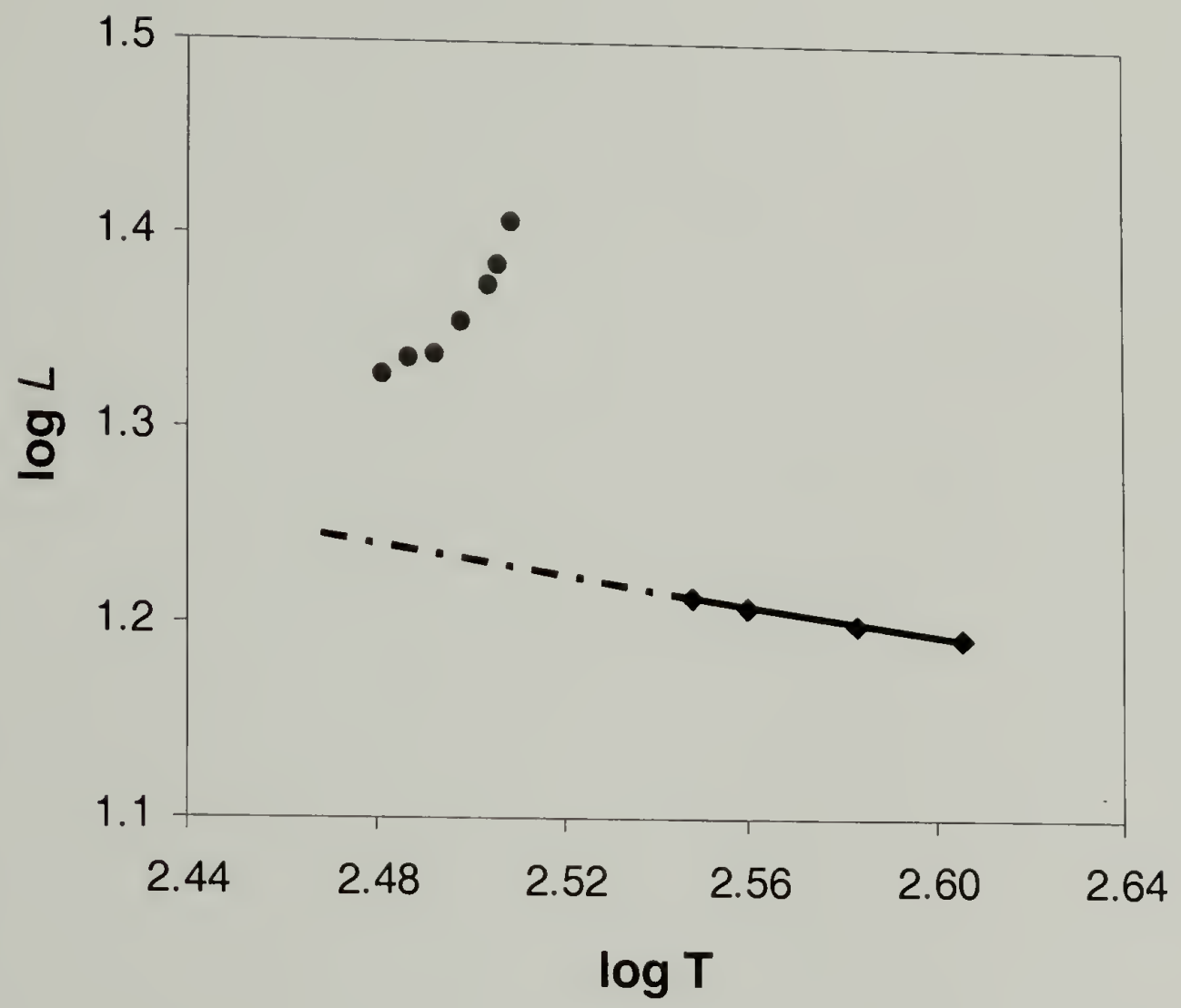

Figure 3.11: Lamellar long spacing as a function of temperature.

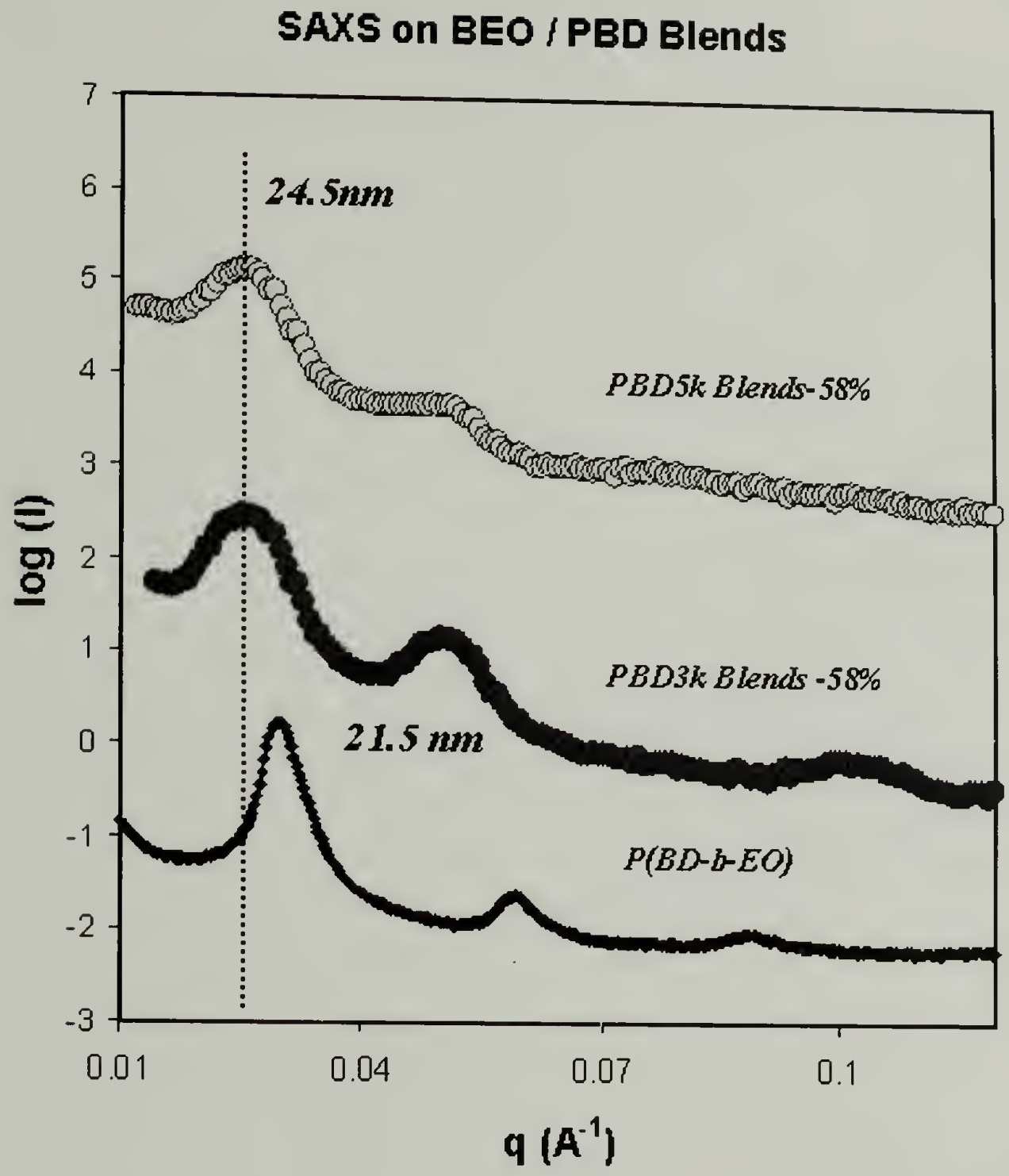

Figure 3.12: SAXS scattering profiles of P(BD-b-EO) / PBD blends.

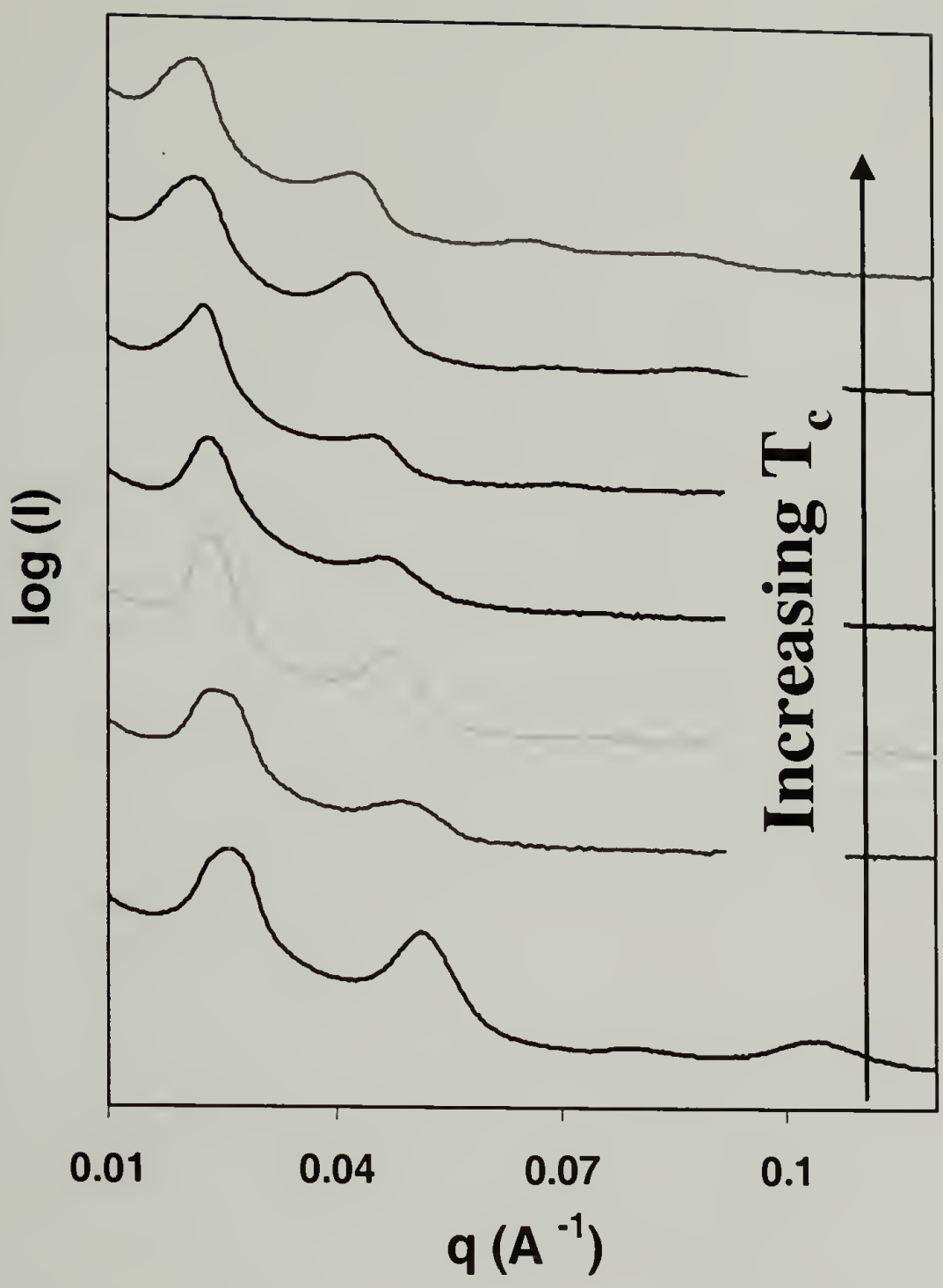

Figure 3.13: SAXS scattering profiles of isothermally crystallized P(BD-b-EO) / PBD blends. The overall volume fraction of PBD was 58% and the molecular weight of the PBD homopolymer was about 5000g/mol.

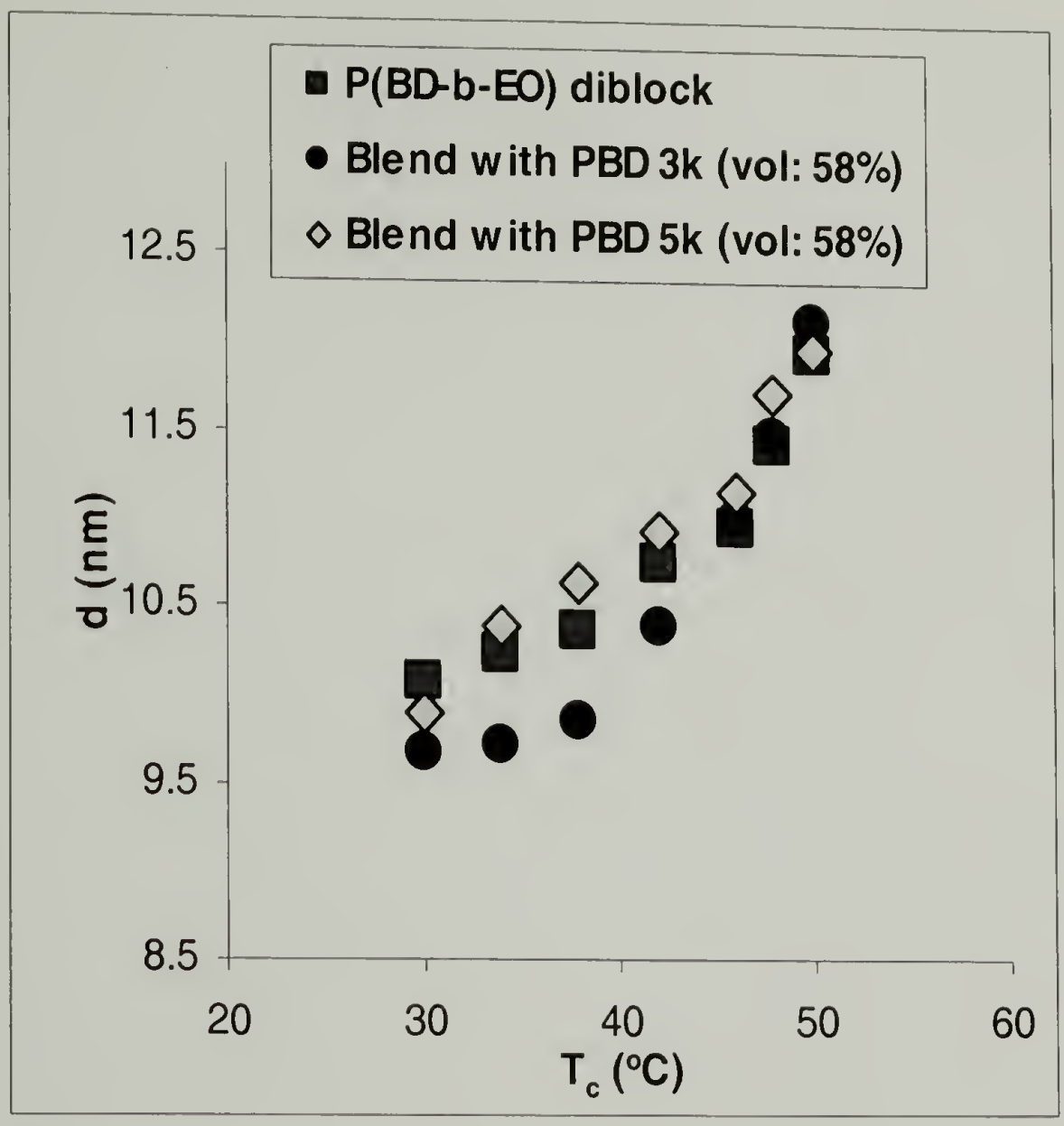

Figure 3.14: Crystalline lamellar thickness as a function of crystallization temperature.

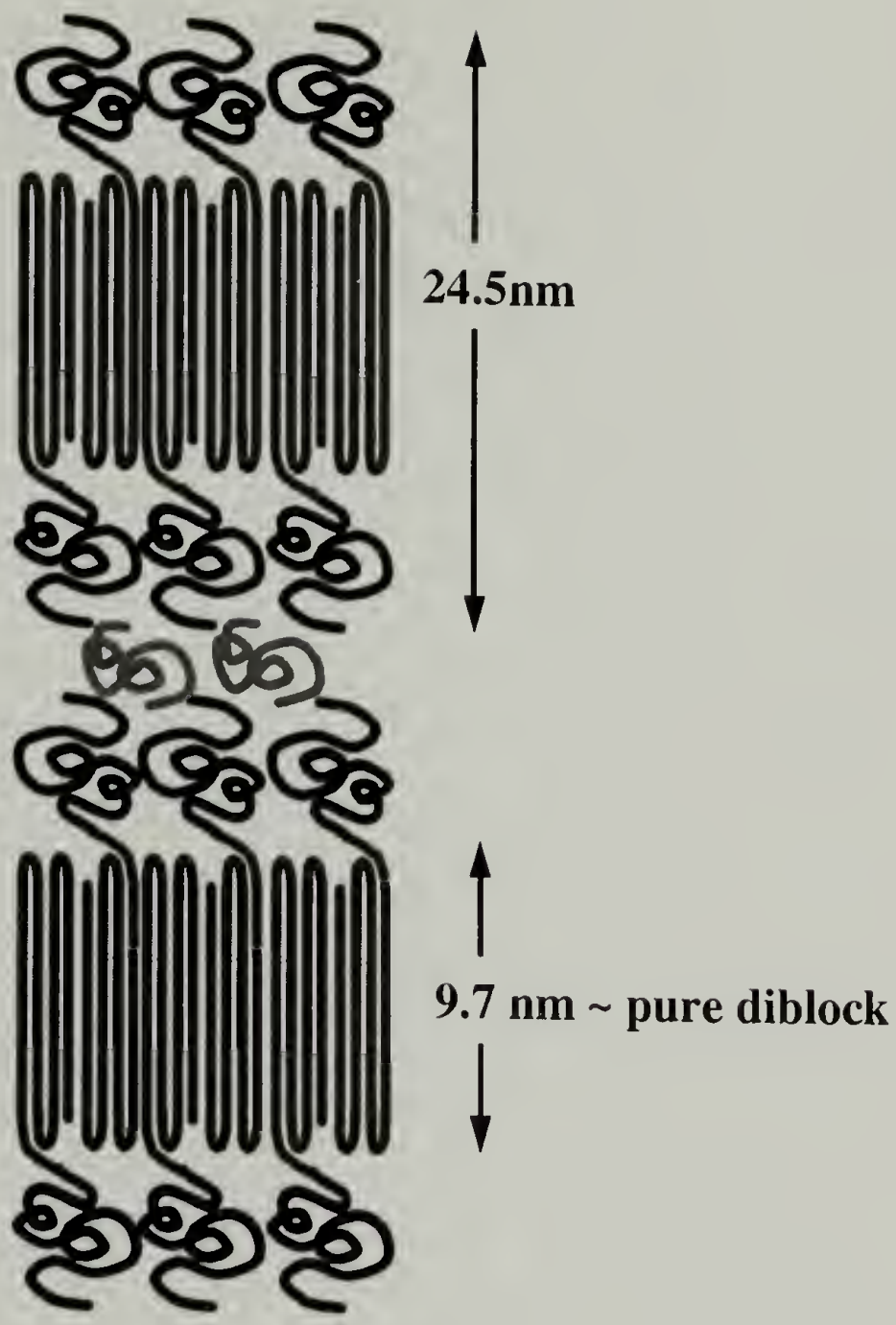

Figure 3.15: Schematic of the morphology of lamellar forming P(BD-b-EO) / PBD homopolymer blends. The crystalline lamellae thickness is not significantly affected by the addition of homopolymers

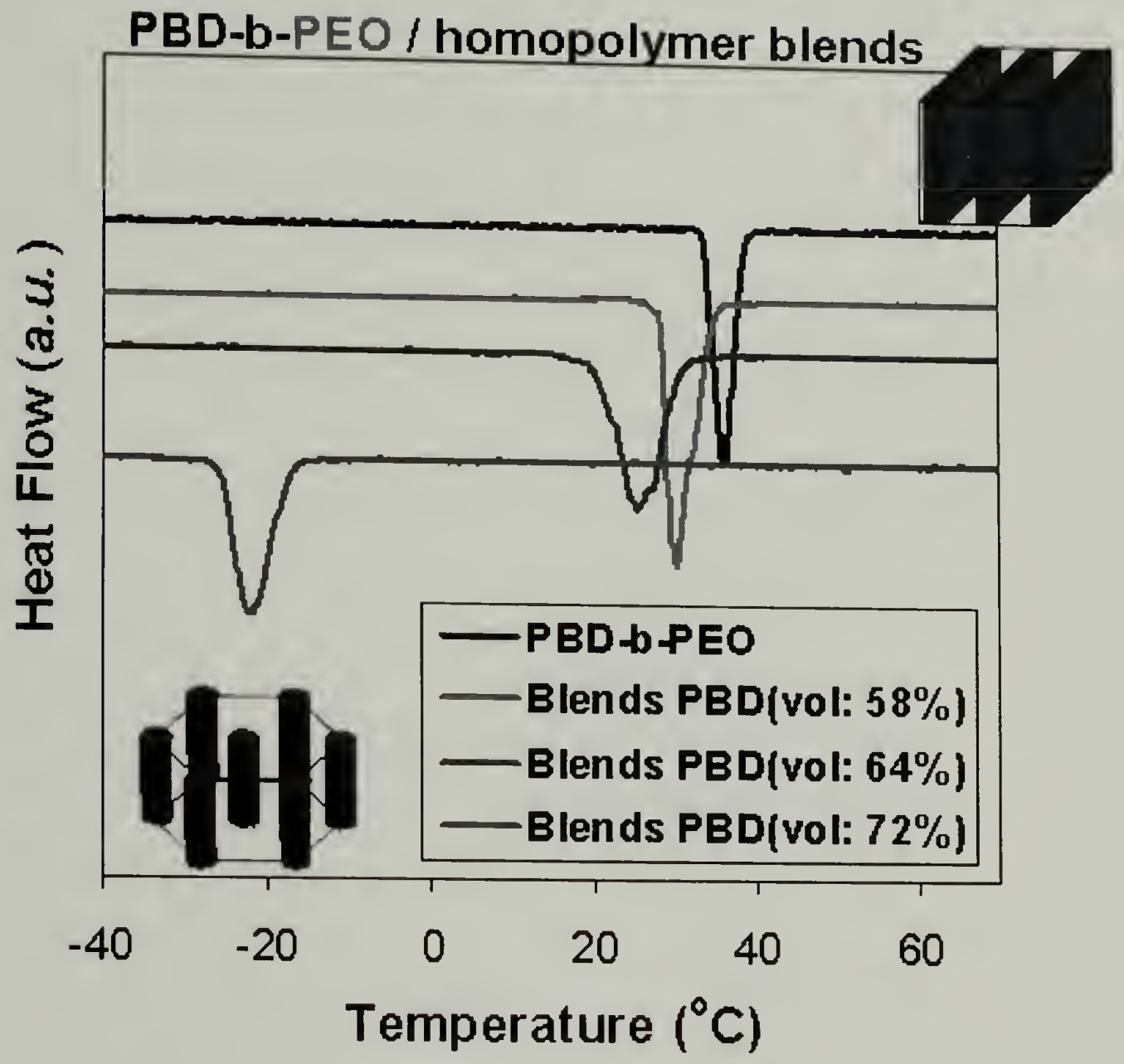

Figure 3.16: DSC cooling thermograms of P(BD-b-EO) / PBD homopolymer blends.

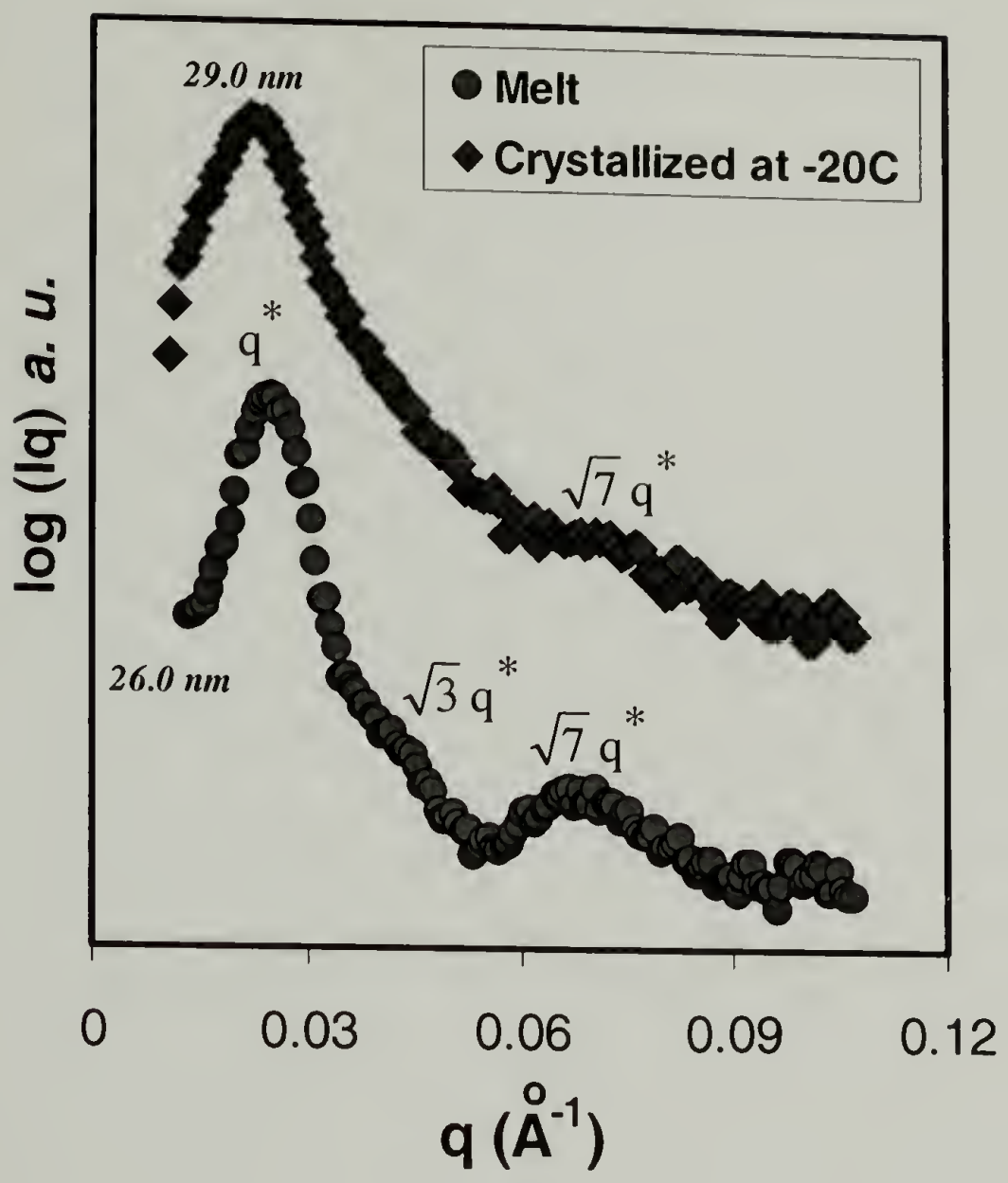

Figure 3.17: SAXS scattering profile of P(BD-*b*-EO) blends with 72% PBD volume fraction.

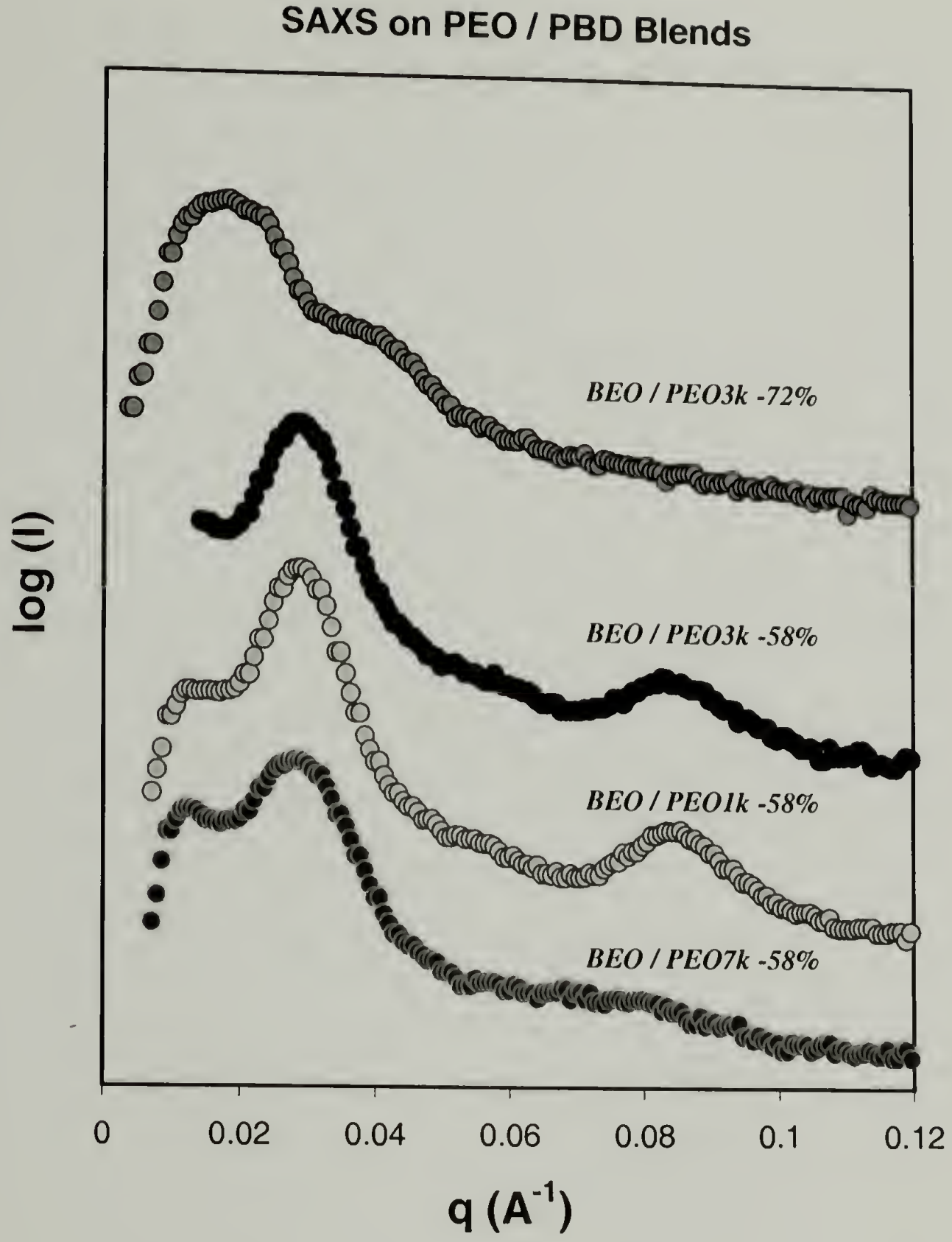

Figure 3.18: SAXS scattering profile of P(BD-b-EO) / PEO homopolymer blends. The corresponding PEO homopolymer molecular weight and the overall PEO volume fraction are indicated on the plot.

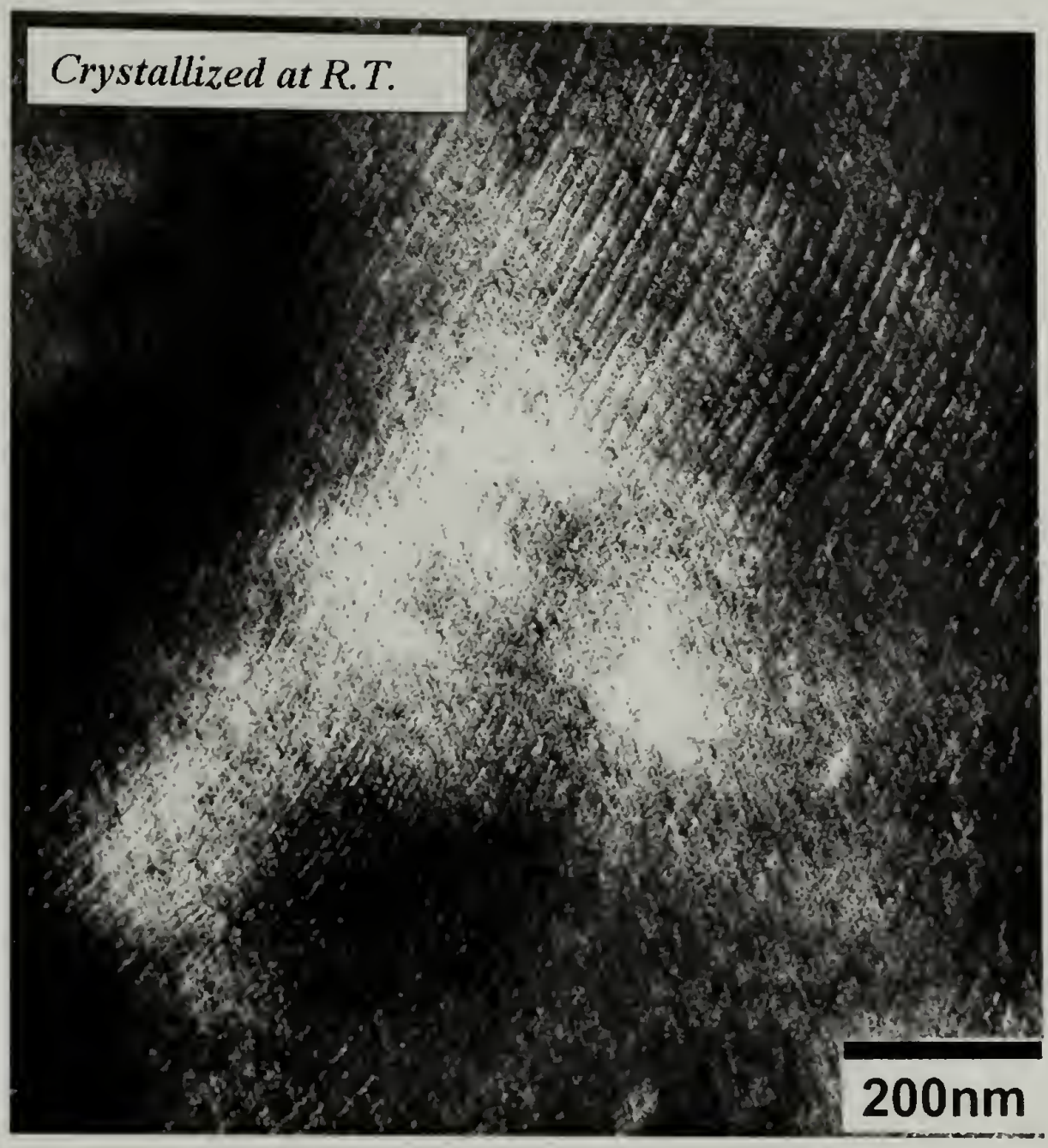

Figure 3.19: TEM micrograph of P(BD-b-EO) / PEO homopolymer blends. The molecular weight of the PEO homopolymer is 3000g/mol and the overall PEO volume fraction in 58%.

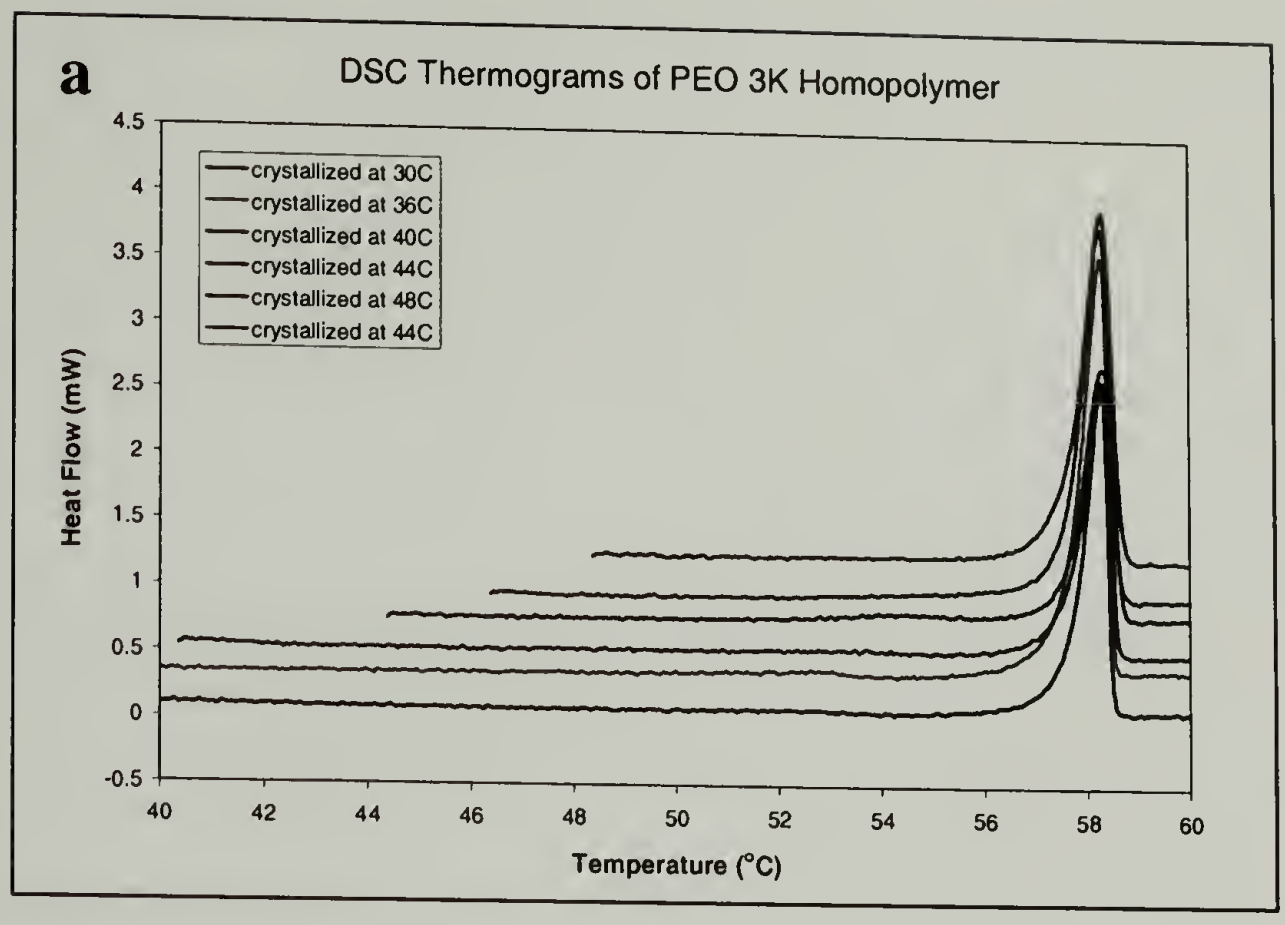

Figure 3.20: DSC melting thermograms: a) PEO homopolymer with 3000g/mol molecular weight; b) P(BD-b-EO) / PEO 3k blends with overall PEO volume fraction of 58%; c) P(BD-b-EO) / PEO 3k blends with overall PEO volume fraction of 72%. The heating rate is 2°C/min.

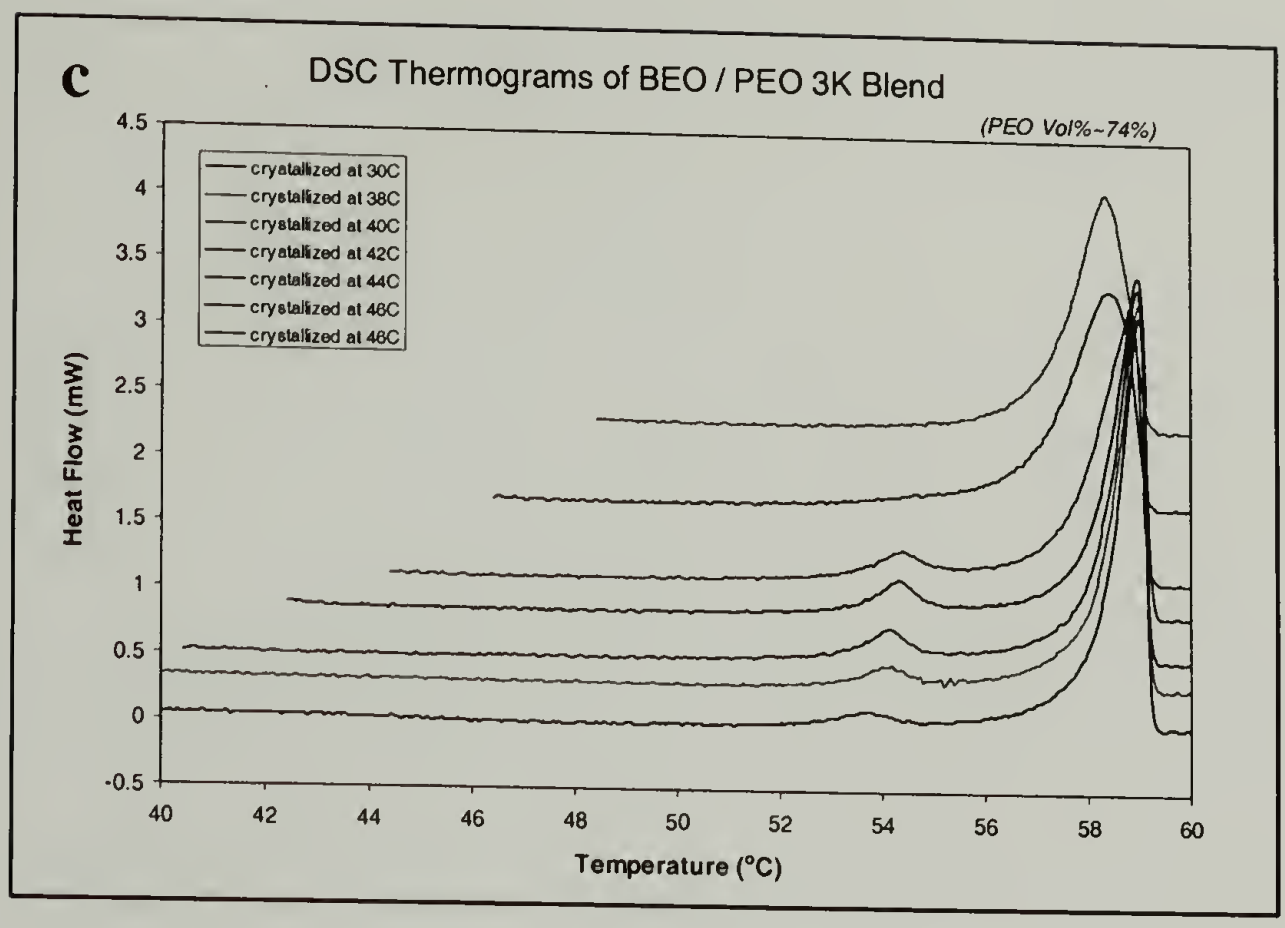
c
DSC Thermograms of BEO / PEO 3K Blend
(PEO Vol%~74%)
crystallized at 30C
crystallized at 38C
crystallized at 40C
crystallized at 42C
crystallized at 44C
crystallized at 46C
crystallized at 46C
Heat Flow (mW)
4.5
4
3.5
3
2.5
2
1.5
1
0.5
0
-0.5
40
42
44
46
48
50
52
54
56
58
60
Temperature (°C)

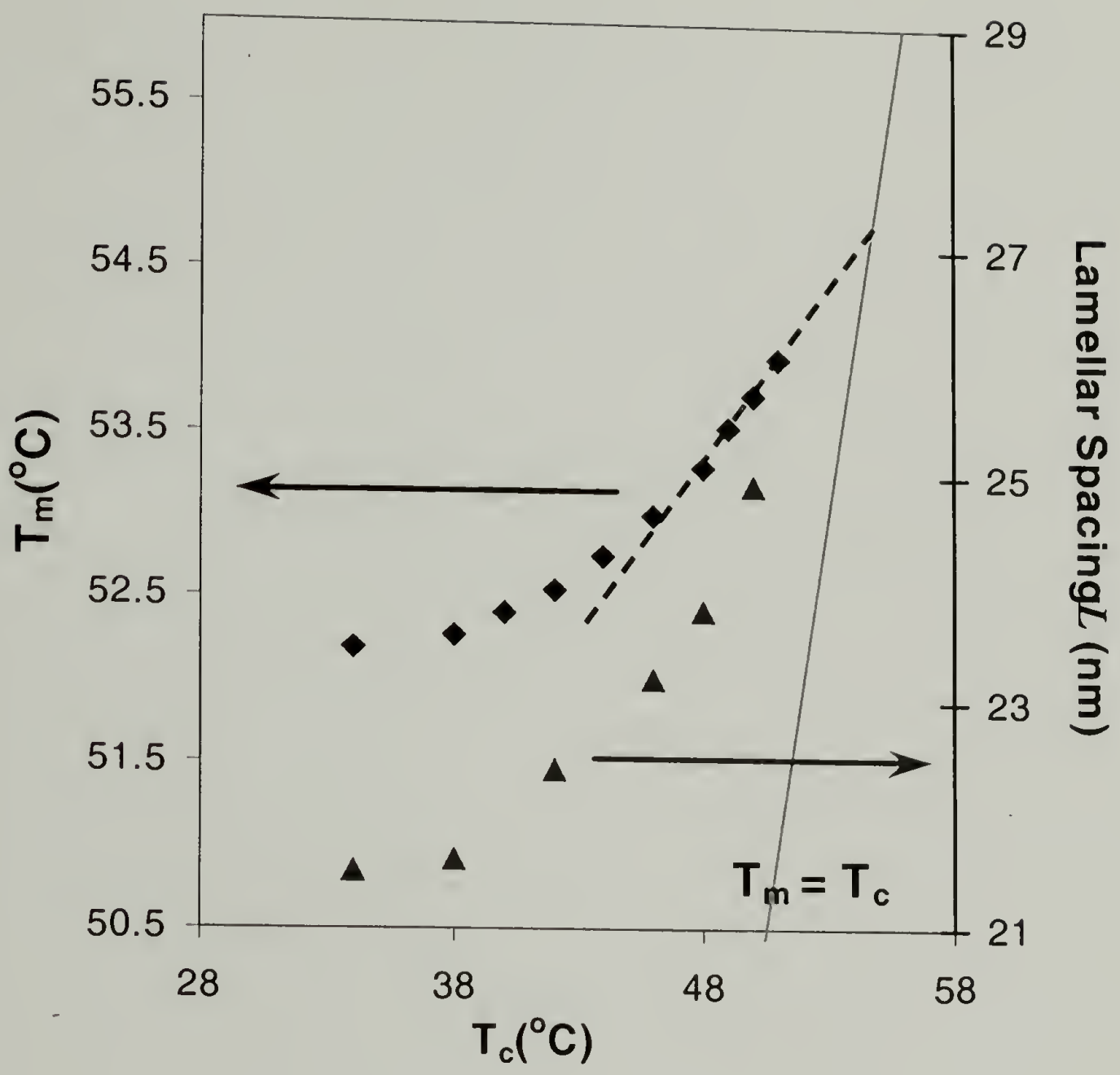

Figure 3.21: Melting temperature (T_m) and lamellar long period dependence on the crystallization temperature (T_c). The $T_m = T_c$ line is also shown on the plot. The dash line is the extrapolation of the experimental T_m data to $T_m = T_c$ based on Hoffman-Weeks method.

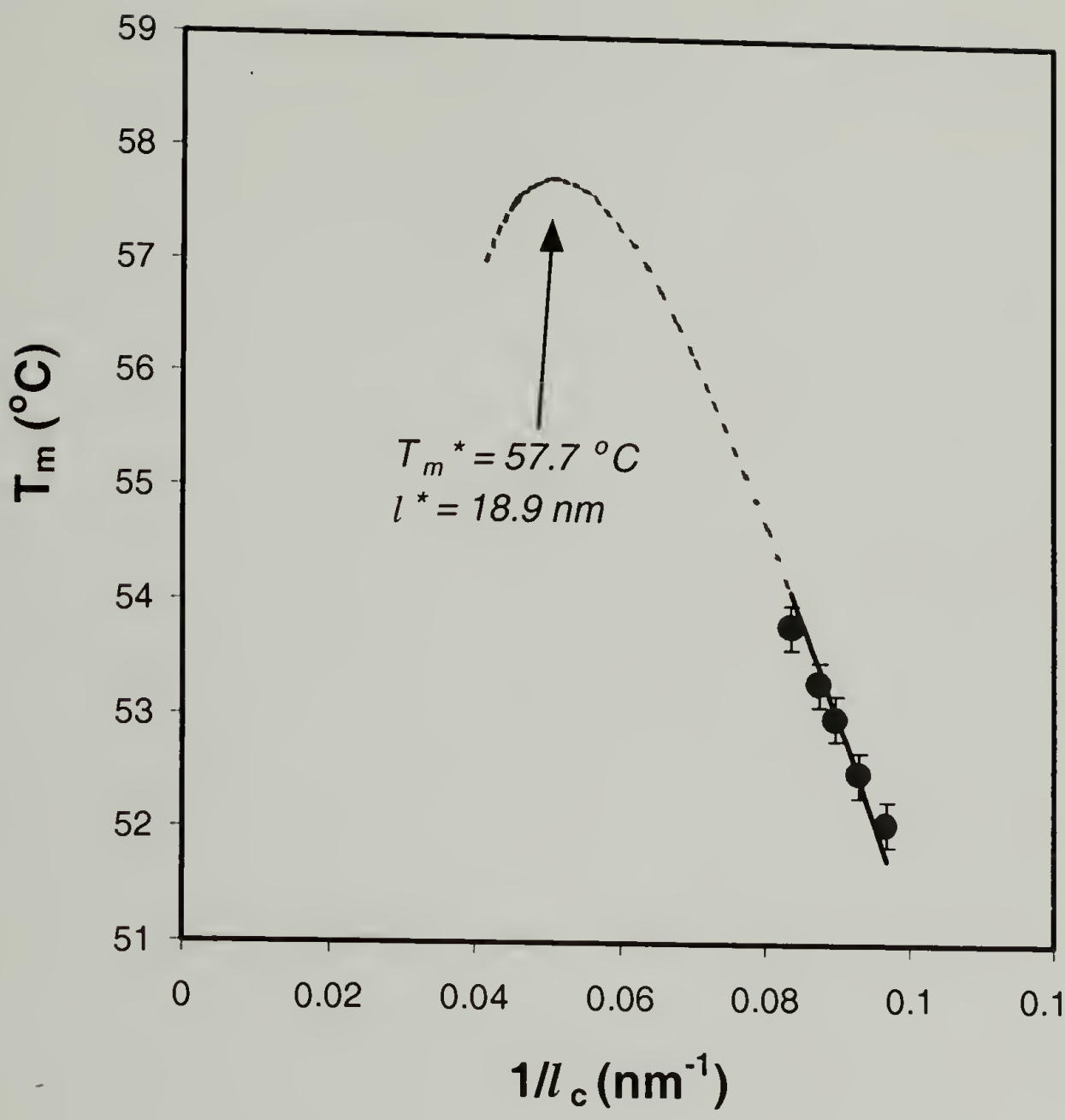

Figure 3.22: T_m **dependence on the reciprocal of crystalline lamellar thickness ($1/L_{PEO}$) of the PEO blocks in P(EO-*b*-BD) block copolymers. The solid line is a fit of Equation 1 to the experimental data (●), and the dash line represents the theoretical model embodied in equation 1 with the interfacial energy parameter obtained by fitting the experimental data.**

CHAPTER 4

SOFT AND RIGID CONFINMENT ON CRYSTALLIZATION: MORPHOLOGY OF A CRYSTALLINE – CRYSTALLINE BLOCK COPOLYMER

4.1 Abstract

The morphology and crystallization behavior of a symmetric crystalline / crystalline block copolymer, poly(ethylene -*b*- ethylene oxide) (P(E-*b*-EO)), were studied under different thermal conditions. The diblock copolymer was found to have an alternating lamellar morphology in both the melt and crystalline states. Transmission electron microscopy (TEM) and electron diffraction indicated that both polyethylene and poly(ethylene oxide) crystalline chains were oriented normal to the interfaces of the microphase separated lamellar domains. Crystallization of the polyethylene block resulted in a significant increase (~3 nm) in the lamellar spacing while the subsequent crystallization of the poly(ethylene oxide) block only caused minimal layer expansion. TEM and optical microscopy indicated that despite the change in lamellar spacing upon PE crystallization, the grain structure of the microphase separated lamellae, was maintained after crystallization. Thus, the pre-existing microphase separated morphology acts as a template for crystallization. The crystallization of PEO inside the rigid confinement provided by the crystallized PE layers of P(E-*b*-EO) was compared with crystallization of PEO in the unsaturated analog poly(butadiene-*b*-(ethylene oxide)) where the confining PBD block is amorphous and flexible. Rigid confinement during

crystallization resulted in lower degrees of crystallinity and suppression of crystallite thickening as compared to the soft confinement.

4.2 Introduction

Research on the morphology and crystallization characteristics of crystalline block copolymers has been an ongoing effort of a number of groups over the past several years.[2,3,7-10,14,16,19,21,25,26,32,34,37,38,44,72,100-103,114] The effect of microphase separated block copolymer morphology formed in the molten state on crystallization has been a major focus of this work.

In our previously reports,[102,114] we studied the morphological behavior of poly(butadiene-*b*-ethylene oxide), an amorphous / crystalline block copolymer, with symmetric volume fractions. The morphology was found to be best described by the schematic model proposed by Whitmore and Noolandi,[3] and DiMarzio and coworkers.[2] The flexible PBD amorphous domains allow moderate deformation to accommodate the crystallization of PEO blocks. The transition from block copolymer lamellar morphology in the molten state to the crystalline/amorphous lamellae in the solid state is accompanied by an increase of microphase separated domain spacing. However, typical block copolymer grain boundaries were still present as observed under transmission electron microscopy (TEM). In addition, on the length scale of tens of microns, as probed by polarizing optical microscopy, typical block copolymer morphology (with the absence of the Maltese cross typical of spherulites) was observed. Apparently, crystallization occurs within the microphase separated lamellar layers and does not destroy the block copolymer grain structures.

In this report, we studied the morphology of poly(ethylene-*b*-ethylene oxide) (P(E-*b*-EO)), which is the hydrogenated product of the same P(BD-*b*-EO) diblock used in our previous work.[102,114] Very little work has been reported on the morphology of crystalline / crystalline block copolymers.[66] As temperature is lowered from the melt P(E-*b*-EO) undergoes two sequential crystallization processes: in the first step, PE crystallizes in an environment where the PEO domain is amorphous and flexible, which is analogous to the situation of PEO crystallization in P(BD-*b*-EO). In the second step, when PEO crystallizes, the PE domains are rigid, providing less flexible confinement. Since the P(E-*b*-EO) employed in this study is a direct derivative of previously studied P(BD-*b*-EO), the PEO block has exactly the same molecular weight. This enables us to directly compare the characteristics of PEO crystallization inside flexible (PBD) domains with that crystallized inside the rigid (PE) domains.

4.3 Experimental

Poly(ethylene-*b*-ethylene oxide) (P(E-*b*-EO)) was synthesized via hydrogenation of the P(1,4-BD-*b*-EO) material whose properties have been reported previously.[114] The PE blocks contain ethyl-branching on 5-7% of the methylene units resulting from the inevitable occurrence of some 1-2 addition of butadiene during the polymerization. The polydispersity of the diblock copolymer was 1.04. The molecular weight of the PE block was 5,200g/mol, and the molecular weight of the PEO block was 5,600 g/mol. In the molten state, the volume fraction of polyethylene in this diblock block copolymer is about 0.54. To avoid absorption of moisture by PEO, samples were dried under vacuum at 140°C prior to use and all the samples were stored under vacuum.

Diblock copolymer films, approximately 1 mm thick, were prepared by dissolving the material in hot toluene first and slowly evaporating the solvent over one day. For samples subject to shearing, the experiments were carried out using an Advanced Rheometric Expansion System (ARES) from Rheometric Scientific Inc. (RSI). The sample was sheared between parallel, 25 mm diameter plates at 5 rad/s for 30 min at 150°C. The bottom plate was stationary while the top rotated unidirectionally. Samples were then annealed in a vacuum oven for 1 day at 150°C. Different thermal treatments (different isothermal crystallization temperatures) were applied to the samples in a DSC instrument.

Differential thermal analyses were carried out using a Perkin Elmer DSC-7 equipped with liquid nitrogen cooling. The isothermal crystallization experiments were conducted by heating the sample up to 150°C and quickly quenching to the desired crystallization temperature at the maximum speed that can be achieved by the instrument. The quantity of the diblock copolymer used for each experiment was smaller than 0.8 mg. The DSC instrument was calibrated daily using indium and eicosane, at the experimental heating rates.

Part of the small angle X-ray scattering (SAXS) data was collected at the Advanced Polymers Beamline (X27C), located at the National Synchrotron Light Source at Brookhaven National Labs (BNL), Upton, NY. Two-dimensional scattering patterns were collected on Fujitsu image plates, then read by a Fujitsu BAS 2000 image plate reader. Custom software at BNL was used to subtract background noise and perform

circular averaging. The wavelength of X-rays was 1.307 Å and the camera length was 1510 mm. Additional SAXS experiments were also conducted at the University of Massachusetts at Amherst. Ni-filtered Cu-Kα radiation from a Rigaku rotating anode operated at 8 kW was used for small-angle X-ray scattering (SAXS) measurements. The primary beam was collimated by a set of three pinholes. A gas-filled area detector (Siemens Hi-Star) 1 m from the sample was used to record the scattering pattern. The flight path between the sample and the detector was evacuated.

Films for optical microscopy were prepared by evaporating a 7% solution of block copolymer in hot toluene onto a glass cover slip, yielding a film approximately 10-100μm thick. These samples were observed with an Olympus BX60F3 optical microscope under crossed polarizers. Two Mettler FP80 hot stages were used in these experiments, one was held at 150°C, while the other was held at the desired crystallization temperature. Melted samples were rapidly transferred from the hot stage at 150 °C to the hot stage at the crystallization temperature and the crystallization process was observed under the optical microscope.

TEM and electron diffraction experiments were conducted on a JEOL 2000 FX-II instrument. The diffraction camera length was calibrated using an internal gold standard sputtered directly onto some of the grids observed. To prepare specimens for TEM, a small piece of copolymer sample was microtomed using a Leica Ultracut Cryomicrotome with a diamond knife at –110°C to obtain ultra thin (about 40nm) sections. No solvent or water was used in microtoming and collecting the specimens in order to minimize moisture absorption by the PEO. The thin sections were stained using RuO_4 and observed

with TEM. RuO_4 stains both PE and PEO, however, it stains amorphous material more readily than crystalline material due to faster diffusion of the stain in the amorphous material.

4.4 Results

4.4.1 General Characterization

Figure 4.1 shows a typical DSC heating thermogram of P(E-*b*-EO) block copolymer. Melting endotherms for both the PEO block and the PE block are present, indicating crystallinity in both blocks. The melting temperature (T_m) of PEO is observed at 50.7°C, while the T_m of PE is at about 95°C. The broad melting endotherm of the PE block is probably due to a distribution of crystallite sizes resulting from the presence of ethyl-branching on 5-7% of the methylene units. The heat of fusion (ΔH) of the crystalline PEO block in the diblock was 144 J/g. Comparing with the heat of fusion for an infinite, perfect PEO crystal (ΔH_f^o) obtained by Buckley and Kovacs on PEO homopolymer (188.9 J/g)[65], the degree of crystallinity of PEO in P(E-*b*-EO) is estimated to be about 76%. The ΔH of the PE block was 84 J/g, which corresponded to about 30% crystallinity in the PE domains. WAXS results (not shown) indicate that both PEO and PE crystallize in their common structures: monoclinic and orthorhombic respectively.

4.4.2 Morphological Study

Figure 4.2 shows SAXS data for the P(E-*b*-EO) block copolymers under several different thermal conditions. At 130°C, both the PE and the PEO blocks were molten. The SAXS data taken at this temperature (Figure 4.2a) shows four orders of reflection at integral multiples of the scattering vector of the primary peak, corresponding to a

microphase separated lamellar morphology with a lamellar long spacing of 17.2 nm. When the sample was cooled to 80°C, PE crystallized while the PEO domains remained amorphous. As shown in Figure 4.2b, the lamellar spacing increased from 17.2 nm to 20.4 nm upon crystallization of the PE domains at 80°C. When the temperature of this same sample, with the PE already crystalline, was further decreased to 30°C, the crystallization of PEO caused a small increase of the spacing from 20.4 nm to 21.5 nm as indicated by the SAXS data in Figure 4.2c. When the same sample was heated back up to 80°C the PEO crystallites melted, and the lamellar spacing returned to about 20.3nm, as indicated by the SAXS in Figure 4.2d. A different sample was quenched from the melt at 130°C into liquid nitrogen, and the SAXS from this sample is shown in Figure 4.2e. The lamellar spacing of 21.2 nm is similar to that obtained by sequential crystallization of PE and then PEO (Figure 4.2c).

To further study the effect of crystallization upon the melt morphology, TEM studies on samples with different grain structures were conducted. Figure 4.3a shows a TEM micrograph of P(E-*b*-EO) block copolymer that was annealed at 150°C for 12 hours and then crystallized stepwise first at 80°C and then at 30°C. The bright regions are more lightly stained PEO crystalline domains, and the dark regions are more heavily stained PE domains with their greater amorphous content. The enlarged inset shows small unstained PE crystallites that appear bright inside the dark PE domains. The sample formed an alternating lamellar morphology (although with a relatively small grain size), consistent with the SAXS data. Figure 4.3b shows a TEM micrograph from another sample that was subjected to shear in a plate-plate rheometer at 150°C prior to the same stepwise crystallization procedure. In contrast to Figure 4.3a, a lamellar morphology with a

moderate degree of alignment and significantly enhanced long range order was observed. It is well known that shearing can dramatically improve the long-range order of amorphous block copolymers.[115] However, in the present system, this improved long range order is observed in the crystalline state. Thus, the characteristics of the lamellar morphology in molten state act as a template for the crystalline morphology. These results are consistent with optical microscopy experiments (not shown) in which the Maltese cross, characteristic of unconstrained crystallization, was absent. TEM and optical microscopy results both indicate that crystallization of both PE and PEO blocks occurred within the confined spaces defined by the microphase separation in the melt.

The orientations of the PE and PEO crystallites inside the microphase separated lamellar domains were determined by TEM and electron diffraction. Figure 4.4a is an indexed electron diffraction pattern of P(E-*b*-EO), taken from the region inside the selected area aperture, shown in Figure 4.4b. The sample was first shear aligned and then crystallized stepwise, first at 80°C and then at 30°C. However, similar behavior was observed for all samples prepared under different thermal conditions. In order to avoid damage to the crystalline structure due to staining, the samples for electron diffraction were not stained. Consequently, the image contrast in Figure 4.4b is from diffraction contrast and mass thickness contrast arising from the degree of crystallinity and density differences between the PE and PEO domains. From Figure 4.4b, the lamellae inside the selected area aperture are observed to all be oriented in approximately the same direction. The diffraction (Figure 4.4c) indicates uniaxial orientation of crystallites with the PEO chain axis perpendicular to the microphase separated lamellar domains. The *120* reflections are oriented parallel to the lamellar layers in the image, indicating that the

[001] crystallographic direction which is also the chain axis is perpendicular to the layers. This diffraction pattern of the PEO block is the same as that observed in P(BD-*b*-EO) previously.[114]

The *110* reflections arising from PE crystallites are also visible in Figure 4.4a as arcs oriented parallel to the lamellar layers in Figure 4.4b. The *200* reflections from the PE crystallites have similar spacing as stronger reflections from the PEO crystallites and thus cannot be clearly resolved. These results suggest that the *c*-axis of the PE crystallites is also oriented normal to the microphase separated domain interfaces. Base on our results, a schematic of the morphology of P(E-*b*-EO) is illustrated in Figure 4.5.

4.4.3 Crystallization Behaviors

Figure 4.6 shows the PEO crystallization exotherms of both P(E-*b*-EO) and P(BD-*b*-EO) block copolymers recorded during a DSC cooling run. The cooling rate is 10°C/min. Confining the PEO crystallization between rigid PE microdomains as compared to flexible PBD microdomains results in a noticeable decrease in the crystallization temperature. Figure 4.7 gives the DSC heating thermograms of P(E-*b*-EO) block copolymers prepared under different isothermal crystallization temperatures (T_c). The samples were all crystallized at 80°C first and then at different PEO isothermal crystallization temperatures (30°C-44°C). Thus, the crystallization condition for the PE block is identical and any variation observed can be ascribed to the different PEO crystallization conditions. Also shown in Figure 4.7 is a DSC thermogram of P(BD-*b*-EO) crystallized at 34°C. Comparing the data, the most significant difference between the heating thermograms is that the second melt endotherm observed in P(BD-*b*-EO), which is due to reorganization during heating,[114] is absent in P(E-*b*-EO). Reorganization

and thickening of the crystalline lamellae require large changes in the domain size, which are possible for P(BD-*b*-EO) since the PBD block is well above its T_g. However, in P(E-*b*-EO) the rigid, crystalline PE domains inhibit such reorganization. As a result of the rigid confinement, the melting temperature and the degree of crystallinity of PEO were found to be lower than in P(BD-b-EO), 76% in P(E-b-EO) as compared to 88% in P(BD-*b*-EO). The melting endotherms were also broader in P(E-b-EO) as compared to P(BD-b-EO).

Figure 4.8a gives SAXS results for P(E-b-EO) samples that were crystallized at different PE crystallization temperatures and subsequently quenched to 30°C where the PEO crystallization takes place. Shown in Figure 4.8b are SAXS results for samples crystallized at 80°C first and then quenched to different temperatures for PEO crystallization. The resulting lamellar long periods as a function of crystallization temperature are plotted in Figure 4.9. As shown in Figure 4.9a, for samples crystallized at different PE crystallization temperatures (75°C - 90°C) but identical PEO crystallization temperature (30°C), a linear increase in lamellar long period with increasing PE crystallization temperatures was observed. On the other hand, as shown in Figure 4.9b, for samples where PE was crystallized at the same temperature (80°C) but PEO crystallization temperatures were varied (30°C - 46°C), the lamellar long periods were nearly constant.

4.5 Discussion

In the present study, the PE blocks were found to orient perpendicular to the microdomain interfaces. This is in contrast to previous studies on PE containing block

copolymers where the PE crystalline chains were found to orient parallel to the microdomain interfaces when crystallized at room temperature or above.[8,9,11] As illustrated in Figure 4.10, the difference in orientation between our material and those used in previous studies may result from a difference in the interfacial area per molecule between the PE containing block copolymers previously studied and the current system. For strongly segregated diblocks in the amorphous state,[1] the interfacial area per junction scales as $N^{1/3}$. However, the crystalline PE lamellar thickness is much more dependent on the crystallization temperature than on molecular weight. For high molecular weight PE containing crystalline / amorphous block copolymers studied previously, the interfacial area per junction is large enough to allow the PE crystalline chains to orient parallel to the microdomain interface. Such an orientation allows crystallization to proceed without deformation of the microdomain structures.[1] In contrast, the block copolymer of the present study has a low molecular weight resulting in a much smaller interfacial area per junction of $A \approx 2.1$ nm^2. If the parallel orientation is adopted, it would require very thin PE crystalline lamellae, on the order of $A^{1/2}$ or 1.5 nm which are not stable. Consequently, the perpendicular orientation is preferred for these low molecular weight materials.

Crystallization of PE and PEO in P(E-*b*-EO) results in an increase in lamellar long period in addition to a density change upon crystallization. However, the characteristic lamellar grain structure present in the molten state is retained. This observation is consistent with previous work on P(BD-*b*-EO).[114] Increases of microdomain spacing upon crystallization in crystalline / amorphous block copolymers have been reported previously,[38] where it was considered to be evidence of disruption of the microphase

separated morphology formed in the molten state. In our study, it is clearly shown that even with significant variation in the domain spacing, the characteristics of the block copolymer grain structures are still maintain after crystallization.

When PE starts to crystallize at 80°C or above, the PEO domains are amorphous and flexible. The confinement influencing PE crystallization is solely from block incompatibility, similar to PEO crystallization in P(EO-*b*-BD), and thus changes in the domain spacing are possible. Furthermore, the lamellar spacing of the PE domains in the melt is only about 8 nm, smaller than the thickness of typical PE crystalline lamellae. Consequently, only one crystalline PE lamella can form across each domain. This may help prevent crystalline lamellar branching, which is a typical feature of spherulitic growth, and help preserve the melt morphology. In addition, due to the small domain size in the melt-state, there is a driving force for the domains to thicken and form more stable PE crystallites. Consequently, the lamellar spacing was found to increase upon PE crystallization and to be a linear function of the PE crystallization temperature (Figure 4.9a). Subsequent crystallization of PEO blocks resulted in little or no change in domain spacing (Figure 4.9b) because the previously crystallized PE lamellae act as rigid and almost undeformable walls and the situation becomes similar to poly(styrene-*b*-ethylene oxide) block copolymers.[37,72] For crystallization of crystalline / amorphous block copolymers inside flexible domains, the energy barrier to form thicker or eventually extended chain crystals is the entropic term due to stretching of the amorphous chains.[2,3] On the other hand, for crystallization in rigid domains, the polymer chains are anchored to an undeformable interface. The previously crystallized PE microdomains restrict the motion of the PEO chains and resist changes in lamellar spacing. Thus, a larger

thermodynamic driving force is required for PEO to crystallize and the crystallization temperature is depressed (Figure 3.6).

A plot of PEO T_m vs. isothermal crystallization temperature (T_c) is given in Figure 4.11. For comparison, data from our previous study of P(BD-b-EO) are also shown.[114] In the previous study of P(BD-*b*-EO) block copolymers, we observed non-integral folding of PEO crystallites and both the melting temperatures and the crystalline lamellar long periods were also found to be dependent on the crystallization temperature (T_c). Unlike P(BD-*b*-EO) systems, the melting temperatures shown in Figure 4.11of P(E-*b*-EO) display only small changes as the PEO crystallization temperature is varied. Furthermore, the highest temperature at which PEO blocks were experimentally observed to crystallize was depressed in P(E-*b*-EO) to 46°C from a value of 52°C in P(BD-*b*-EO). Table 4.1 gives the PEO crystalline domain thickness (l_{PEO}) calculated from lamellar long period (L) based on percentage crystallinity and volume fraction. Comparing the data for P(BD-*b*-EO) and P(E-*b*-EO), for crystallization temperatures higher than 46°C, the PEO chains prefer to form crystalline lamellae that are thicker (11.4 nm) than allowed by the PE microdomain confinement (10.5 nm). As a result, stable nuclei with the preferred thickness cannot be formed at these temperatures and crystallization of the PEO is hindered.

4.6 Conclusions

The P(E-*b*-EO) block copolymers in the crystalline state were found to have an alternating lamellar morphology with both PE and PEO crystalline chain stems orienting normal to the microphase separated microdomain interface. Crystallization of the PE

block results in a substantial increase in the domain spacing. However, the lamellar grain structure that existed in the molten state is maintained after crystallization of both blocks. The melt morphology thus acts as a template for crystallization. When crystallization occurs within a flexible microdomain, such as PE crystallization in P(E-*b*-EO), the lamellar spacing is found to be a function of the crystallization temperature. On the other hand, when crystallization proceeds under rigid nano-scale confinement, the lamellar spacing was nearly invariant and little change in the morphology was observed. Crystallization of PEO under rigid confinement from PE domains in P(E-*b*-EO) results in decreases in percentage crystallinity and crystallization temperature relative to PEO crystallization under soft confinement by PBD domains in the analogous P(BD-*b*-EO).

Table 4.1: Lamellar spacing as a function of crystallization temperature of P(E-*b*-EO) and P(BD-*b*-EO) diblock copolymers. L is the overall long period and l_{PEO} is the PEO layer thickness.

T_c (°C)	P(BD-*b*-EO)		P(E-*b*-EO)	
	L (nm)	l_{PEO} (nm)	*L* (nm)	l_{PEO} (nm)
34	21.5	10.3	22.3	10.5
38	21.6	10.4	22.2	10.4
42	22.4	10.8	22.4	10.6
46	23.2	11.1	22.3	10.5
48	23.8	11.4	-	-
50	24.9	12.0	-	-

T_c: isothermal crystallization temperature; *L*: lamellar long period measured by SAXS; l_{PEO}: PEO crystalline domain spacing based on volume fraction and percentage crystallinity.

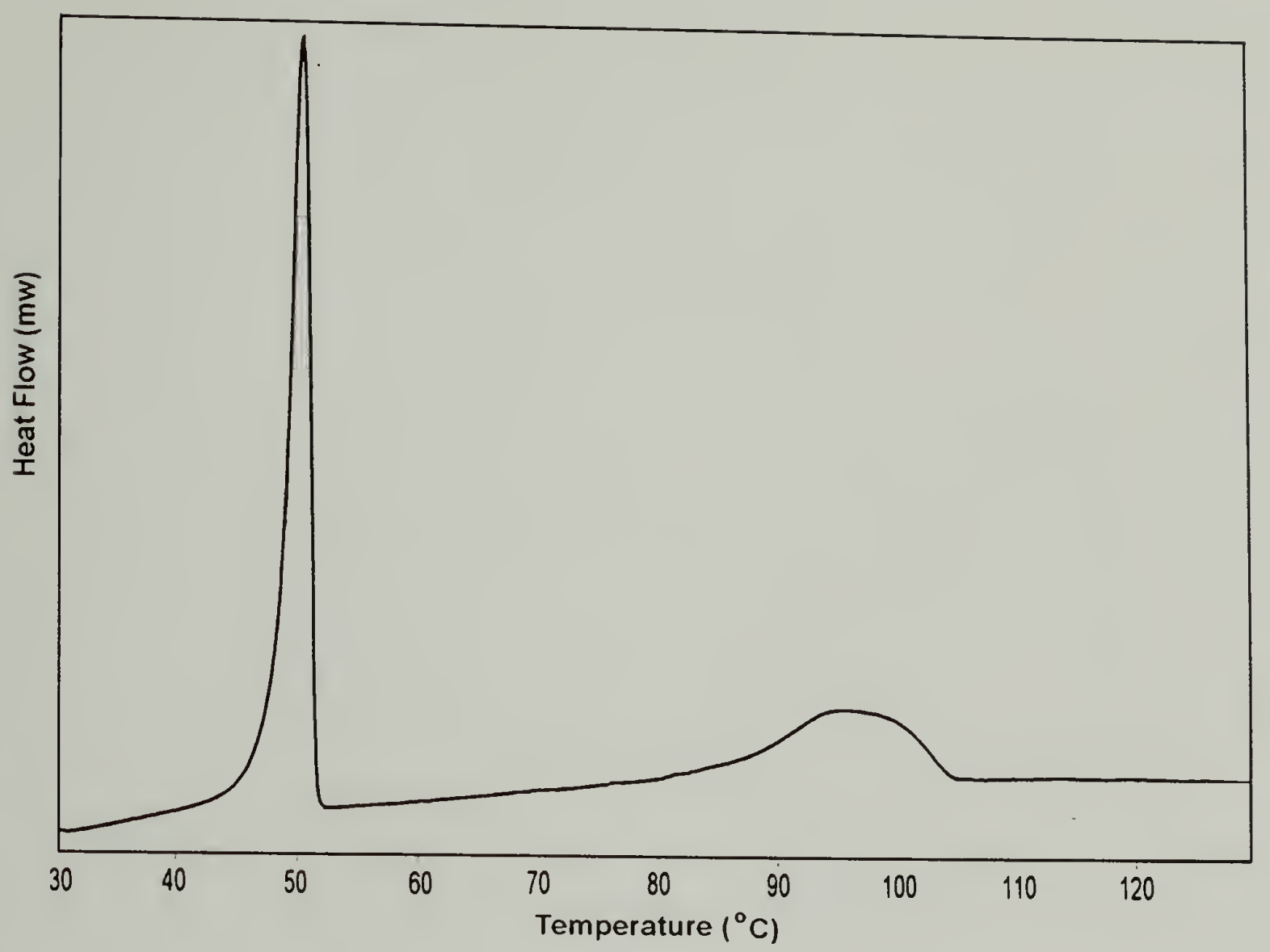

Figure 4.1: DSC heating thermogram of P(E-*b*-EO) diblock copolymer. The heating rate is 10°C/min. The data shown was taken at the second heating run.

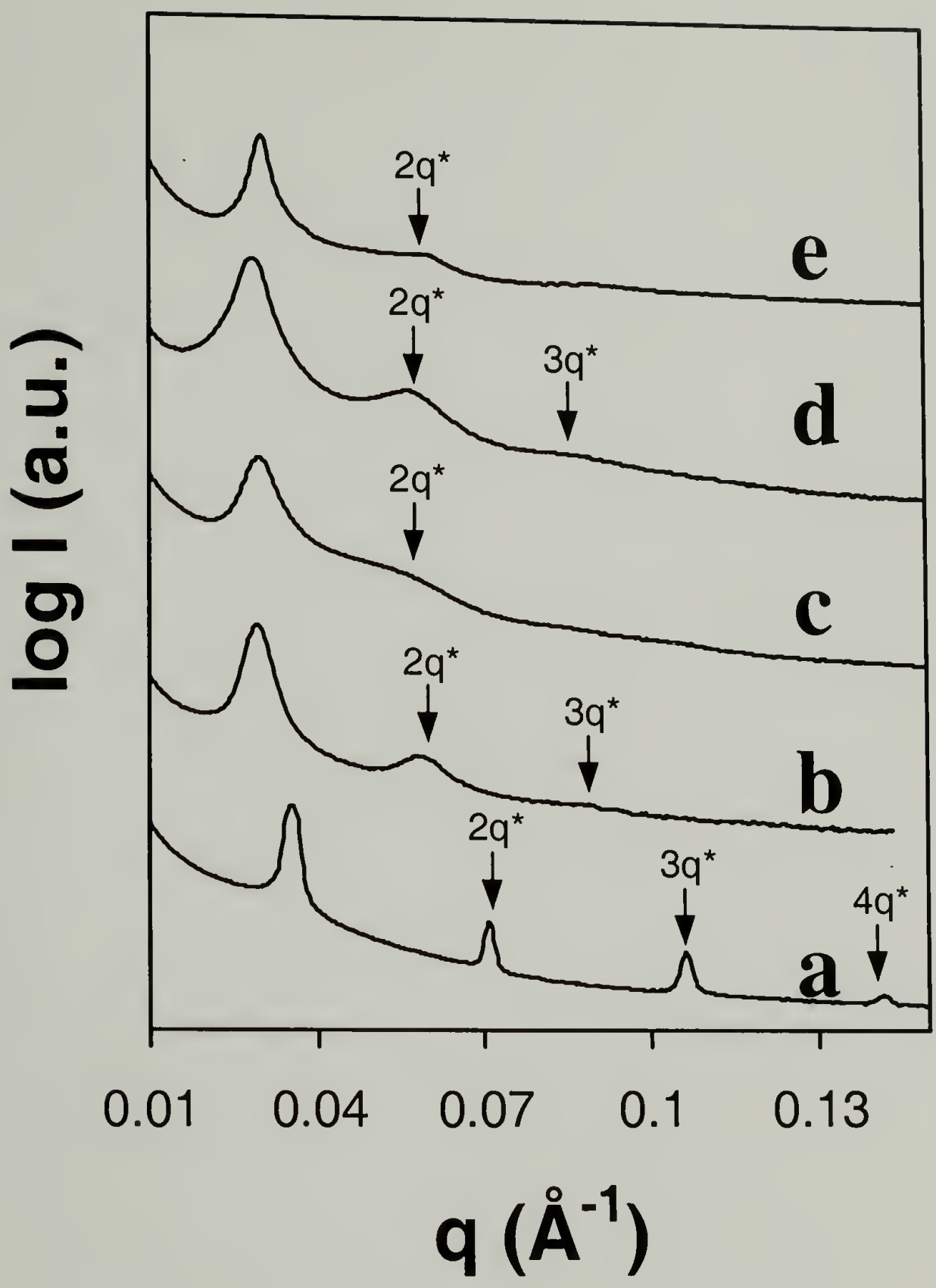

Figure 4.2: SAXS of P(E-*b*-EO) in the melt state and crystallized under different conditions; (a) Melt; (b) Sample held at 80°C after *step-a*; (c) Sample held at 30°C after *step-b*; (d) Sample re-melted at 80°C after *step-c*; (e) Sample quenched in liquid nitrogen from melt.

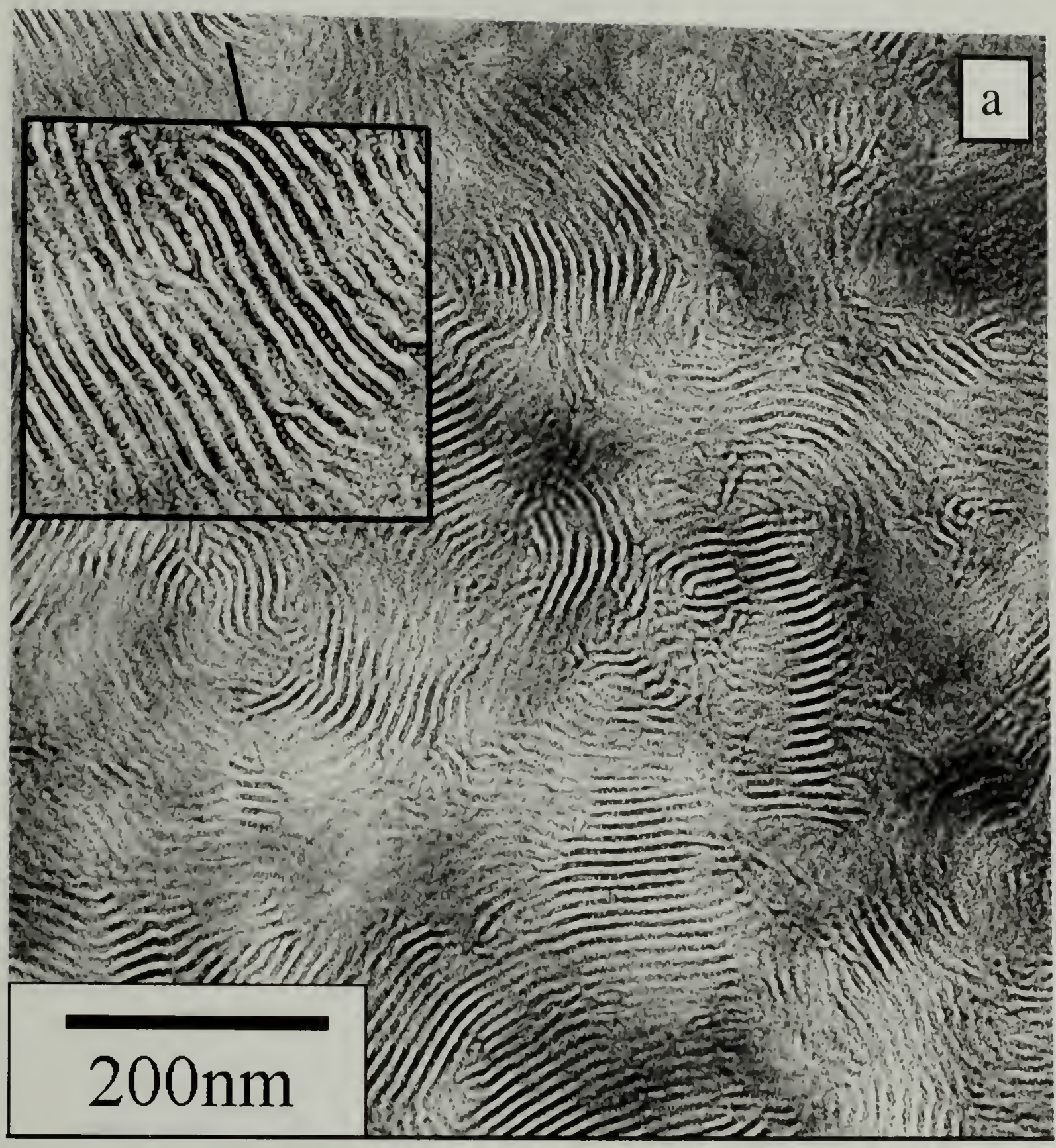

Figure 4.3: TEM micrographs of P(E-*b*-EO) diblock copolymers crystallized at 80°C first and then crystallized at 30°C. (a) Sample was prepared by solution casting followed by annealing at 140°C. (b) Sample was shear aligned in the melt state.

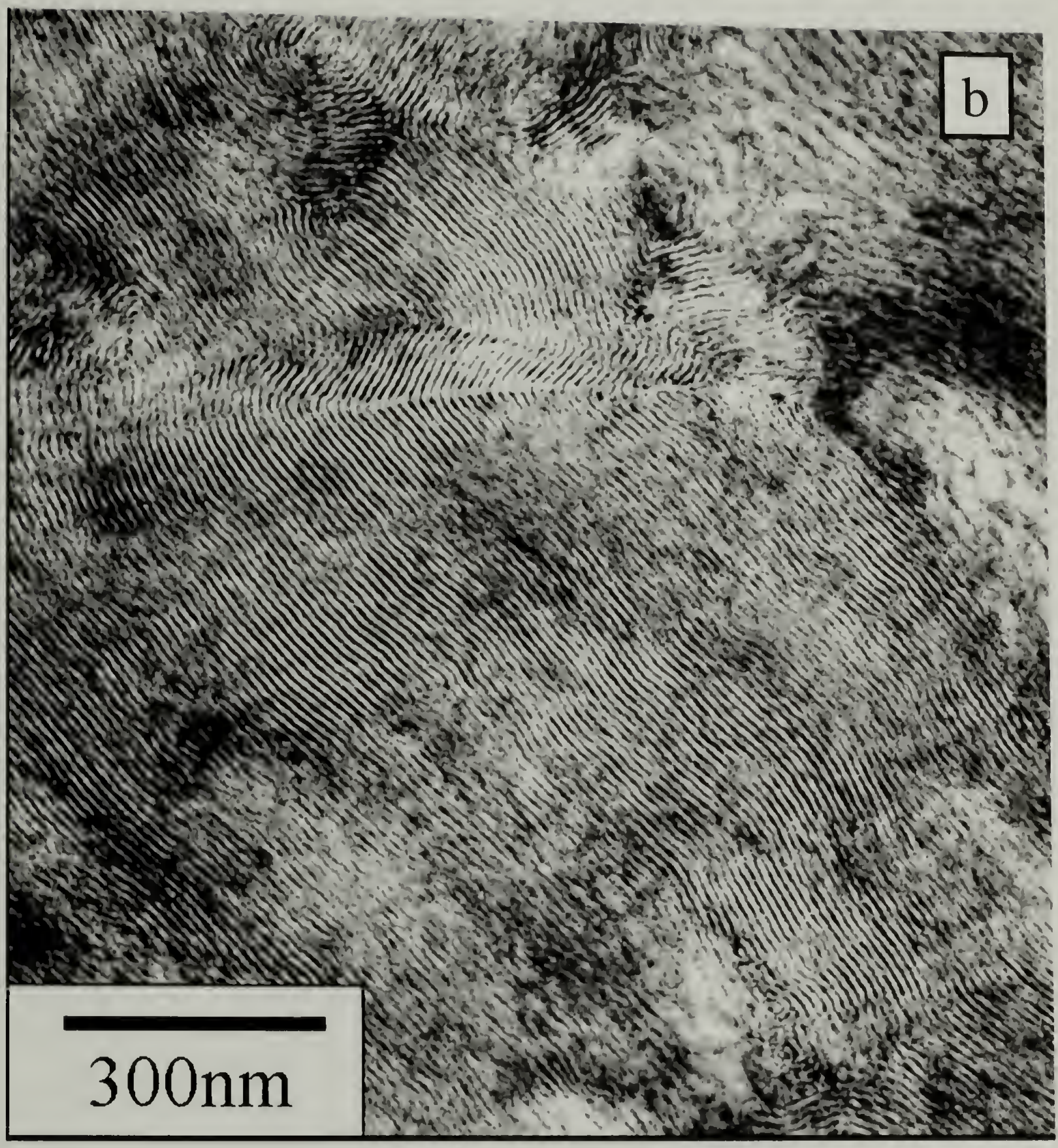
b
300nm

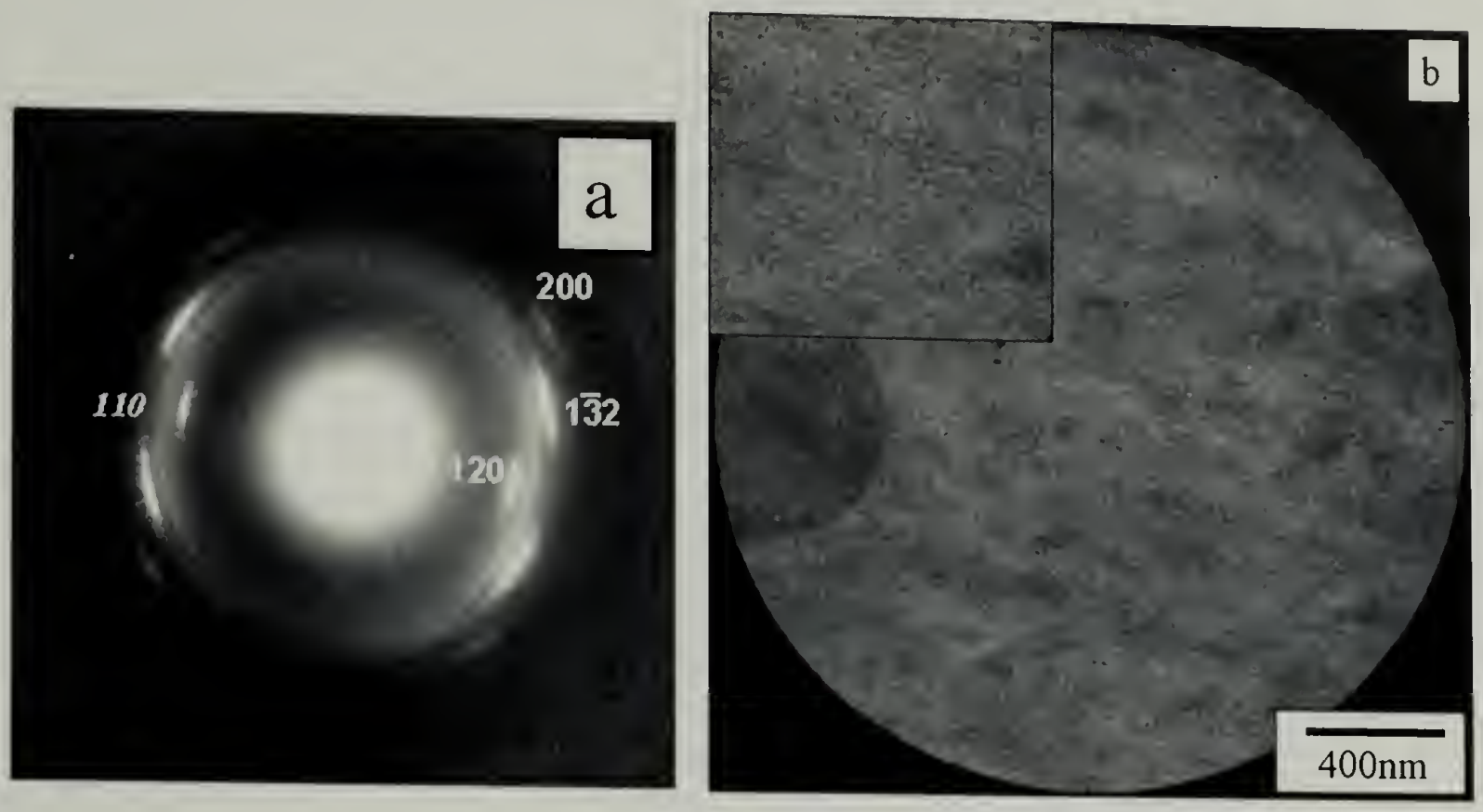

Figure 4.4: Crystalline chain orientation of P(E-*b*-EO) diblock copolymer in the solid state: (a) Electron diffraction pattern; (b) TEM micrograph inside the selected area aperture of the area from which the diffraction pattern was taken; (c) Indexed diffraction pattern schematic.

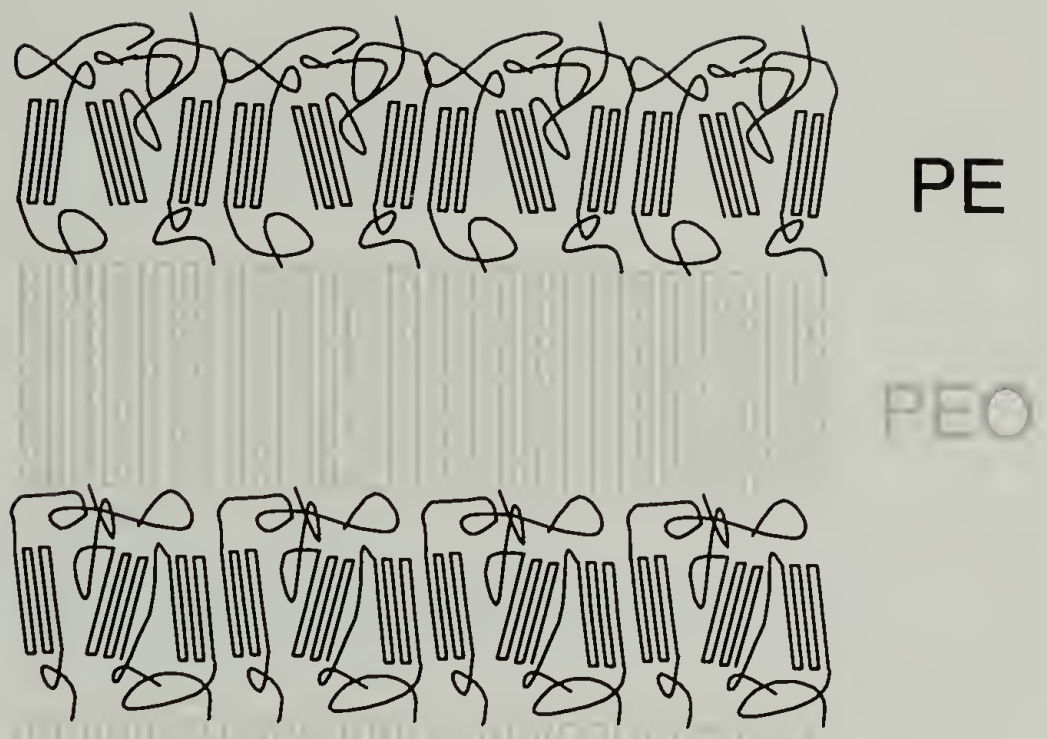

Figure 4.5: Schematic of the morphology of P(E-*b*-EO) in the solid state.

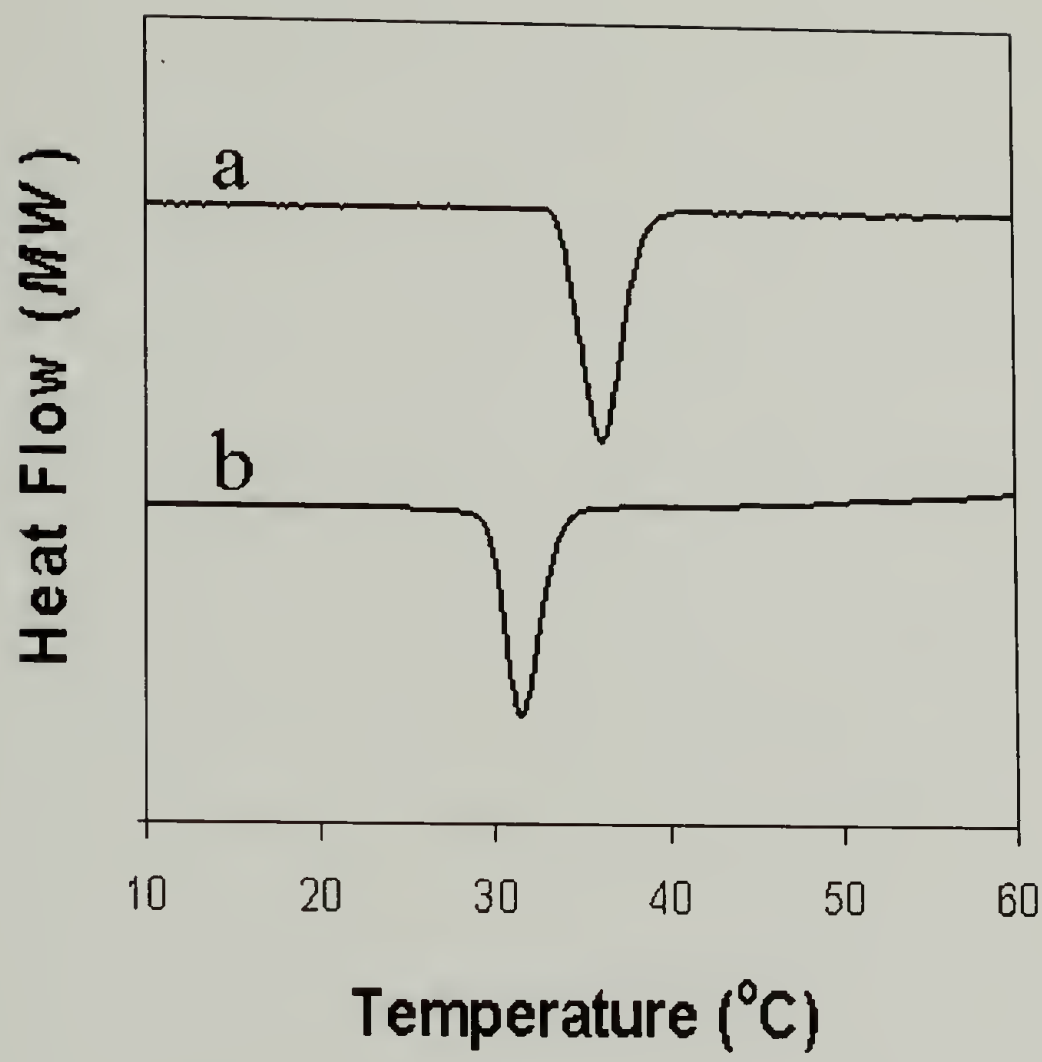

Figure 4.6: DSC cooling exotherms of P(E-*b*-EO) diblock copolymers. The peaks correspond to the crystallization temperature of the PEO block: (a) P(BD-*b*-EO); (b) P(E-*b*-EO)

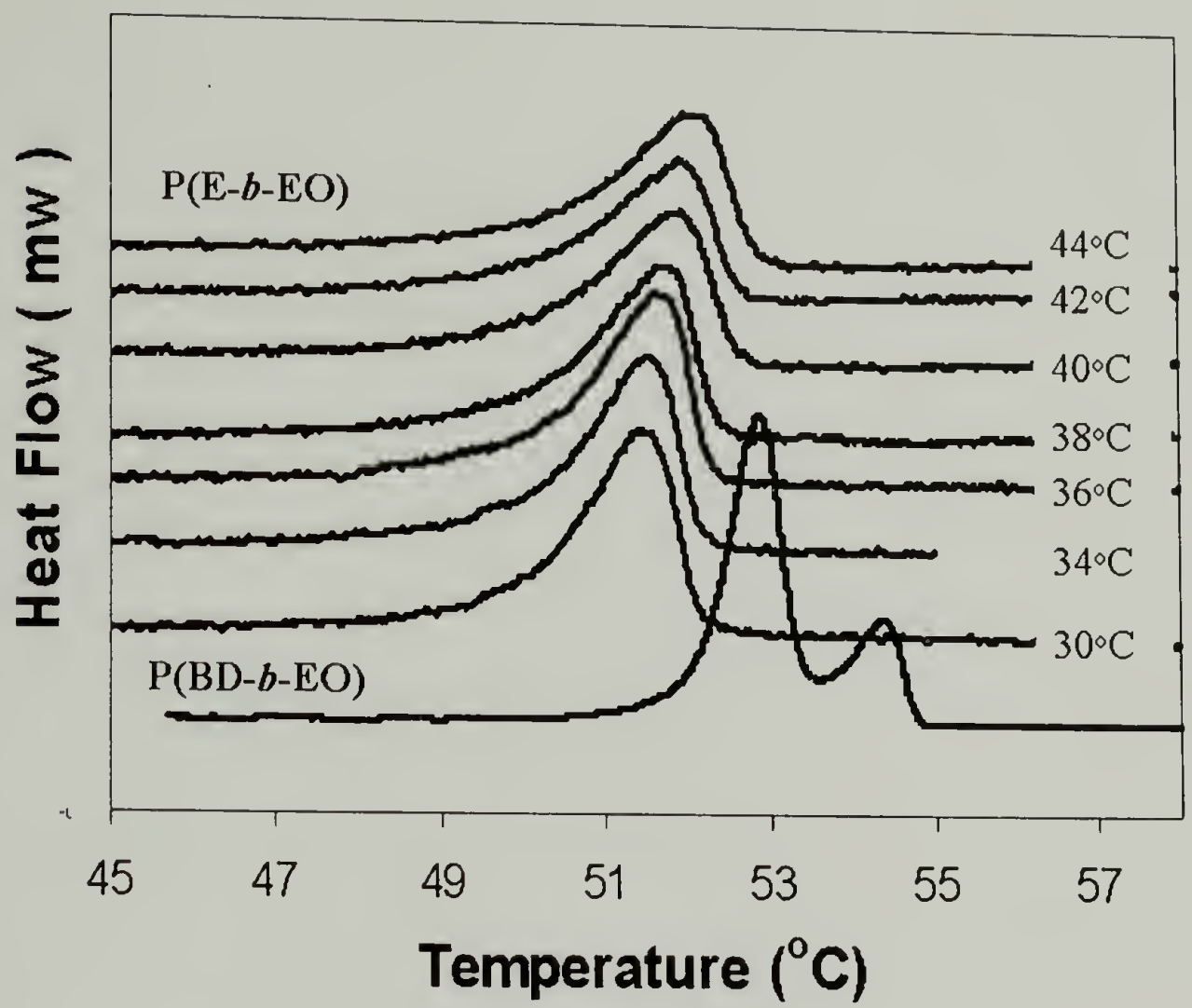

Figure 4.7: DSC melting endotherms of isothermally crystallized P(E-*b*-EO) diblock copolymer samples. The corresponding isothermal crystallization temperature for each run is labeled on the graphs. The heating rate was 2°C/min. For comparison, the melting endotherm of P(BD-*b*-EO) isothermally crystallized at 30°C is also shown.

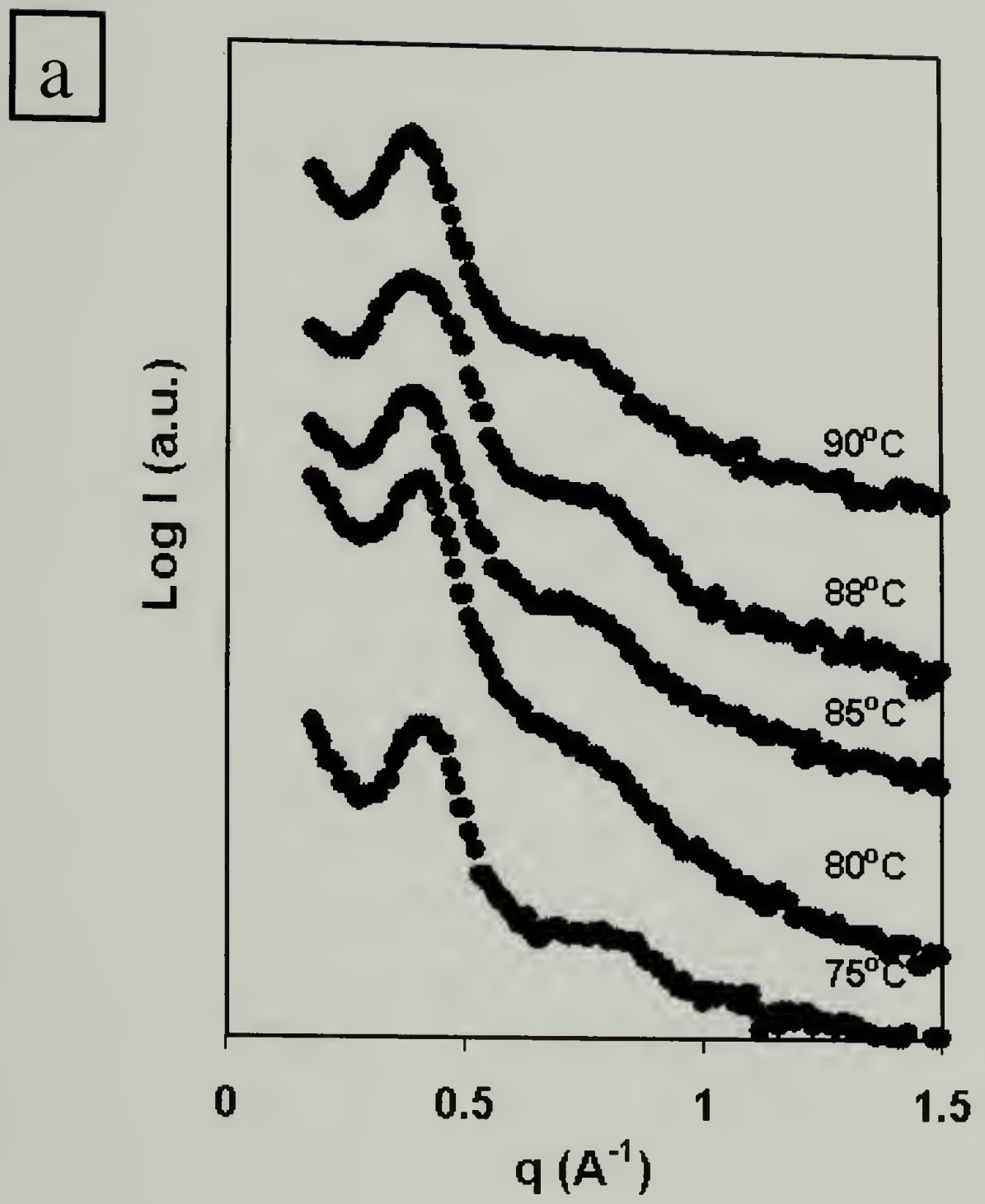

Figure 4.8: SAXS data of P(E-b-EO) diblock copolymers crystallized isothermally at different conditions.

a) PE was first crystallized isothermally at different temperature and then PEO was crystallized isothermally at 30°C;

b) PE was first crystallized isothermally at 80°C and then PEO was crystallized isothermally at different temperatures.

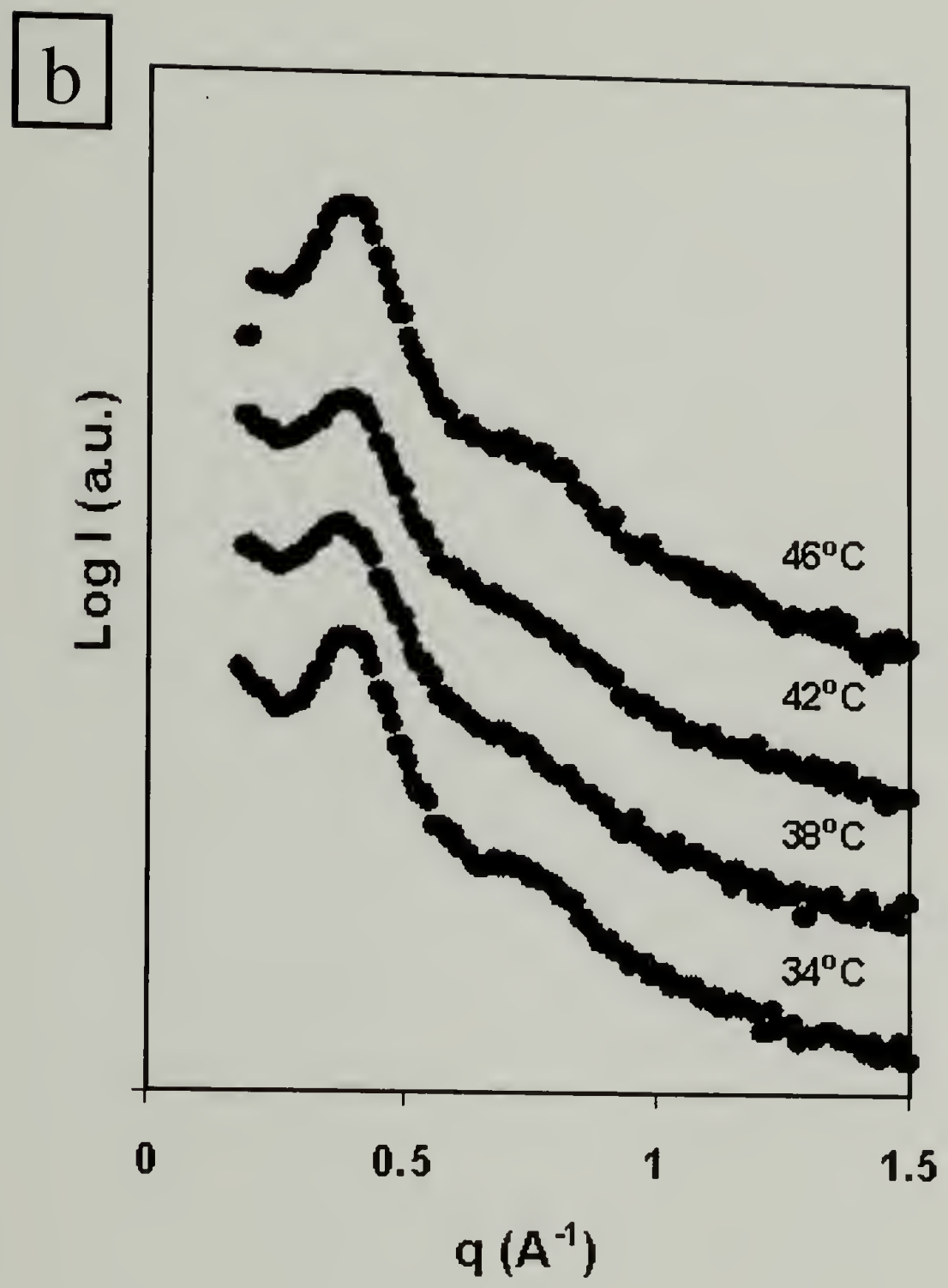
b
Log I (a.u.)
46°C
42°C
38°C
34°C
0
0.5
1
1.5
q (A-1)

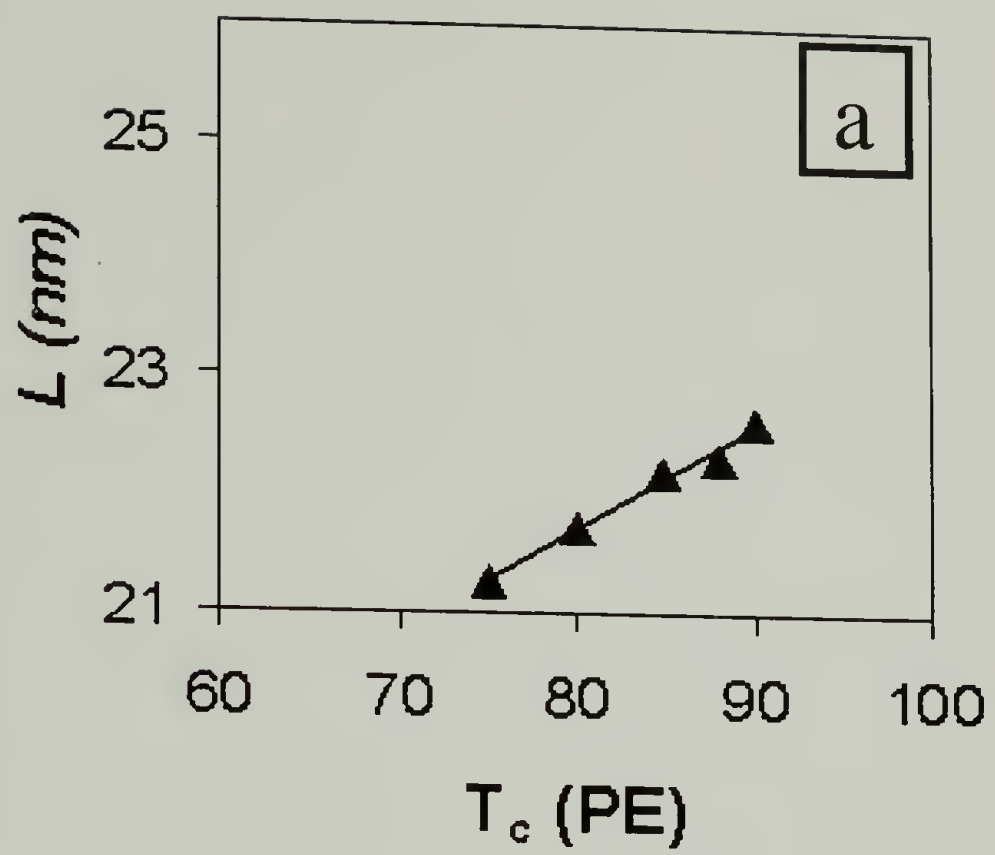

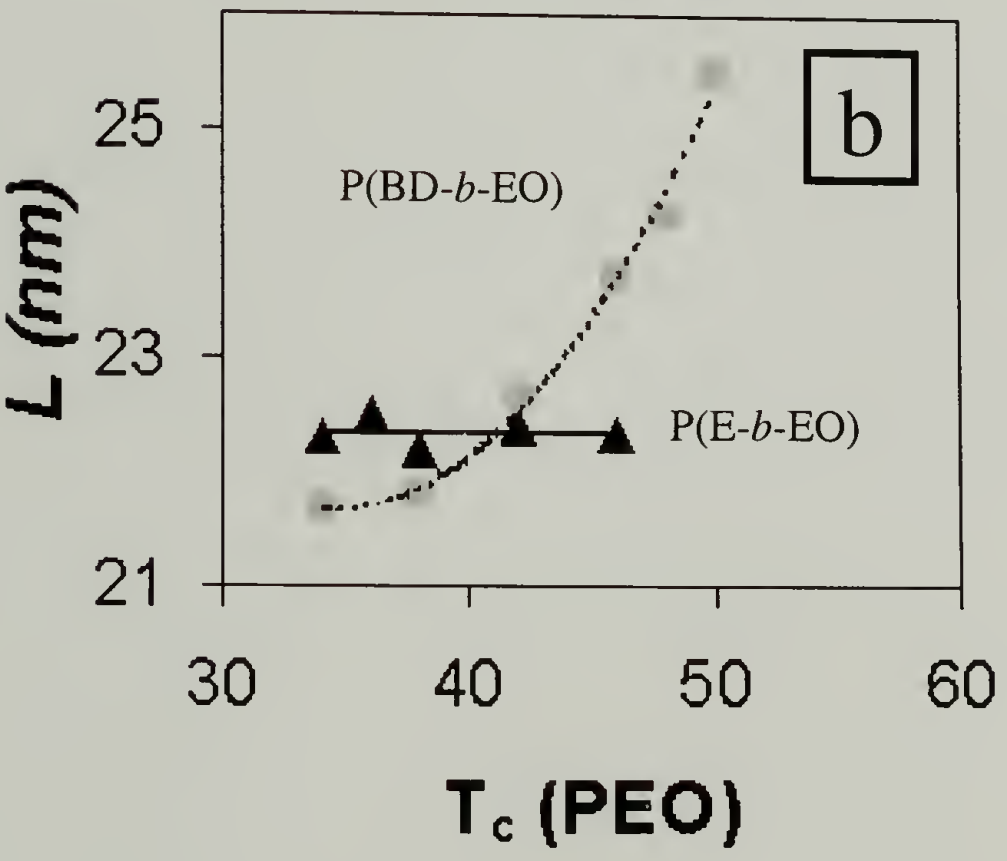

Figure 4.9: Lamellar spacing as a function of isothermal crystallization temperature: (a) PE block crystallized at different temperatures followed by PEO crystallization at 30°C; (b) PE block crystallized at 80°C followed by PEO block crystallization at different temperatures.

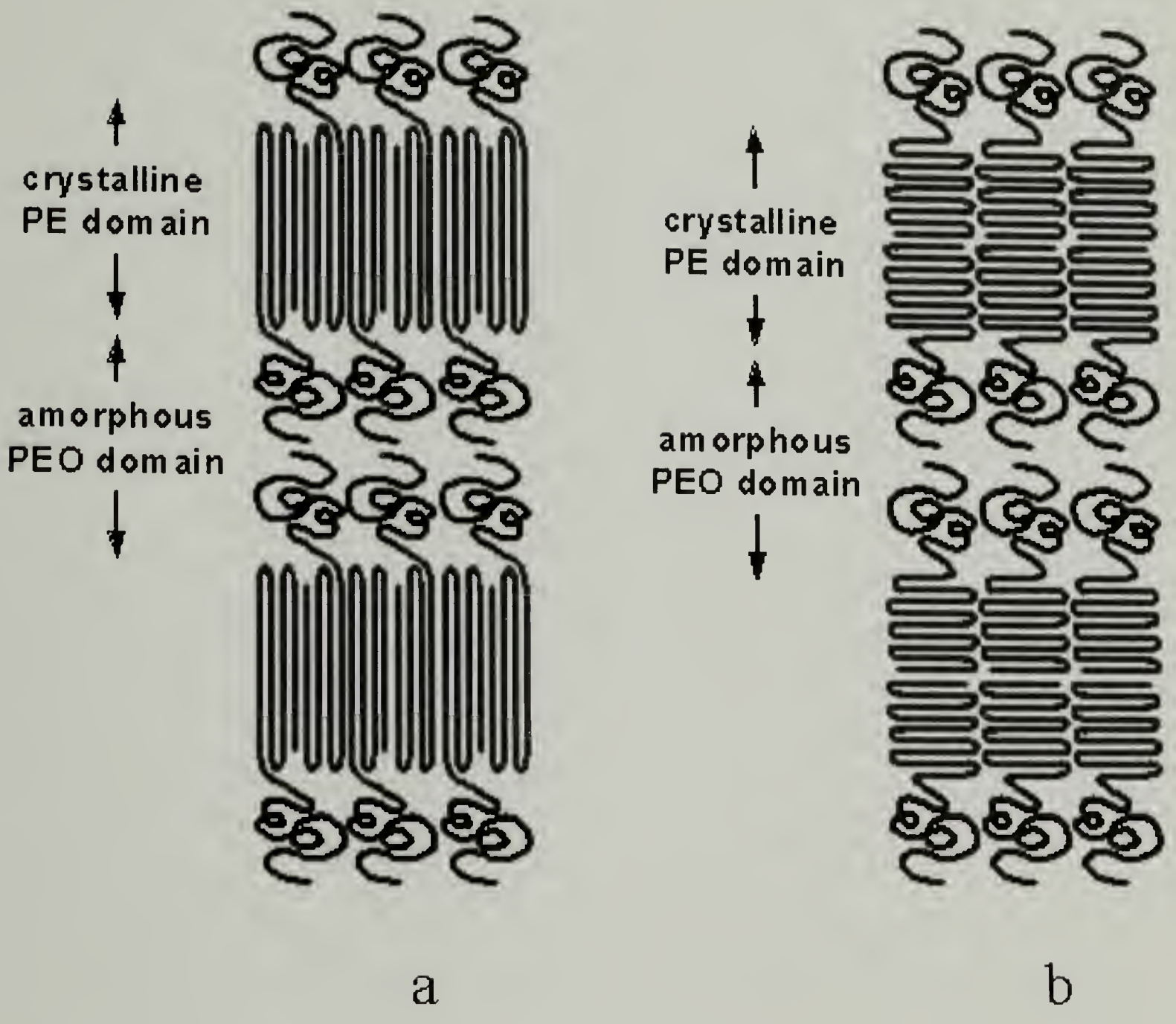

Figure 4.10: Schematics of morphology with different PE crystalline chain orientations: (a) crystalline chain stems perpendicular to interface; (b) crystalline chain stems parallel to interface

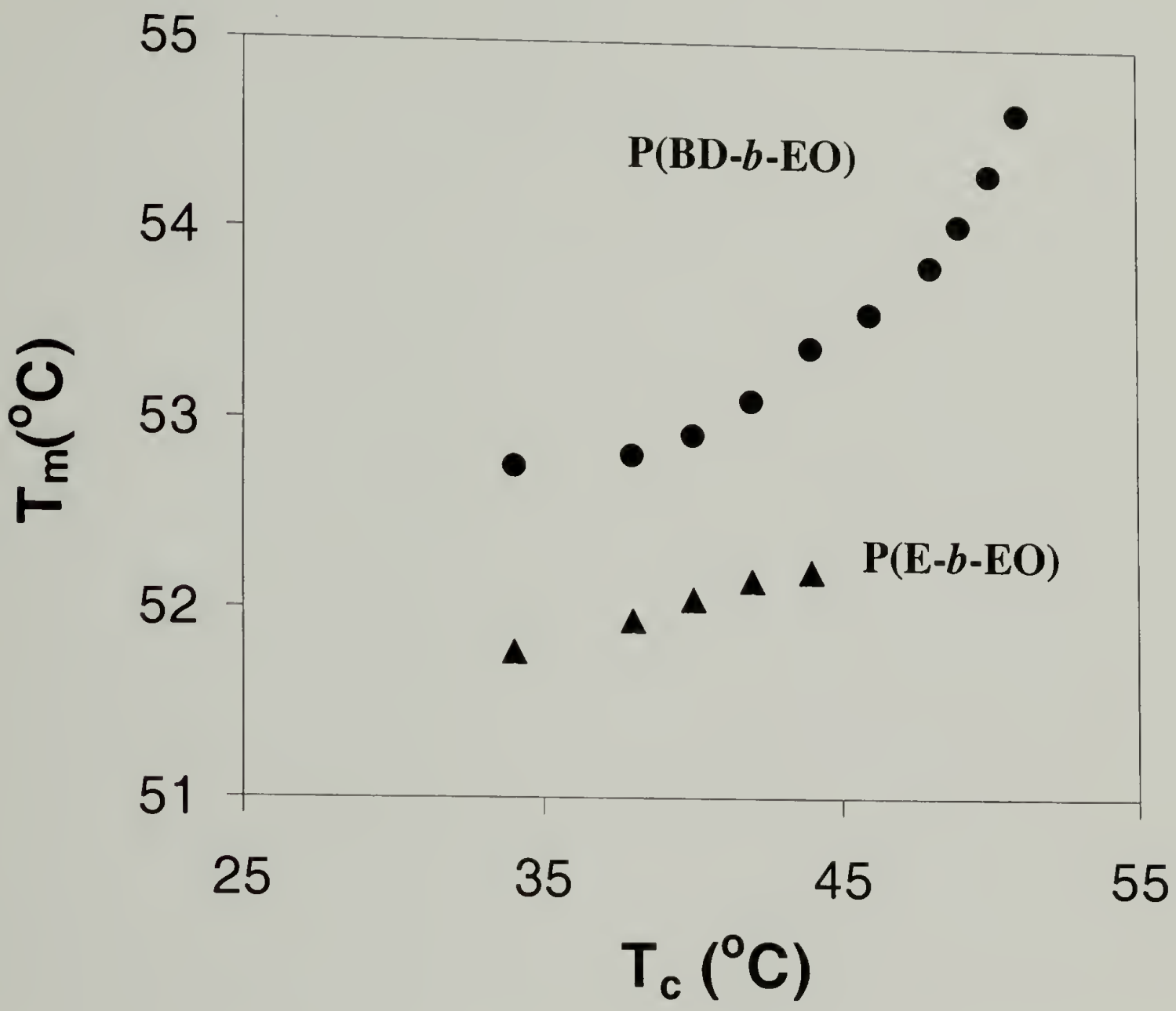

Figure 4.11: Comparison of PEO-block T_m as a function of T_c between P(E-*b*-EO) and P(BD-*b*-EO).

CHAPTER 5

MORPHOLOGICAL EVOLUTION OF CRYSTALLINE-AMORPHOUS BLOCK COPOLYMER IN THIN FILMS

5.1 Abstract

The evolution of the morphology of a crystalline/amorphous diblock copolymer poly(ethylene oxide -*b*- 1,4 butadiene) (P(EO-*b*-BD)) upon crystallization in thin films was studied via interference optical microscopy. Two-dimensional crystallization confined within the PEO lamellar layers was observed with retention of the microphase separated lamellar morphology formed in the melt-state. The morphology was further characterized by TEM and electron diffraction which showed it to consist of alternating layers of PEO and PBD with PEO crystalline chains oriented perpendicular to the lamellar layers of the microphase separated structure. Multiple parallel layers of crystalline PEO were found by electron diffraction to be in *crystallographic registry* even though they were separated by approximately 10 nm thick layers of amorphous PBD.

5.2 Introduction

The morphology of crystalline/amorphous block copolymers has attracted considerable attention recently. Studies on these materials have the potential to shed light on the fundamental physics of polymer crystallization, in general, as well as on crystallization in confined geometry. Theoretical predictions concerning the morphology of semicrystalline diblock copolymers have been developed by DiMarzio and

coworkers[2], Whitmore and Noolandi[3], and Vilgis and Halperin[4] assuming that a thermodynamic equilibrium state can be achieved.

Many diblock copolymer systems with a crystallizable block have been investigated. Crystallizable blocks including poly(ethylene),[4,6,7,10,11,14,17,21,25,42] poly(ethylene oxide),[22,29,30,32,33,115,116] poly(ε-caprolactone)[38] and poly(tetrahydrofuran)[39,40] have been studied. The amorphous blocks investigated vary considerably, in term of their glass transition temperatures and segregation interactions with the crystallizable block. The earliest work on PEO and polystyrene diblock copolymers was done by Lotz and Kovacs[68,69] in 1966, where the crystalline structure of PEO was investigated by solution grown diblock copolymer single crystals. The morphology of P(EO-*b*-S) diblock copolymers as function of the concentration of preferential solvent was investigated by Gervais and Gallot in the 1970's.[30,71] Hamley, Ryan and coworkers recently studied the morphology and crystallization kinetics of a series of P(EO-*b*-BO) (polybutylene oxide) and P(EO-*b*-PO) (polypropylene oxide) diblock copolymers.[10,32,70,116] More recently, the effect of ODT on bulk morphology of P(EO-*b*-S) and crystalline orientation were studied by Cheng and coworkers.[37]

In many of these previous studies, the final morphology was found to be path-dependent. When crystallizing the sample from a microphase separated melt state, one of two results is obtained: (1) The microphase separated morphology is maintained and the crystallizable block crystallizes within volume defined by the block copolymer microphase separated morphology. (2) Crystallization destroys the microphase-separated morphology and a spherulitic texture formed. The morphology of crystalline/amorphous

block copolymers was found to be heavily influenced by kinetics, similar to the case of crystallizable homopolymers. The crystalline chain orientation within the microphase-separated microdomains was also found to vary depending upon the diblock systems and the crystallization conditions.

Although a relatively large body of work exists on crystallizable block copolymers in the bulk, much less work has been done in thin films.[70] Here, we presented a study on thin films of a symmetric poly(ethylene oxide -*b*- 1,4-butadiene) (P(EO-*b*-BD)) diblock copolymer. P(EO-*b*-BD) is in the strong segregation limit, yet with a low T_g amorphous block. The confinement of crystallization arises from the large enthalpic penalty of segmental interactions between the blocks rather than the immobility of the amorphous block. Nonetheless, the molecular weight of the diblock copolymer is low enough so that the thickness of the lamellar microdomains is much smaller than the thickness of crystals in PEO homopolymers. Each of these characteristics contributes to unusual morphological behavior in thin films of this copolymer.

5.3 Experimental

Poly(ethylene oxide -*b*- 1,4 butadiene) (P(EO-*b*-BD)) was obtained from Polymer Source. It was synthesized via sequential anionic polymerization where polybutadiene (PBD) was polymerized first. The molecular weights and molecular weight distributions of the PBD block and the entire diblock copolymer were characterized by GPC. The polydispersity of PBD before the addition of ethylene oxide was 1.05. The polydispersity of the final diblock copolymer was 1.04. The molecular weight for the PBD block was 5,000 g/mol by using PBD standards. The molecular weight for the PEO block was

calculated from ^{1}H NMR and was found to be 5,500 g/mol. The densities of crystalline and amorphous PEO are 1.13 g/cm^3 and 1.03g/cm^3, respectively, while the density of PBD is 0.94 g/cm^3. For a high degree of PEO crystallinity, the volume ratio of PEO to PBD in the diblock copolymer is about 1:1. The melting temperature of the PEO block was found to be around 53°C from DSC measurements.

The thermal stability of P(EO-*b*-BD) was examined by thermogravimetric analysis (TGA). The sample was held at 150°C in the TGA for one hour and no weight loss was observed. GPC results on the material used in this TGA experiment indicated a slight increase of polydispersity to 1.13. The most severe thermal treatment encountered in all of our studies is the melting of the diblock material by holding it at 80°C for at most 5 minutes. TGA results indicate that the copolymer is thermally stable under such conditions without noticeable degradation. To avoid absorption of moisture by PEO, samples were dried under vacuum at 50°C prior to use and all the samples were stored under vacuum.

Silicon wafers were obtained from International Wafer Service and cleaned according to standard procedures in order to remove adsorbed organic contaminates.[117] The substrates was examined by a Rudolph Research AutoEL-II ellipsometer using a helium-neon laser (λ=632.8nm) at an incidence angle of 70°, and found to be free of organic contaminates. Thin films of P(EO-*b*-BD) were prepared by spin casting a 2% toluene solution onto a silicon wafer. Films with different thickness can be prepared by changing the concentration of the solution and the spinning speed. The average thickness of the films was characterized by ellipsometry. The diblock copolymer films, on the

substrates, were melted at 80°C for ~ 5 minutes in a Mettler FP80 hot stage. The sample films were subjected to a step change in temperature by quickly transferring them to a second Mettler hot stage preset at the crystallization temperature of interest. The samples were then observed directly with an interference optical microscope. For lower crystallization temperatures (large undercooling) nucleation was fast, whereas for higher crystallization temperatures, nucleation was very slow. Nucleation could be promoted, however, by touching the edge of the wafer with tweezers or by using the self-seeding method described by Kovacs and Gonthier.[48] Experiments at low undercooling can also be conducted by nucleation at a lower temperature followed by a rapid transfer of the sample to another hot stage at a higher temperature.

The structures of the thin films were studied using an Olympus BX60F3 optical microscope. All the optical images were obtained under reflection conditions to obtain interference colors from a white-light source. Normarski conditions were used to enhance the contrast of the terraced surface of the copolymer thin films.[118] The change in birefringence upon crystallization can not be seen under reflection conditions in the optical microscope. However, crystallization does produce a slight, yet observable, change in the surface topography that enables the study of crystallization in microphase separated diblock copolymer thin films.

X-ray photoelectron spectroscopy (XPS) was carried out using a Physical Electronics Model 5100 with a Mg K_α X-ray source at 500 W. The incident beam angle was 45° and the sampling depth was about 4nm.

Silicon nitride (Si_3N_4) membranes (100nm thick) with a window size of 0.46 mm x 0.46 mm were obtained from Structure Probe Inc. A toluene solution of the diblock copolymer was spin coated onto the membranes. The thin films have the same characteristics as those on silicon wafers as observed via optical microscopy. The polymer thin film was then melted at 80°C and crystallized at various temperatures. The experimental conditions were exactly the same as those cast on silicon wafers. The silicon nitride membranes permit a direct transmission electron microscope (TEM) observation of and diffraction from thin films.[119] TEM and electron diffraction experiments were performed on a JEOL 2000 FX-II transmission electron microscope. The diffraction camera length was calibrated by using an internal gold standard that was evaporated onto one of the membranes.

5.4 Results and Discussion

5.4.1 Linear Growth of Crystallites:

Thin films of P(EO-*b*-BD) with an average thickness of 40nm were spin coated and then heated to 80°C. The reflectance optical micrograph shown in Figure 5.1a shows the distinct color contours across the entire surface of the sample indicative of a microphase separated morphology with lamellar layers oriented parallel to the wafer.[118] Different colored regions indicate different number of layers in an "island and hole" or "terraced" morphology. When this sample was cooled to 25°C, initially no changes were observed. Subsequently, as seen in Figure 5.1b, a front, indicated by a change in the topography, was seen moving across the sample. The direction of the front advancement is given by the arrow. The lower magnification image in Figure 5.1c demonstrates the planar, radial mode of growth associated with the crystallization of PEO block.

The micrographs in Figure 5.1 show that the terraced surface topography arising from the layered morphology of the copolymer is retained as crystallization proceeds. Consequently, PEO crystallizes within the confined spaces defined by the microphase separated morphology without disrupting it. As noted, there is a slight color change before and after crystallization indicating that the film thickness and therefore, the lamellar period of the microphase separated structure has changed only slightly upon crystallization at 25°C. In Figure 5.1, striations and cracks are visible in the crystallized regions. These result from a combination of the density change upon crystallization of the PEO block and the correspondingly small change in the layer thickness. Laterally constraining the multilayered copolymer morphology to substrate surface precludes any large-scale lateral contraction of the film during crystallization. Any contraction must occur locally, resulting in crack formation. XPS results (not shown) on the thin films before and after crystallization show that PBD is always located at the polymer-air interface. The thickness of the film measured by AFM was found to be an integral number of lamellar periods. Consequently, PBD must also be located at the polymer-substrate interface.

Crystallizing the diblock copolymer thin film at higher temperatures (lower undercoolings) yields a lower radial growth rate of the crystallization. Optical micrographs of the crystallization front observed at 45°C are shown in Figure 5.2. The time interval between Figure 5.2a and Figure 5.2b is only seconds. As seen, the island and hole morphology is still preserved. However, a significant change in the interference colors between the crystallized and molten regions of the film is seen in the micrographs.

These color changes correspond to a change in the lamellar period from about 19nm to 24nm brought about by the PEO crystallization. It should be noted, that the discrete terracing of the interference colors is still evident after crystallization, showing that crystallization has not destroyed the multilayered structure initially present and has occurred within the layered framework, even though there is a significant increase in the period. However, the extent of cracking in the sample has dramatically increased over that seen at 25°C. The larger increase in lamellar spacing necessitates a greater lateral contraction in the PEO layers in order to conserve volume. This results in more dramatic cracking.

Figure 5.2c is an enlargement of the growth front from Figure 5.2b. These data show that the crystalline growth front proceeds in three separate layers independently as indicated by distinct interference colors, providing direct visual evidence that PEO crystallization proceeds separately in different layers. There are slight differences in the times at which the fronts reach a given position in the film. This type of staggered crystal growth is observed in the spiral overgrowths of chain folded polymer crystals grown from dilute solution,[120] where the growth in one layer initiates the growth of adjacent layers through a screw dislocation defect.

A careful examination of Figure 5.2a and b shows another unusual feature of the crystallization within the two-dimensional layered morphology. On the right hand side of the figures, holes corresponding to film thickness changes are visible. As the crystallization front advances towards these areas, they strongly distended towards the growth front, even when the growth front is ~10μm away! While one would expect

transport of PEO chains to the growth front from the fluid phase, the confinement of the crystals within the layered structure along with the large increase in the period results in a substantial contraction laterally causing a distortion of the surface features over very large distances.

The radial growth rate was found to be constant at a given temperature. A plot of this linear growth rate as a function of crystallization temperature is shown in Figure 5.3. For PEO homopolymers, the temperature dependence of the growth rate is usually discontinuous and can be separated into different regimes due to a change in the integral fold number.[49,50] However, such discontinuities were not observed here over the temperature range studied.

5.4.2 Self-seeding Experiments

When crystallization was conducted at 45°C or higher, nucleation was very slow and only a few nuclei formed across the entire film. By using a self-seeding method[48], the number of nuclei increases and they form more rapidly and at much higher density. In our studies, the sample film was melted by heating to 80°C for 5 minutes. It was then quenched to 30°C and held at this temperature until crystallization was complete. The sample was then heated to 58°C (slightly higher than the T_m determined by DSC) for 5 minutes. Figure 5.4a is an optical micrograph of the thin film at 58°C where the PEO crystals have melted leaving only a few stable nuclei. Upon cooling to 45°C, crystallites were found to nucleate at many places in the sample as shown in Figure 5.4b. As the crystallization proceeds (shown in Figure 5.4c), the crystallites grow independently in each of layers. Crystallites growing in the same layer are seen to impinge upon one

another. Two crystallites growing in separate, parallel layers appear in the optical micrographs to grow through one another without impinging. The enlarged insets in Figure 5.4c show these two different cases. These results suggest that nucleation and crystallization can occur independently in different layers.

A series of optical micrographs of a sample film crystallized at 50°C is shown in Figure 5.5. The self-seeding method was used to ensure fast nucleation. It is most interesting to notice that the growing crystallites adopt a hexagonal shape that resembles the shape of a PEO single crystal.[48,69] The hexagonal shape of the growing crystallite shows little change when the crystallite becomes larger (up to 100μm in diameter). Previous observations of PEO single crystals have revealed both square and roughly hexagonal shaped crystals.[69] We have also observed (not shown) square growth patterns in these diblock thin films. Subsequent crystallization of the PEO blocks in adjacent layers was found, leading to what appear to be overgrowths on the original crystallites. The crystallites in different layers propagate "cooperatively" across the sample, which is consistent with the observation of distinct layers in the crystallization front in Figure 5.2b. Clearly in this case, the crystalline order in one layer induces the crystallization in adjacent layers, even though the PEO layers are separated by an approximately 100Å of amorphous PBD.

5.4.3 Crystalline Chain Orientation

To further investigate the crystalline structure of PEO blocks, electron diffraction patterns were taken. Diblock copolymer solutions were spin coated onto silicon nitride membranes that are transparent to the electron beam. The samples were melted at 80°C

and crystallized at various temperatures. The same terraced morphology as that of thin films cast on bare silicon wafers was observed by optical microscopy. Figure 5.6 shows a low magnification TEM image of a sample crystallized at 35°C taken by projecting the electron beam through the silicon nitride membrane and, thus, perpendicular to the microphase separated layers of PBD and PEO. The island and hole structure is clearly visible from mass thickness contrast arising from the integral number of layers in different areas. The film has, on average, about 6-7 layers of diblock copolymer lamellae on it. Cracking during crystallization has resulted in the small striations on this image. Marked on this image are locations where electron diffraction patterns were taken. The general pattern obtained is a four-fold spot pattern corresponding to the (120) reflections of PEO. This is identical to the diffraction pattern obtained from PEO single crystals.[69] Numerous diffraction patterns for samples crystallized from 30°C to 45°C were obtained, and all showed the same spot diffraction pattern regardless of the crystallization temperature. The results indicate that PEO chains in the crystal are oriented parallel to the electron beam and the fold surface plane is normal to the electron beam. Since the microphase-separated layers are oriented parallel to the substrate, the crystalline PEO chain stems are oriented perpendicular to the microphase-separated layers. The results are consistent with the observation of hexagonal-shaped crystalline growth at 50°C. The morphology of PEO-*b*-PBD thin films is thus very similar to that proposed theoretically, shown schematically in Figure 1.1. However, the lamellar long period may not follow the scaling law as predicted by equilibrium argument and may instead be kinetically controlled.

In electron diffraction patterns 1-8 and 10-12 in Figure 5.6 only 1 set of four fold spots are observed even though the beam is projecting through multiple layers of the structure and thus multiple crystalline layers of PEO. This can only occur if PEO crystals in adjacent layers are in registry. In the TEM image in Figure 5.6, there are at least 3 different sections that are from different nuclei as characterized by straight boundaries among them. The diffraction patterns within these regions (1-3; 4-8; 10-13) have the same (or very similar) crystallographic orientation. Pattern #9 shows eight reflections, however, it was taken at the boundaries between regions where the PEO orientation was different. Consequently two different oriented regions contribute to this pattern. The eight spot pattern is a result of the overlap of two four-fold patterns corresponding to the two adjacent regions and is actually a superposition of patterns 8 and 10.

5.4.5 Lamellar Domain Spacing in Thin Films

It is observed from interference color obtained during crystallization process that the thickness of PEO block varies upon different crystallization temperatures. To obtain an accurate measure of domain spacing and to investigate the surface topology of the diblock copolymer thin film, samples crystallized at different temperatures were further studied by AFM. Shown in Figure 5.7 are representative AFM micrograph and its corresponding height profile for a thin film sample crystallized at 45°C. The step height corresponds to lamellar long period of microphase separation. The lamellar spacing as a function of crystallization temperature is summarized in Figure 5.8. For comparison, the lamellar spacing of bulk sample is also shown. The thin film results agree with the bulk results quantitatively, indicating that PEO crystallites in both thin film and bulk are not integral folded.

5.4.6 Morphology of Very Thin Films

For diblock copolymer films with thickness less than 10nm, we observed a peculiar surface morphology as shown in Figure 5.9. The dendritic pattern of the crystalline growth is obvious. The most interesting phenomenon is that the center of each branch appears to be hollow, given the overall morphology a "hollow tree" like pattern. The dendritic growth of PEO homopolymers on thin film has been studied previously.[121] However, such morphology was not observed. This phenomenon may be due to edge thickening of the crystallites combined with limited mobility of block copolymers.

5.5 Conclusions

In the melt, the PEO-*b*-PBD diblock copolymers form a lamellar morphology oriented parallel to the substrate. Crystallization confined within the microphase separated PEO layers progresses across the sample with retention of the preformed microphase-separated lamellar morphology. Crystallization at higher temperatures thickens the lamellae but still preserves the layered morphology formed in the melt-state.

The crystallization of one layer was found to induce the crystallization of adjacent layers. The crystallographic registry between adjacent crystalline layers was an unexpected, yet remarkable result since the crystals are separated by intervening layers of amorphous PBD (~100Å thick). This can only occur if the PEO crystallites in adjacent layers originated from the same nucleus and if there is a crystallographic connection between the layers. The development of overgrowth crystallites on a single initial crystallite in Figure 5.5 supports this conclusion. Notice that the facets of the overgrowth crystallites are aligned with those of the parent crystallite. Also notice in Figure 5.5b and

c that each overgrowth appears to be either centered around a hole (white in the image) or located at a point where there is a change in the film thickness, i.e. at the edge of an island or hole. This suggests a defect-controlled mechanism for the spreading of crystallinity between PEO layers. Figure 5.10a illustrates how an edge dislocation that occurs at the boundary of an island or hole results in the spreading of crystallinity to an adjacent layer. A screw dislocation, as illustrated in Figure 5.10b, provides a spiral ramp by which crystallinity can spread to many adjacent layers. This screw dislocation mechanism is the same mechanism that leads to overgrowths in solution grown crystallites.[120,122] The difference here is that the screw dislocation is formed in a two-component layered material rather than a single component material. The structure of screw dislocations in microphase separated lamellar systems has been discussed by Gido and Thomas.[106] These screw dislocations do not require a discontinuity in the core, but rather have the core structure of a helicoid minimal surface. This structure is similar to that of a parking garage in which each circuit around the core moves one up or down between adjacent layers of the same type. When a growing crystallite in a single layer encounters this screw dislocation structure, its growth will carry it up and down the screw dislocation and allow it to spread outward in all the adjacent layers. The crystallographic alignment of all these layers follows since the crystallites in all the layers are actually one single crystal connected through the defect. The edge dislocation mechanism also allows for alignment of crystallites in adjacent layers.

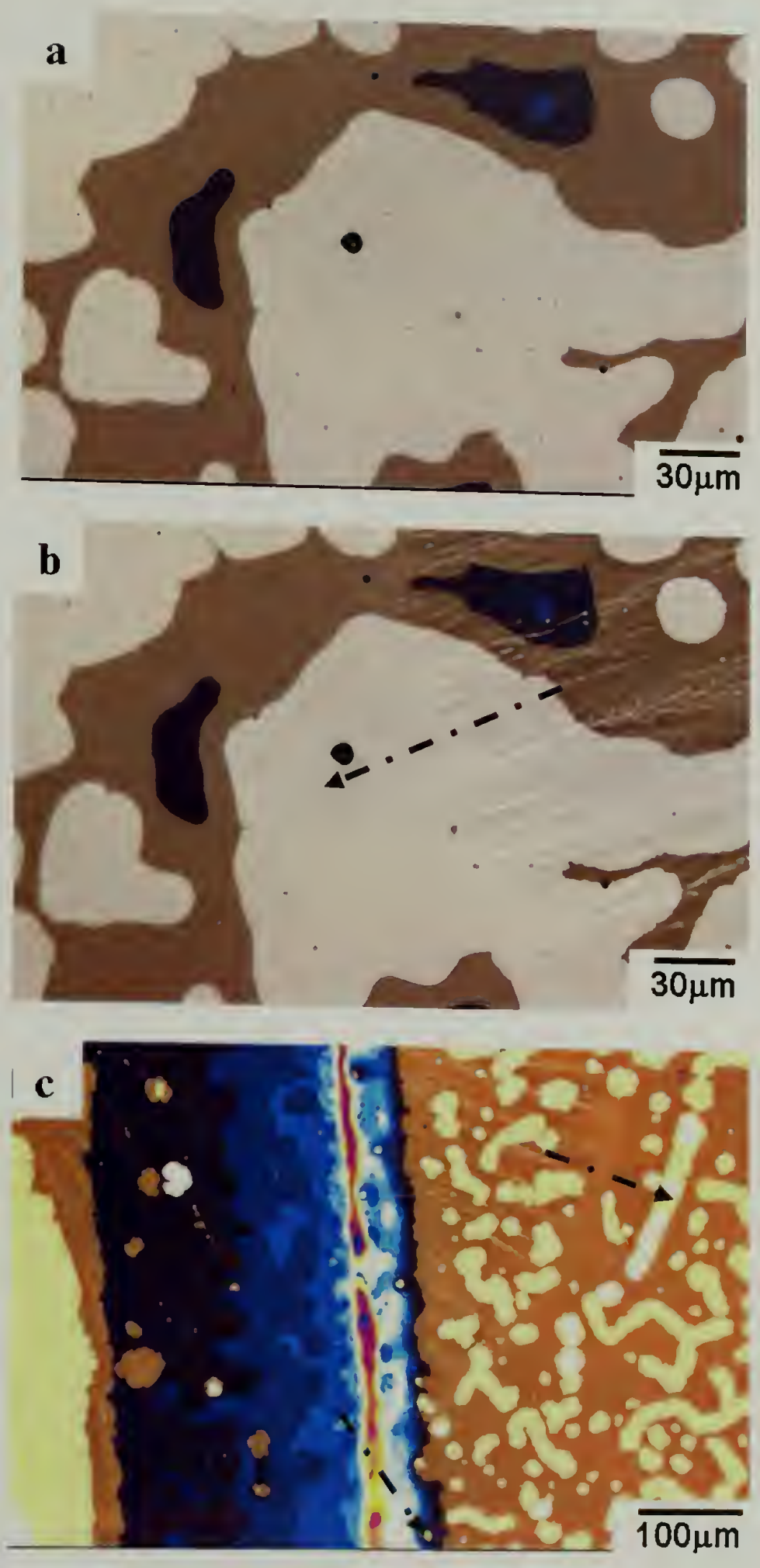

Figure 5.1: Crystallization at 25°C. (a) Thin film at 80°C; (b) Crystallization front at 25°C; (c) Observation at smaller magnification. (arrows indicate crystallization directions)

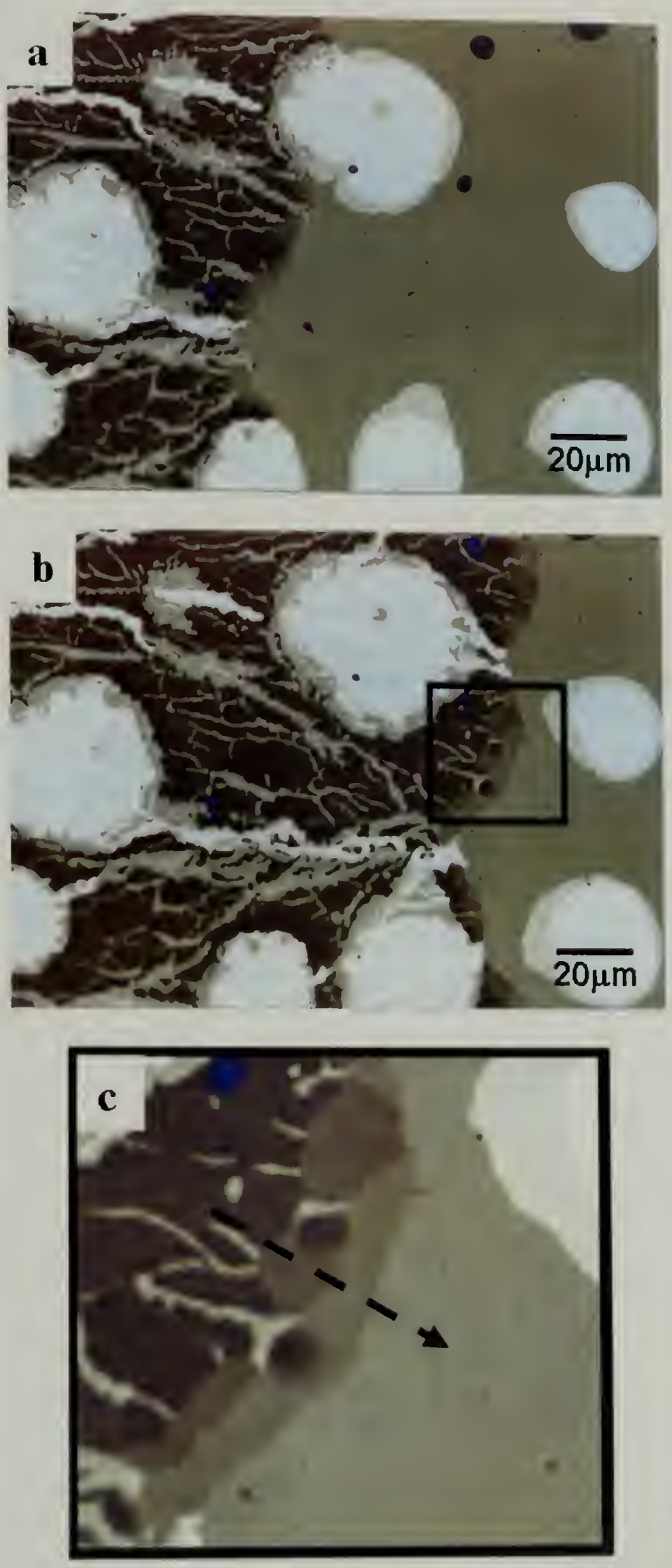

Figure 5.2: Crystallization at 45°C. a) earlier time; b) later time; c) inset from (b). (arrow indicates crystallization direction)

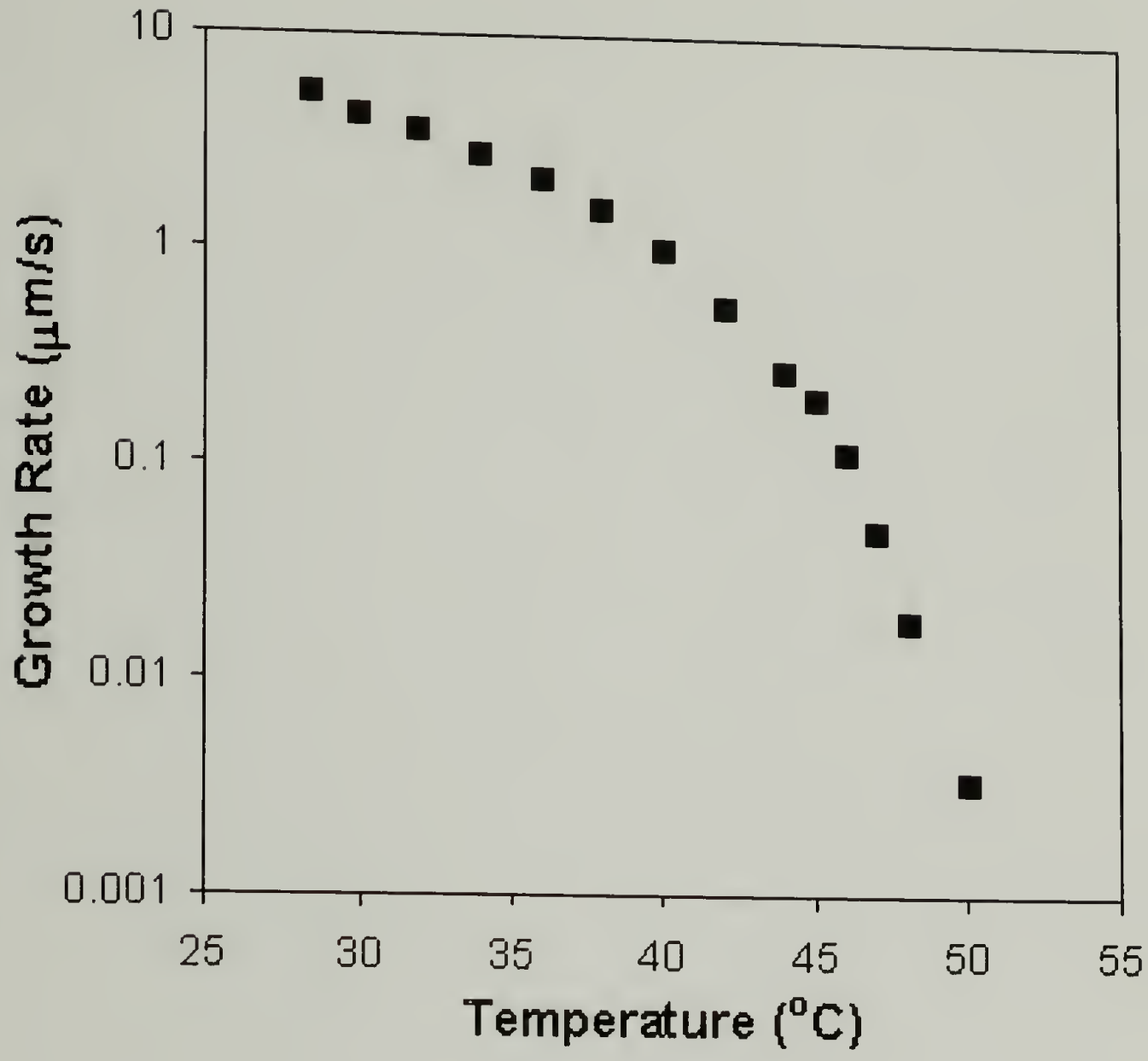

Figure 5.3: Linear crystallite growth rate in thin film.

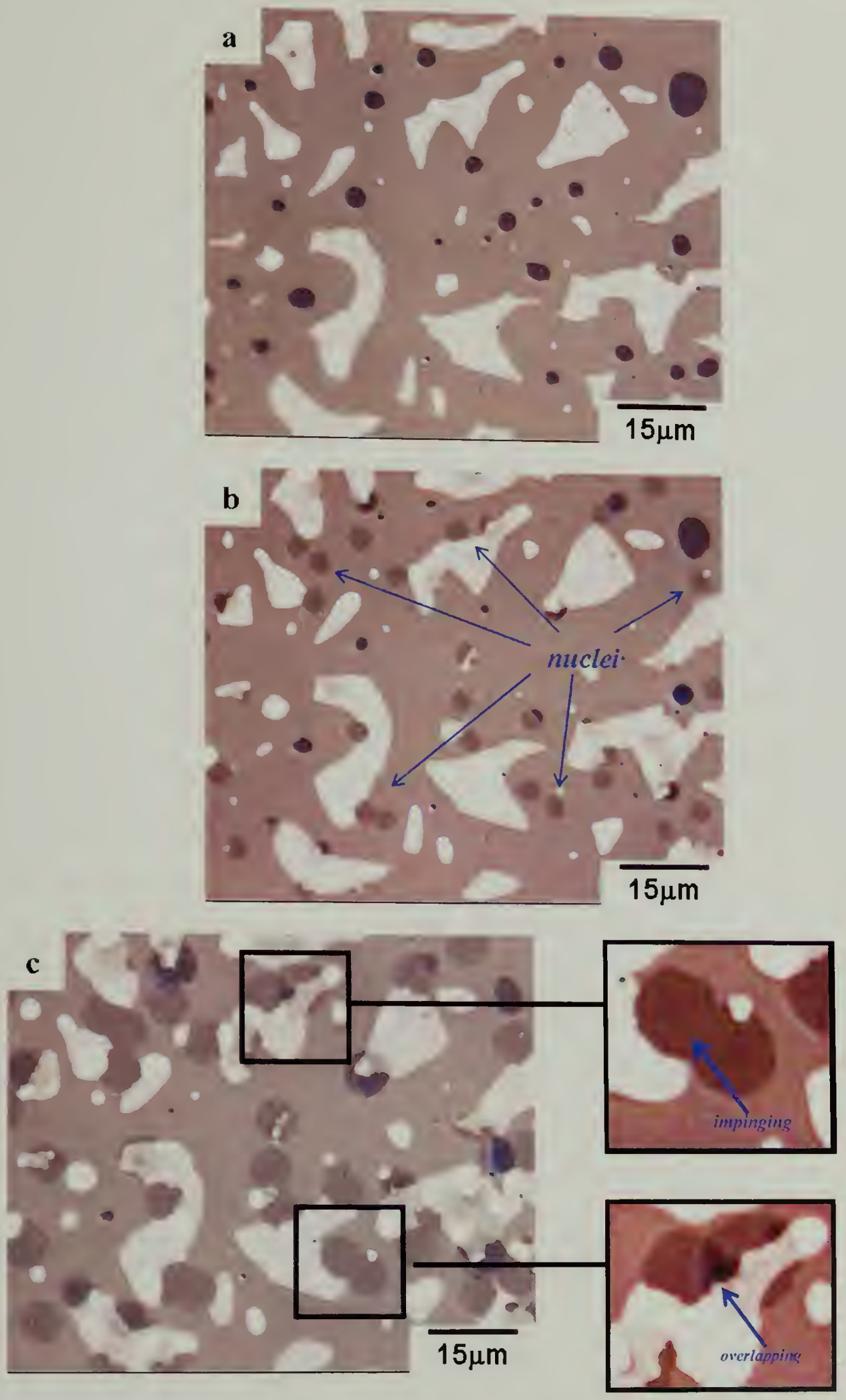

Figure 5.4: Self-seeding crystallization at 45°C. a) Thin film held at 58°C; b) Nuclei started to emerge when temperature was lowered, c) Crystallites grew larger and start to impinge or overlap each other.

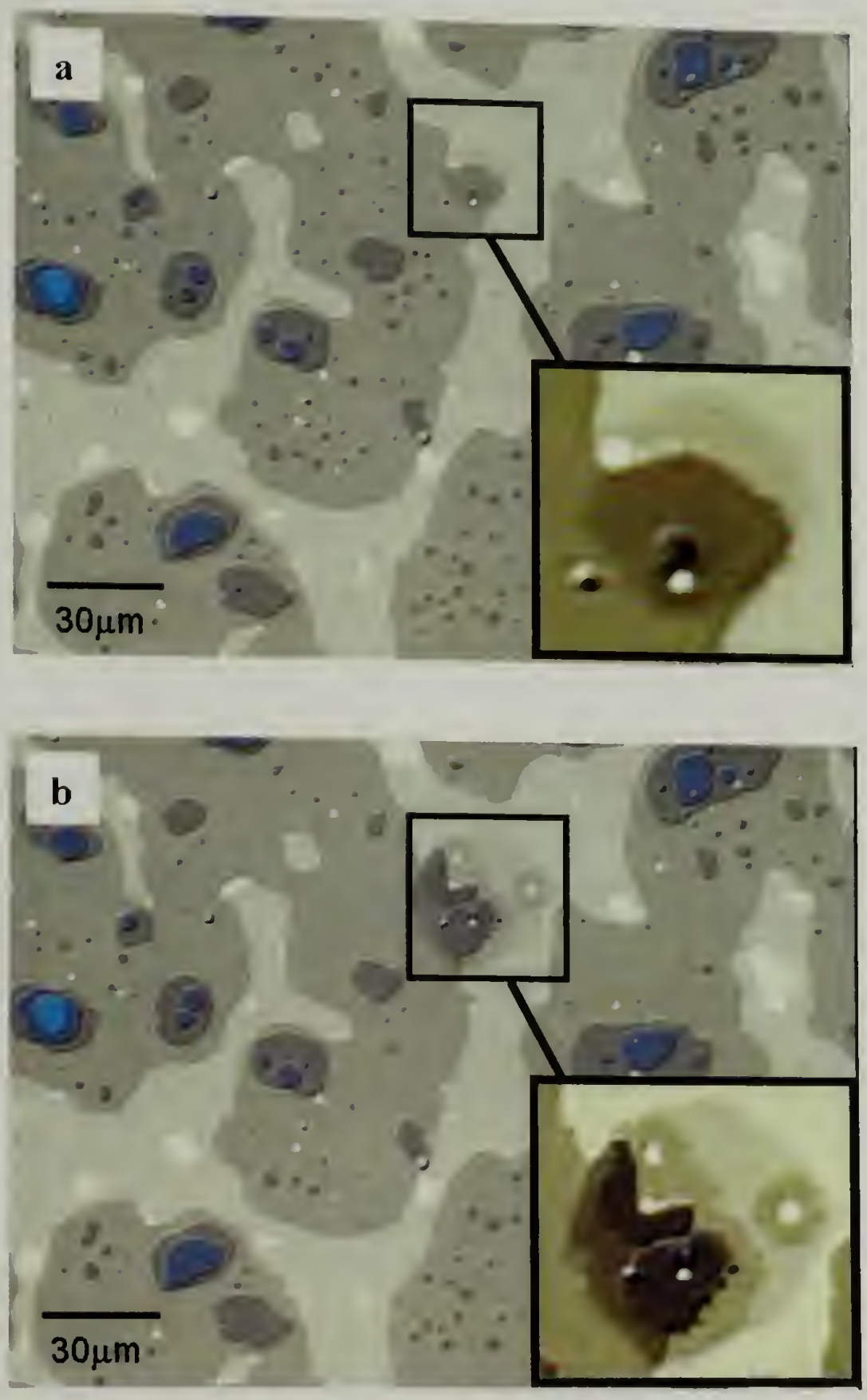

Figure 5.5: Crystal growth and layer propagation at 50°C. a) -b) -c) -d) morphology evolution with time.

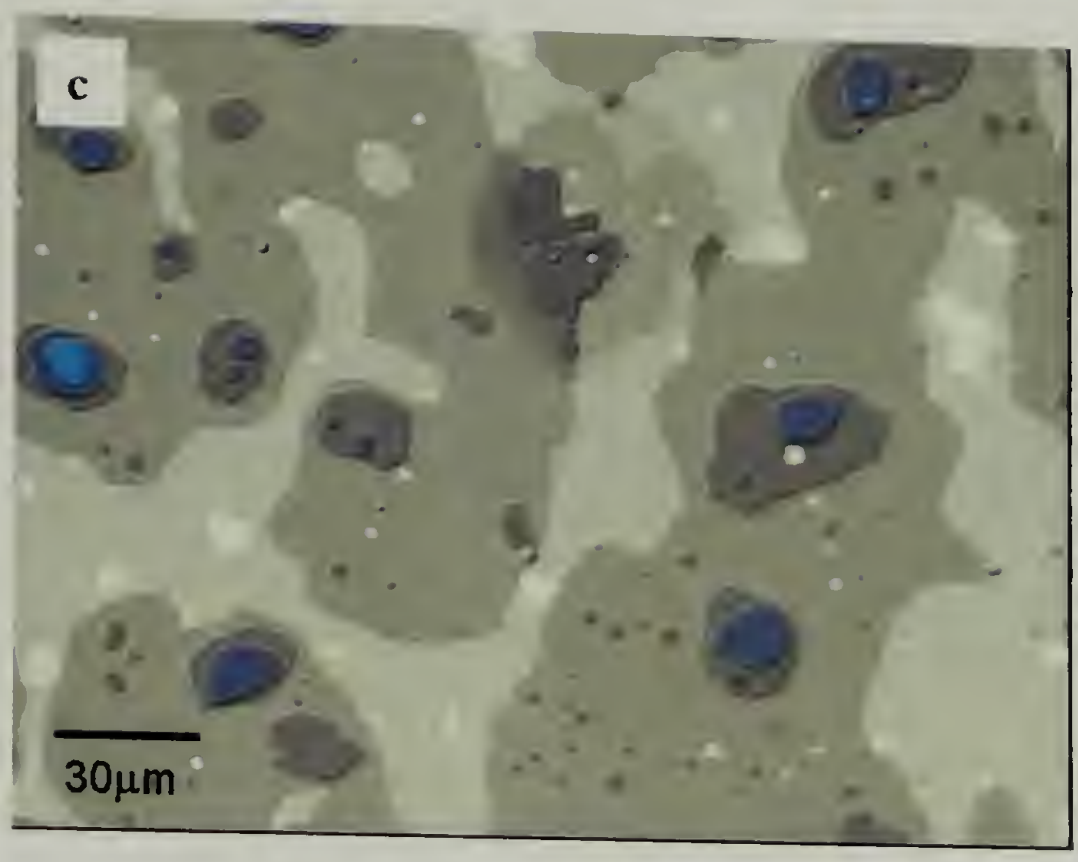
c
30µm

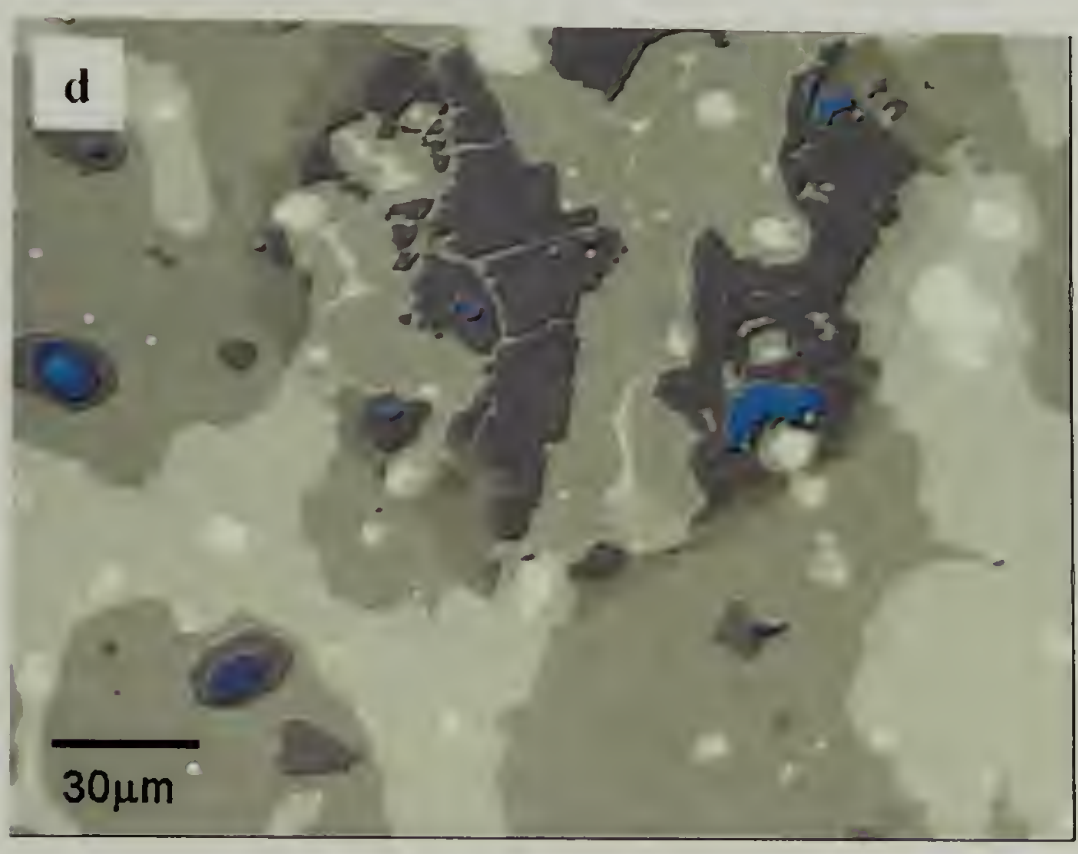
d
30µm

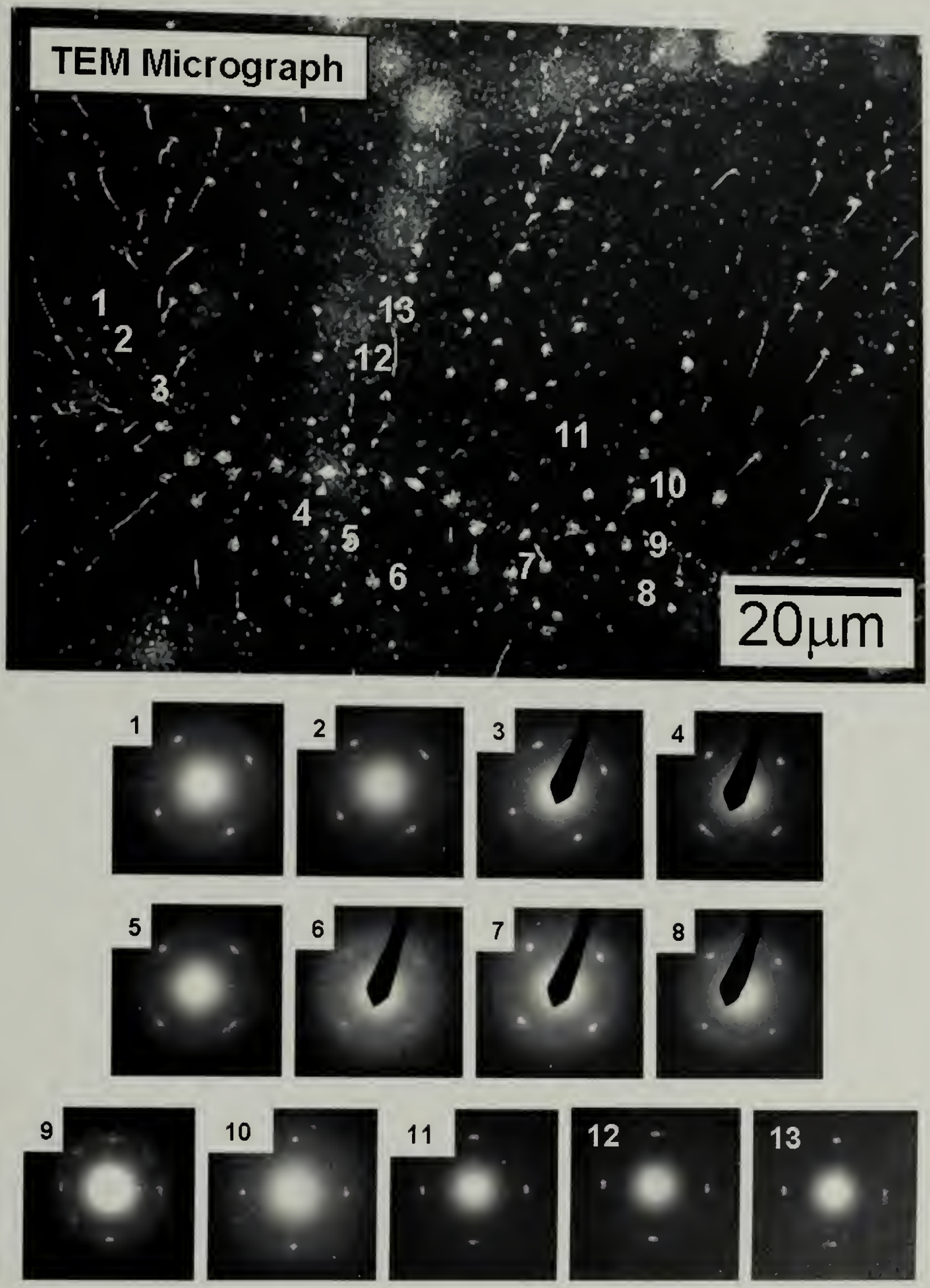

Figure 5.6: TEM image and the electron diffraction patterns showing (120) diffraction from various positions of the film

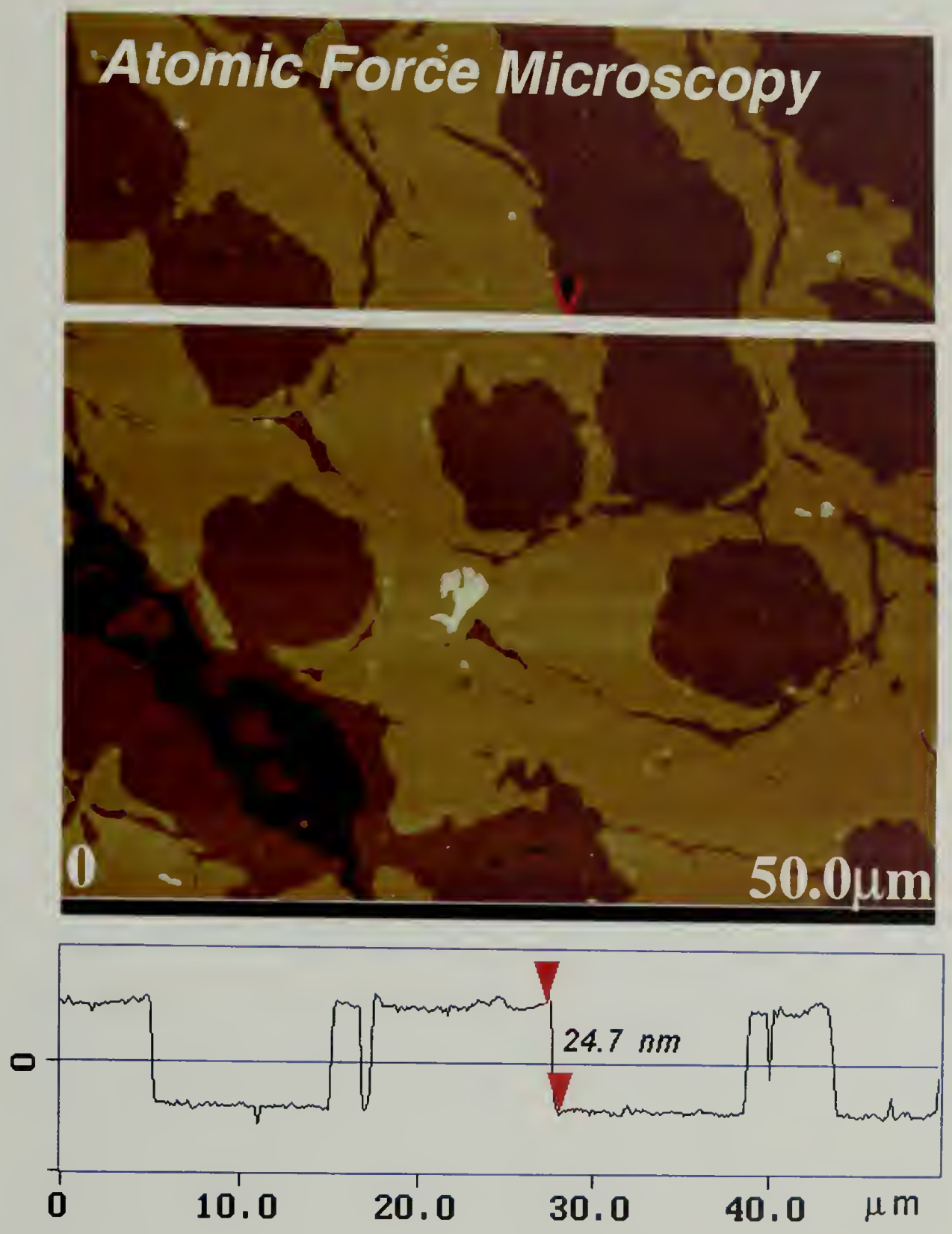

Figure 5.7: AFM micrograph and height profile of P(BD-b-EO) diblock copolymer thin film surface. The sample was crystallized at 45°C.

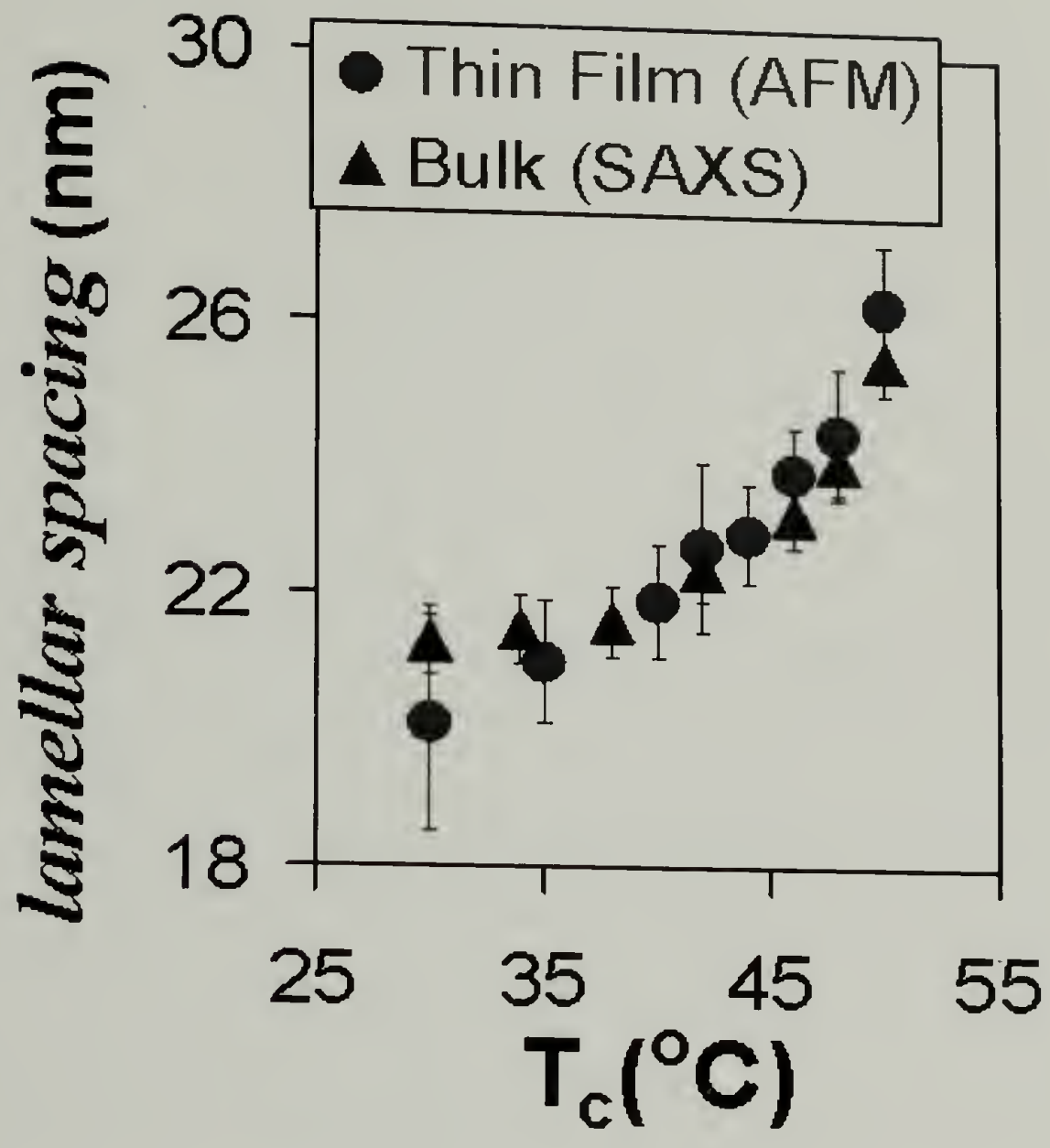

Figure 5.8: Thin film lamellar spacing as a function of crystallization temperature as determined by AFM. For comparison, bulk sample data were as shown.

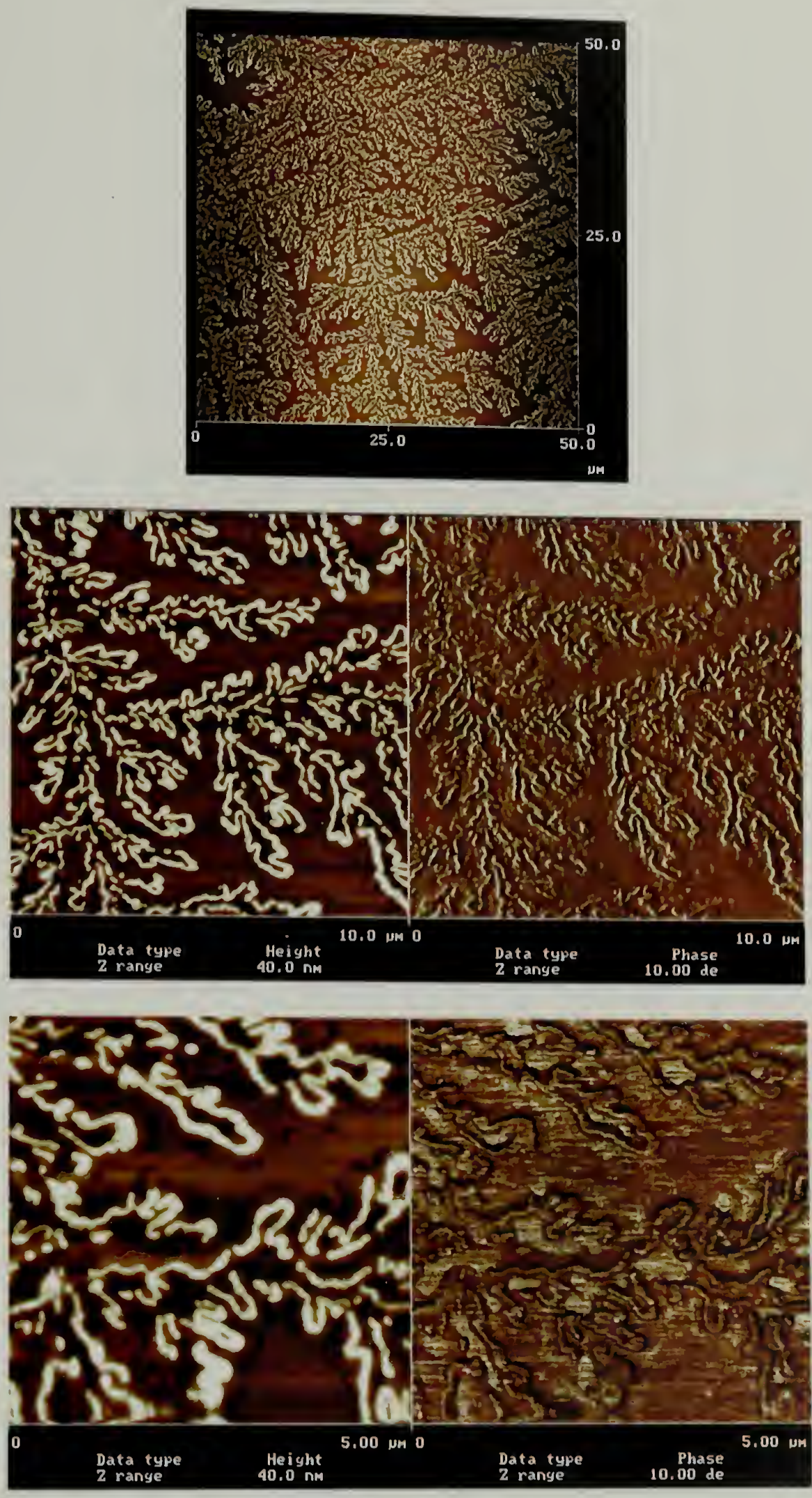

Figure 5.9: AFM micrographs of P(BD-*b*-EO) diblock copolymer films. The films thickness is around 5 – 10nm as determined by ellipsometry.

a

b

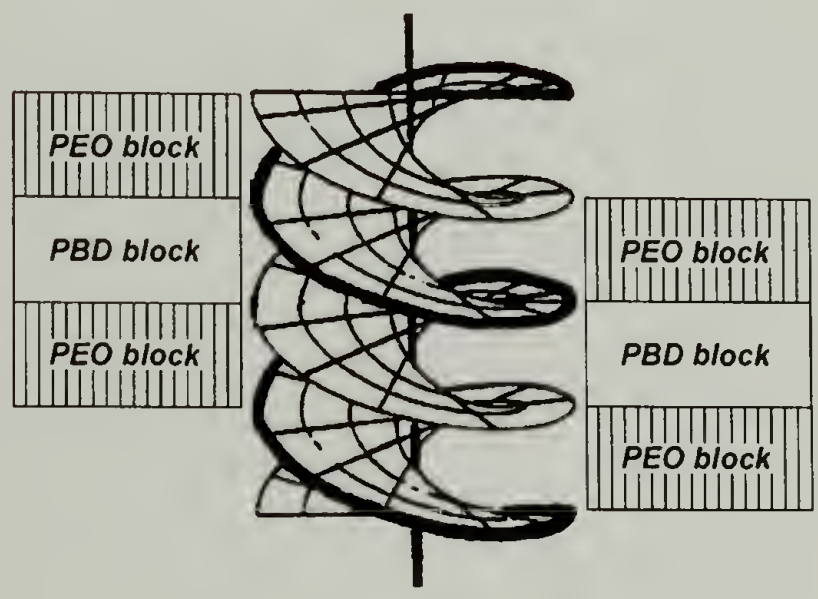

Figure 5.10: Schematics for: a) edge dislocation, b) screw dislocation.

CHAPTER 6

CONCLUSIONS AND FUTURE WORK

6.1 Conclusions

In this study, the phase behavior of strongly segregated crystalline – amorphous diblock copolymers with rubbery amorphous block was investigated. Three different systems were studied, including poly(ethylene-b-atactic propylene) (PE-*b*-aPP), poly(ethylene oxide-b-butadiene) (PEO-*b*-PBD) and poly(ethylene oxide-b-ethylene) (PEO-*b*-PE). All of diblock copolymers formed a well-ordered microphase separated morphology in the melt-state. The objective of this research is to understand the effect of crystallization on pre-existing microphase separated morphology and the effect of morphology on the crystallization behavior of the crystalline block.

For PE-*b*-aPP diblock copolymers, upon crystallization, in most cases, two-dimensional crystallization confined within the microphase-separated microdomains was observed with retention of the microphase-separated morphology formed in the melt-state. The crystallization temperature was found to have significant effect on morphology. Both the extent of microdomain confinement on crystallization and the crystalline chain orientation inside the microdomain were observed to be crystallization temperature dependent. It was shown in this study that utilizing the improved solvent resistance of crystalline block copolymers, a novel method to prepare photonic band gap crystals was developed.

In order to find a system behaving morphologically similar to the theoretical morphological model of crystalline-amorphous diblock copolymers, a low molecular weight yet high crystallinity PEO-*b*-PBD diblock copolymer was chosen as a model system. TEM coupled with electron diffraction revealed a microphase separated, alternating lamellar morphology with PEO crystalline chains oriented perpendicular to the microdomain interface. A significant increase in the microphase separated, lamellar domain spacing was observed upon crystallization. On the length scale of tens of microns, as probed by polarizing optical microscopy, a non-spherulitic crystalline texture (with the absence of the Maltese-cross), corresponding to the microphase separated lamellar grain morphology, was observed. The melt microphase separated morphology acts as templates for crystallization. Crystallization at high temperature resulted in a modest yet observable increase in microphase separated lamellar grain size. In contrast to the integral chain folding observed in PEO homopolymers, the increase in PEO lamellar thickness with decreasing undercooling is continuous in the block copolymers. In addition, at equilibrium the PEO crystalline chain in block copolymer was found to have one fold. This is in contrast to the extended chain crystallites preferred by homopolymers. The crystallization and phase behavior of PEO-*b*-PBD diblock copolymer / homopolymer blends were also studied. By blending low molecular weight homopolymers with PEO-*b*-PBD diblock copolymers, the melt morphology of the system changed from lamella to cylinder. It was observed that confining PEO crystallization inside small cylindrical domains could result in significant retardation in PEO crystallization (more than 40°C).

The morphology of crystalline-crystalline diblock copolymer: PEO-b-PE was investigated and compared with the morphology of its unhydrogenated precursor: PEO-b-PBD. Transmission electron microscopy (TEM) and electron diffraction indicated that both polyethylene and poly(ethylene oxide) crystalline chains were oriented normal to the interfaces of the microphase separated lamellar domains. Crystallization of the polyethylene block resulted in a significant increase (~3 nm) in the lamellar spacing while the subsequent crystallization of the poly(ethylene oxide) block only caused minimal layer expansion. TEM and optical microscopy indicated that despite the change in lamellar spacing upon PE crystallization, the grain structure of the microphase separated lamellae, was mostly maintained after crystallization. The results were analogous to PEO crystallization in PEO-b-PBD diblock copolymers. In addition, it was found that crystallization within rigid microdomains was retarded as compared to crystallization within flexible microdomains.

The morphological evolution of PEO-*b*-PBD diblock copolymers upon crystallization in thin films was studied in detail. Multiple parallel layers of crystalline PEO were found by electron diffraction to be in *orientational crystallographic registry* even though they were separated by approximately 10 nm thick layers of amorphous PBD. A defect controlled mechanism was proposed to explain this unusual observation. The material represents a first example of organic, self-assembled, channel cut crystals.

6.2 Future Work

The current study focused on the morphology of strongly segregated crystalline block copolymers with low T_g amorphous block. Although quite extensive study was

carried out to investigate the morphology in both bulk and thin film, there are still many unanswered questions and many interesting directions worth exploring.

In PE-b-aPP diblock copolymers, the PE crystalline lamellae were observed to have a sphero-disk like orientation when crystallized at high temperature. However, in the case of PE-b-PEO, the PE crystalline chains were found to orient perpendicular to the microdomain interface. This may be due to molecular weight difference between the two systems. In the case of PE-b-PEO, the small spacing does not allow twisting of the crystalline lamellae within the microdomain. The results suggested in addition to a temperature dependent crystalline chain orientation, there might also be molecular weight dependence. It would be very interesting to investigate in this direction for both PE and PEO containing diblock copolymers. If possible, comparison between flexible and rigid confinement on crystallization should be conducted along with the study.

The mechanical properties of PE-b-aPP diblock copolymers were also explored in this study, which showed very different behavior as compared to PE homopolymers. As shown in Figure 6.1 the diblock copolymers had much better elongation at break than pure PE (also hydrogenated PBD) yet the toughness of the two materials were very similar. Also shown in this figure, PE-b-aPP diblock copolymers with well defined microphase separation had much better elongation at break and toughness compared to solution cast samples, where the morphology consisted of short crystalline PE lamellae yet no well define microphase separation. WAXS study Figure 6.2a indicated that PE crystallites in the diblock copolymers were oriented upon stretching with crystalline chains oriented parallel to the stretching direction. If combined with TEM and electron

diffraction (Figure 6.2b), the results indicated that not only the crystalline PE chains were oriented the PE-b-aPP microdomains were also oriented parallel to the stretching direction. In addition, PE crystalline chain stems were found to be parallel to the microdomain interface. A schematic of the morphology is shown in Figure 6.2c. The result suggests that it may be possible to orient a crystalline amorphous diblock copolymer via solid state stretching. It would also be worthwhile to further this study on a series of PE containing diblock copolymers with different PE volume fractions and different chain lengths.

In PBD-b-PEO diblock copolymers, the current study established a method to study the equilibrium state of crystalline/amorphous diblock copolymers based on experimentally obtained data. The current study has only focused on one diblock copolymer. It would be interesting to expand this research to diblock copolymers with a series of different molecular weights.

For PBD-b-PEO diblock copolymer thin films with thickness less than 10nm, we observed very interesting "hollow dendritic" morphology. Although similar conditions were applied to PEO homopolymers, such morphology was not observed. The results suggested that it was unique for diblock copolymers. It may be due to a combination of edge thickening of crystallites and limited diffusion of absorbed diblock copolymers. A detailed study of different crystallization temperatures may shed more light. It may also be necessary to conduct electron diffraction to investigate the crystalline chain orientation on very thin films: whether it is perpendicular or tilted with respected to microdomain interfaces.

The majority of this current study focused on lamellar forming diblock copolymers. It would be very interesting to extend this study to block copolymers forming more complex morphologies, such as cylinder, sphere or even gyroid. The morphology evolution upon crystallization, crystalline chain orientation and the crystallization kinetics are all worth investigating.

One of the most exciting observation in this study is that we can use crystalline / amorphous block copolymer to prepare flexible photonic band gap crystals. The main advantage of our current procedure is the potential to make 2 or 3 dimensional photonic crystals with relatively low molecular weight diblock copolymers. In thinking of potential application of crystalline amorphous block copolymers, this is definitely a direction that shall be explored further.the crystallization kinetics would all be interesting subjects for further investigations.

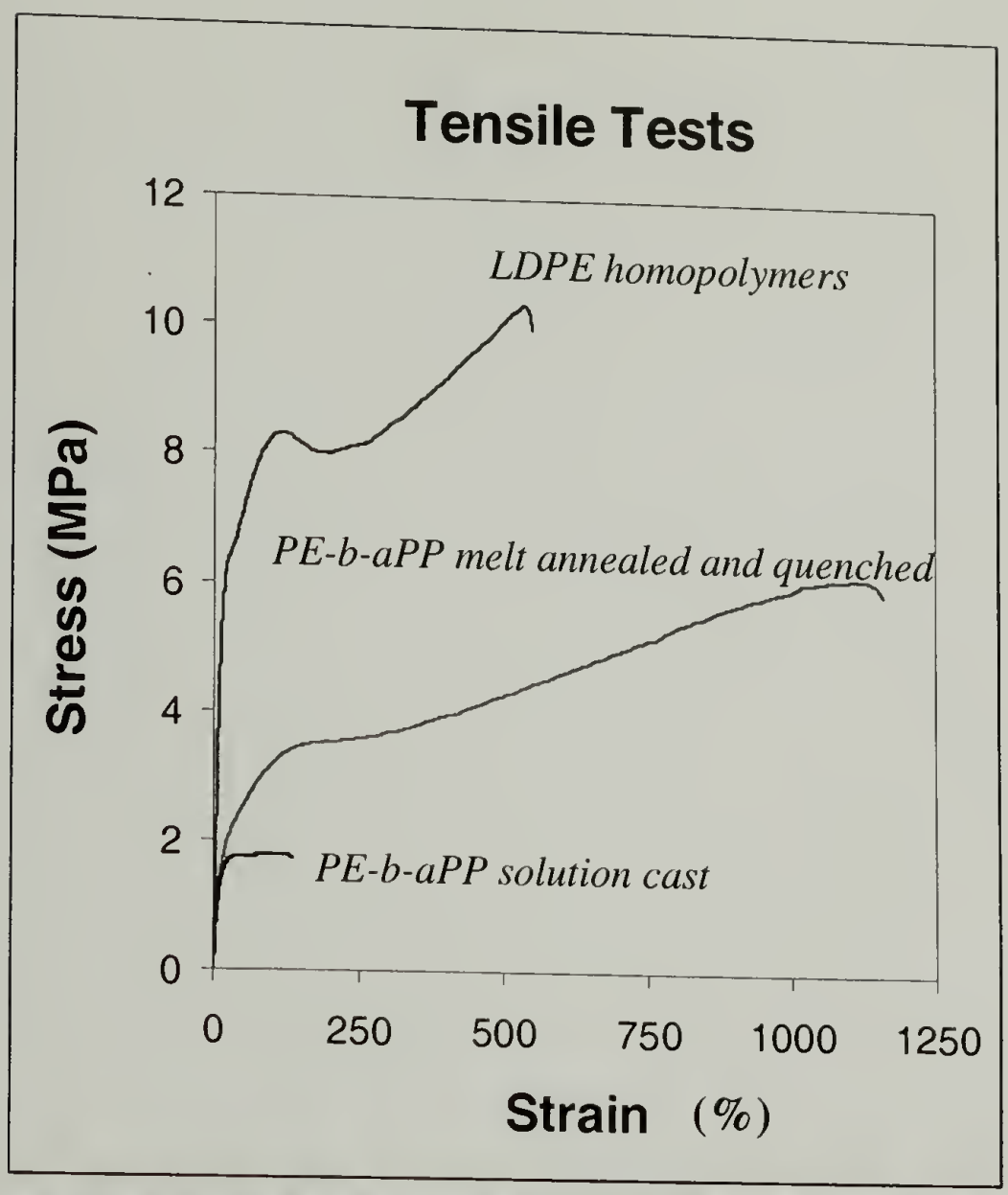

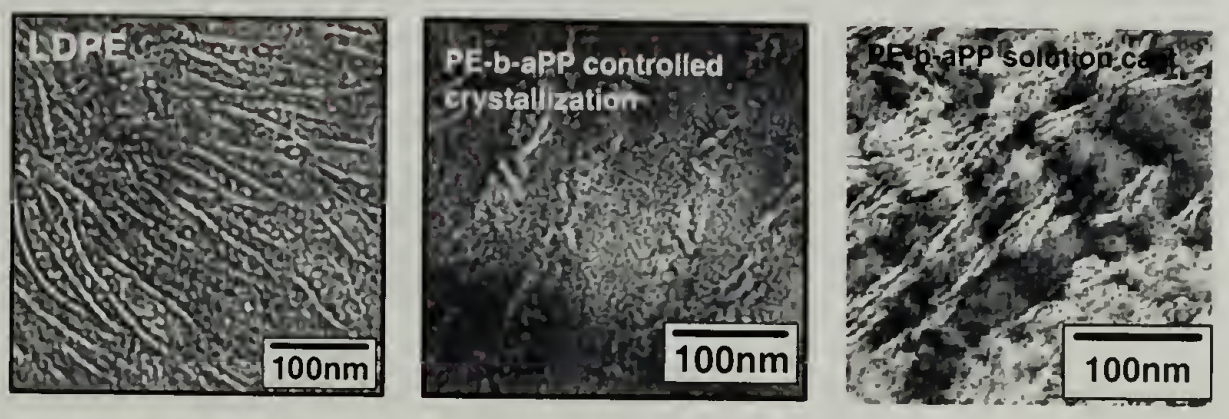

Figure 6.1: Comparison of tensile properties of LDPE and PE-b-aPP diblock copolymers.

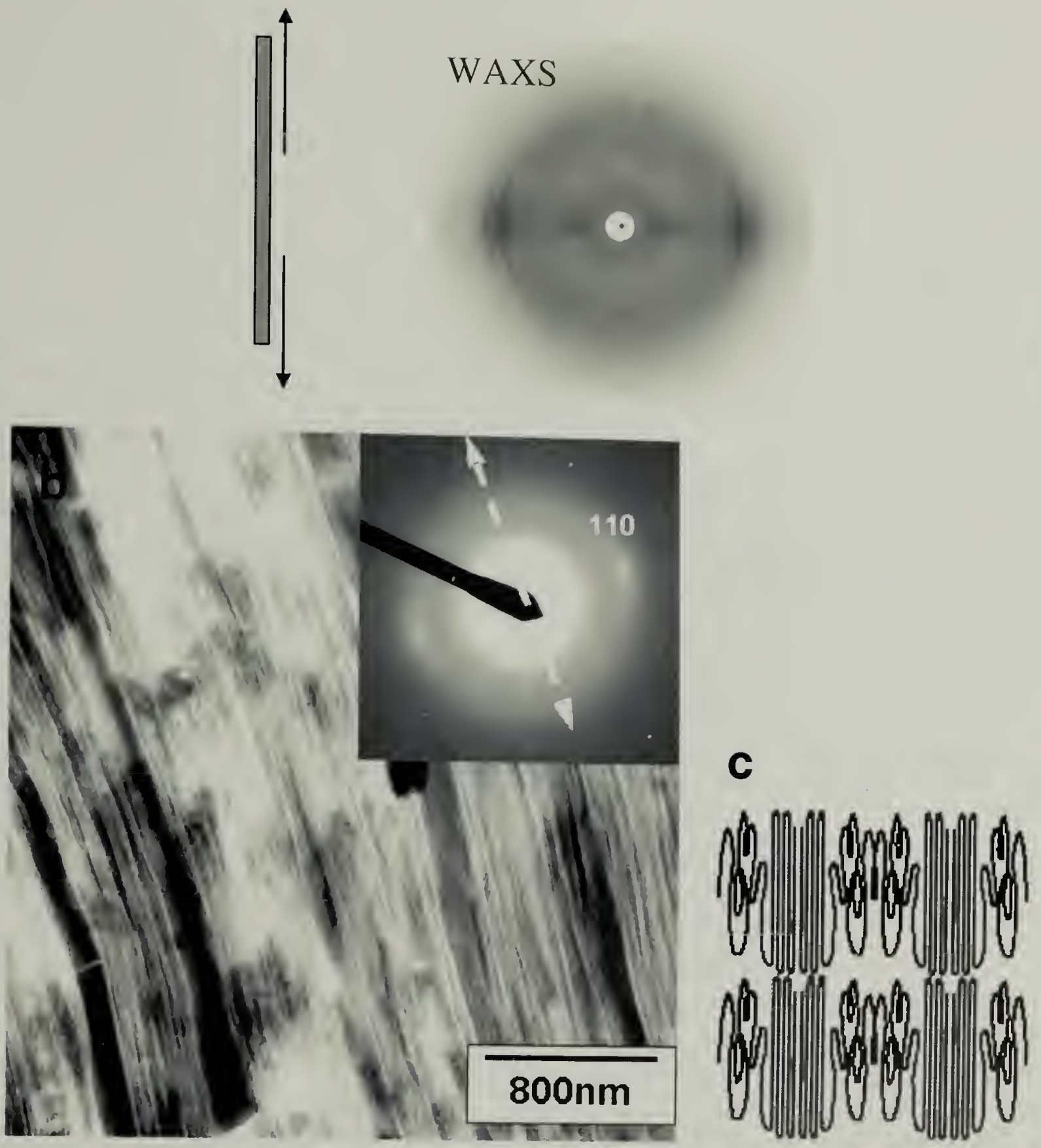

Figure 6.2: Morphology of PE-b-aPP diblock copolymers upon strecthing. a) WAXS (arrows indicates drawing direction); b) TEM Micrograph and electron diffraction pattern; c) Schematic of morphology.

BIBLIOGRAPHY

1. Hamley, I. W. *The Physics of Block Copolymers* (Oxford University Press, Oxford, 1998).

2. DiMarzio, E. A., Guttman, C. M., Hoffman, J. D. *Macromolecules* **1980**, *13*, 1194.

3. Whitmore, M. D., Noolandi, J. *Macromolecules* **1988**, *21*, 1482.

4. Vilgis, T., Halperin, A. *Macromolecules* **1991**, *24*, 2090.

5. Seguela, R., Prud'Homme, J. *Polymer* **1989**, *30*, 1446.

6. Cohen, R. E., Cheng, P. L., Douzinas, K., Kofinas, P., Berney, C. V. *Macromolecules* **1990**, *23*, 324.

7. Douzinas, K. C., Cohen, R. E., Halasa, A. F. *Macromolecules* **1991**, *24*, 4457.

8. Douzinas, K. C., Cohen, R. E. *Macromolecules* **1992**, *25*, 5030.

9. Hamley, L. W., Fairclough, J. P. A., Terrill, N. J., Ryan, A. J., Lipic, P. M., Bates, F. S., Towns-Andrews, E. *Macromolecules* **1996**, *29*, 8835.

10. Hamley, I. W., Fairclough, J. P. A., Bates, F. S., Ryan, A. J. *Polymer* **1998**, *39*, 1429.

11. Kofinas, P., Cohen, R. E. *Macromolecules* **1994**, *27*, 3002.

12. Kofinas, P., Cohen, R. E., Halasa, A. F. *Polymer* **1994**, *35*, 1229.

13. Kofinas, P., Cohen, R. E. *Macromolecules* **1995**, *28*, 336.

14. Loo, Y. L., Register, R. A., Ryan, A. J. *Phys. Rev. Let.* **2000**, *84*, 4120.

15. Quiram, D. J., Register, R. A., Marchand, G. R., Ryan, A. J. *Macromolecules* **1997**, *30*, 8338.

16. Quiram, D. J., Register, R. A., Marchand, G. R. *Macromolecules* **1997**, *30*, 4551

17. Quiram, D. J., Register, R. A., Marchand, G. R., Adamson, D. H. *Macromolecules* **1998**, *31*, 4891.

18. Rangarajan, P., Register, R. A., Fetters, L. J. *Macromolecules* **1993**, *26*, 4640.

19. Rangarajan, P., Register, R. A., Fetters, L. J., Bras, W., Naylor, S., Ryan, A. J. *Macromolecules* **1995**, *28*, 4932.

20. Rangarajan, P., Register, R. A., Adamson, D. H., Fetter, L. J., Bras, W., Naylor, S., Ryan, A. J. *Macromolecules* **1995**, *28*, 1422.

21. Rangarajan, P., Haisch, C. F., Register, R. A., Adamson, D. H., Fetters, L. J. *Macromolecules* **1997**, *30*, 494.

22. Ryan, A. J., Hamley, I. W., Bras, W., Bates, F. S. *Macromolecules* **1995**, *28*, 3860.

23. Sakurai, K., MacKnight, W. J., Lohse, D., Schulz, D. N., Sissano, J. A. *Macromolecules* **1993**, *26*, 3236.

24. Sakurai, K., MacKnight, W. J., Lohse, D. J., Schulz, D. N., Sissano, J. A. *Macromolecules* **1994**, *27*, 4941.

25. Sakurai, K., MacKnight, W. J., Lohse, D. J., Schulz, D. N., Sissano, J. A., Lin, J. S., Agamalyan, M. *Polymer* **1996**, *37*, 4443.

26. Sakurai, K., Shinkai, S., Ueda, M., Sakurai, S., Nomura, S., MacKnight, W. J., Lohse, D. J. *Macromol. Rapid Commun.* **2000**, *21*, 1140.

27. Ashman, P. C., Booth, C. *Polymer* **1975**, *16*, 889.

28. Ashman, P. C., Booth, C., Cooper, D. R., Price, C. *Polymer* **1975**, *16*, 897.

29. Gast, A. P., Vinson, P. K., Cogan-Farinas, K. A. *Macromolecules* **1993**, *26*, 1774.

30. Gervais, M., Gallot, B. *Makromol. Chem.* **1973**, *174*, 193.

31. Wittmann, J. C., Lotz, B., Candau, F., Kovacs, A. J. *J. Polym. Sci., Poly. Phys. Ed.* **1982**, *20*, 1341.

32. Mai, S., Fairclough, J. P. A., Hamley, I. W., Matsen, M. W., Denny, R. C., Liao, B., Booth, C., Ryan, A. J. *Macromolecules* **1997**, *30*, 8392.

33. Ryan, A. J., Fairclough, J. P. A., Hamley, I. W., Mai, S., Booth, C. *Macromolecules* **1997**, *30*, 1723.

34. Reiter, G., Castelein, G., Hoerner, P., Riess, G., Blumen, A., Sommer, J. *Phys. Rev. Lett.* **1999**, *83*, 3844.

35. Floudas, G., Reiter, G., Lambert, O., Dumas, P. *Macromolecules* **1998**, *31*, 7279.

36. Floudas, G., Ulrich, R., Wiesner, R. *J. Chem. Phys.* **1999**, *110*, 652.

37. Zhu, L., Chen, Y., Zhang, A., Calhoun, B. H., Chun, M., Quirk, R. P., Cheng, S. Z. D., Hsiao, B. S., Yeh, F., Hashimoto, T. *Physical Review B* **1999**, *60*, 10022.

38. Nojima, S., Kato, K., Yamamoto, S., Ashida, T. *Macromolecules* **1992**, *25*, 2237.

39. Ishikawa, S., Ishizu, K., Fukutomi, T. *European Polymer Journal* **1992**, *28*, 1219.

40. Liu, L.-Z., Yeh, F., Chu, B. *Macromolecules* **1996**, *29*, 5336.

41. Cohen, R. E., Bellare, A., Drzewinski, M. A. *Macromolecules* **1994**, *27*, 2321.

42. Khandpur, A. K., Macosko, C. W., Bates, F. S. *J. Polym. Sci., Polym. Phys. Ed.* **1995**, *33*, 247.

43. Loo, Y.-L., Register, R. A., Adamson, D. H. *J. Polym. Sci. B: Polym. Phys.* **2000**, *38*, 2564.

44. Loo, Y.-L., Register, R. A., Adamson, D. H. *Macromolecules* **2000**, *33*, 8361.

45. Wu, Z., Grubbs, R. H. *Macromolecules* **1994**, *27*, 6700.

46. Gratt, J., Cohen, R. E. *Macromolecules* **1997**, *30*, 3137.

47. Avrami, M. *Journal of Chem. Phys.* **1939**, *7*, 1103.

48. Kovacs, A. J., Gonthier, A. *Kolloid Z. Z. Polym.* **1972**, *250*, 530.

49. Kovacs, A. J., Gonthier, A., Straupe, C. *J. Polym. Sci., Polym. symp.* **1975**, *50*, 283.

50. Kovacs, A. J., Straupe, C., Gonthier, A. *J. Polym. Sci., Polym. symp.* **1977**, *59*, 31.

51. Cheng, S. Z. D., Wunderlich, B. *J. Polym. Sci., Polym. Phys. Ed.* **1986**, *24*, 577.

52. Cheng, S. Z. D., Wunderlich, B. *J. Polym. Sci., Polym. Phys. Ed.* **1986**, *24*, 595.

53. Cheng, S. Z. D., Bu, H. S., Wunderlich, B. *J. Polym. Sci., Polym. Phys. Ed.* **1988**, *26*, 1947.

54. Cheng, S. Z. D., Noid, D. W., Wunderlich, B. *J. Polym. Sci., Polym. Phys. Ed.* **1989**, *27*

55. Cheng, S. Z. D., Chen, J., Janimak, J. J. *Polymer* **1990**, *31*, 1018.

56. Cheng, S. Z. D., Zhang, A., Barley, J. S., Chen, J., Habenschuss, A., Zschack, P. R. *Macromolecules* **1991**, *24*, 3937.

57. Cheng, S. Z. D., Zhang, A., Chen, J., Heberer, D. P. *J. Polym. Sci., Polym. Phys. Ed.* **1991**, *29*, 287.

58. Cheng, S. Z. D., Chen, J., Zhang, A., Heberer, D. P. *J. Polym. Sci., Polym. Phys. Ed.* **1991**, *29*, 299.

59. Cheng, S. Z. D., Barley, J. S., Meerwall, E. D. V. *J. Polym. Sci., Polym. Phys. Ed.* **1991**, *29*, 515.

60. Cheng, S. Z. D., Wu, S. S., Chen, J., Zhuo, Q., Quirk, R. P., Meerwall, E. D. V., Hsiao, B. S., Habenschuss, A., Zschack, P. R. *Macromolecules* **1993**, *26*, 5105.

61. Barnes, W. J., Price, F. P. *Polymer* **1964**, *5*, 283.

62. Bu, H. S., Cheng, S. Z. D., Wunderlich, B. *Polymer* **1988**, *29*, 1603.

63. Buckley, C. P. *Polymer* **1980**, *21*, 444.

64. Buckley, C. P., Kovacs, A. J. *Progr. Colloid and Polym. Sci.* **1975**, *58*, 44.

65. Buckley, C. P., Kovacs, A. J. *Colloid Z. Z. Polym.* **1976**, *254*, 695.

66. Fujiwara, T., Miyamoto, M., Kimura, Y. *Macromolecules* **2000**, *33*, 2782.

67. Hoffman, J. D. *Macromolecules* **1986**, *19*, 1124.

68. Lotz, B., Kovacs, A. J. *Kolloid Z. Z. Polym* **1966**, *209*, 97.

69. Lotz, B., Kovacs, A. J., Bassett, G. A., Keller, A. *Kolloid Z. Z. Polym.* **1966**, *209*, 115.

70. Hamley, I. W., Wallwork, M. L., Smith, D. A., Fairclough, J. P. A., Ryan, A. J., Mai, S.-M., Yang, Y.-W., Booth, C. *Polymer* **1998**, *39*, 3321.

71. Gervais, M., Gallot, B. *Makromol. Chem.* **1973**, *171*, 157.

72. Zhu, L., Cheng, S. Z. D., Calhoun, B. H., Ge, Q., Quirk, R. P., Thomas, E. L., Hsiao, B. S., Yeh, F. J., Lotz, B. *J. Am. Chem. Soc.* **2000**, *122*, 5957.

73. Flory, P. J., Vrij, S. *J. Am. Chem. Soc.* **1963**, *85*, 3548.

74. Yang, Y. W., Tanodekaew, S., Mai, S. M., Booth, C., Ryan, A. J., Bras, W., Viras, K. *Macromolecules* **1995**, *28*, 6029.

75. Nojima, S., Nakano, H., Ashida, T. *Polymer* **1993**, *34*, 4168.

76. Nojima, S., Nakano, H., Takahashi, Y., Ashida, T. *Polymer* **1994**, *35*, 3479.

77. Nojima, S., Yamamoto, S., Ashida, T. *Polymer Journal* **1995**, *27*, 673.

78. Nojima, S., Takahashi, Y., Ashida, T. *Polymer* **1995**, *36*, 2853.

79. Nojima, S., Kuroda, M., Sasaki, S. *Polymer Journal* **1997**, *29*, 642.

80. Nojima, s., Hashizuma, K., Rohadi, A., Sasaki, S. *Polymer* **1997**, *38*, 2711.

81. Nojima, S., Tanaka, H., Rohadi, A., Sasaki, S. *Polymer* **1998**, *39*, 1727.

82. Ishikawa, S., Sasaki, S., Fukutomi, T. *Journal of applied Polymer Science* **1993**, *48*, 509.

83. Ishikawa, S., Fukutomi, T. *European Polymer Journal* **1993**, *29*, 877.

84. Ishikawa, S. *Journal of Applied Polymer Science* **1994**, *51*, 1709.

85. Liu, L., Li, H., Jiang, B., Zhou, E. *Polymer* **1994**, *35*, 5511.

86. Liu, L., Jiang, B., Zhou, E. *Polymer* **1996**, *37*, 3937.

87. Liu, L., Xu, W., Li, H., Su, F., Zhou, E. *Macromolecule* **1997**, *30*, 1363.

88. Deng, S.-S., Zhang, H.-Z., Feng, X.-D. *Polymer Bulletin* **1982**, *8*, 219.

89. Brown, G. M., Butler, J. H. *Polymer* **1997**, *38*, 3937.

90. Montezinos, D., Wells, B. G., Burns, J. L. *J. Polym. Sci., Part C* **1985**, *23*, 421.

91. Bushelman, A. A. *Ph.D. Thesis,* University of Massachusetts, Amherst **1999**

92. Scott, D. B., Waddon, A. J., Lin, Y., Karasz, F. E., Winter, H. H. *Macromolecules* **1992**, *25*, 4175.

93. Keller, A. *J. Polym. Sci.* **1955**, *15*, 133.

94. Balta-Calleja, F. J., Vonk, C. G. *X-Ray Scattering of Synthetic Polymers* (Elsevier, New York, 1989).

95. Urbas, A., R., S., Fink, Y., Thomas, E. L. *Adv. Mater.* **2000**, *12*

96. Weber, M. F., Stover, C. A., Gilbert, L. R., Nevitt, T. J., Ouderkirk, A. J. *Science* **2000**, *287*, 2451.

97. Gates, B., Park, S. H., Xia, Y. *Adv. Mater.* **2000**, *2000*, 653.

98. Hoffman, J. D., Frolen, L. J., Ross, G. S., Lauritzen, J. I. J. *J. Res. Nat. Bur. Std. - A. Phys. Chem.* **1975**, *79A*, 671.

99. Noshay, A., McGrath, J. E. *Block Copolymer, Overview and Critical Survey* (Academic Press, New York, 1977).

100. Hong, S., Bushelman, A. A., MacKnight, W. J., Gido, S. P., Lohse, D. J., Fetter, L. J. *Polymer* **2001**, *42*, 5909.

101. Hong, S., MacKnight, W. J., Russell, T. P., Gido, S. P. *Macromolecules* **2001**, *34*, 2398.

102. Hong, S., MacKnight, W. J., Russell, T. P., Gido, S. P. *Macromolecules* **2001**, *34*, 2876.

103. Reiter, G., Castelein, G., Hoerner, P., Riess, G., Sommer, J. U., Floudas, G. *Euro. Phys. J. E.* **2000**, *2*, 319.

104. Brandrup, J., Immergut, E. H. *Polymer Handbook* (Interscience, New York).

105. Gido, S. P., Thomas, E. L. *Macromolecules* **1994**, *27*, 6137.

106. Gido, S. P., Gunther, J., Thomas, E. L., Hoffman, D. *Macromolecules* **1993**, *26*, 4506.

107. Newstein, M. C., Garetz, B. A., Dai, H. J., Balsara, N. P. *Macromolecules* **1995**, *28*, 4587.

108. Gido, S. P., Schwark, D. W., Thomas, E. L., Goncalves, M. *Macromolecules* **1993**, *26*, 2636.

109. Gido, S. P., Thomas, E. L. *Macromolecules* **1994**, *27*, 849.

110. Burgaz, E., Gido, S. P. *Macromolecules* **2000**, *33*, 8739.

111. Friedel, G. *Ann..Phys. Paris* **1922**, *18*, 273.

112. Gedde, U. W. *Polymer Physics* (Chapman&Hall, 1995).

113. Alfonso, J. C., Russell, T. P. *Macromolecules* **1986**, *19*, 1143.

114. Hong, S., MacKnight, W. J., Russell, T. P., Gido, S. P. *Macromolecules* **2001**, *Accepted for publication*

115. Pople, J. A., Hamley, I. W., Terrill, N. J., Fairclough, J. P. A., Ryan, A. J., Yu, G.-E., Booth, C. *Polymer* **1998**, *39*, 4891.

116. Mai, S., Fairclough, J. P. A., Hamley, I. W., Matsen, M. W., Denny, R. C., Liao, B., Booth, C., Ryan, A. J. *Macromolecules* **1996**, *29*, 6212.

117. Fadeev, A. Y., McCarthy, T. J. *Langmuir* **1999**, *15*, 3759.

118. Coulon, G., Russell, T. P., Deline, V. R., Green, P. F. *Macromolecules* **1989**, *22*, 2581.

119. Morkved, T. L., Lu, M., Urbas, A. M., Ehrichs, E. E., Jaeger, H. M., Mansky, P., Russell, T. P. *Science* **1996**, *273*, 931.

120. Keith, H. D., Padden, F. J. *J. Appl. Phys.* **1964**, *35*, 1286.

121. Reiter, G., Sommer, J. *Phys. Rev. Lett.* **1998**, *80*, 3771.

122. Khoury, F., Passaglia, E. in *Treatie on Solid State Chemistry* Chap. 6. New York: Plenum (1976).